Département
Génie Énergétique et
Environnement

Domaine scientifique de la Doua
Institut National des Sciences Appliquées
Bâtiment Sadi Carnot
9 rue de la physique
69621 Villeurbanne Cedex
Tel. (+33) 04 72 43 87 00 (secrétariat)

New Energy Research Center (NERC) Turku
Turku University of Applied Sciences
Joukahaisenkatu 3A
20520 TURKU
FINLAND
+358 22 63350
www.tuas.fi

Internship Report

Thermal energy storage with valorisation of industrial solid wastes

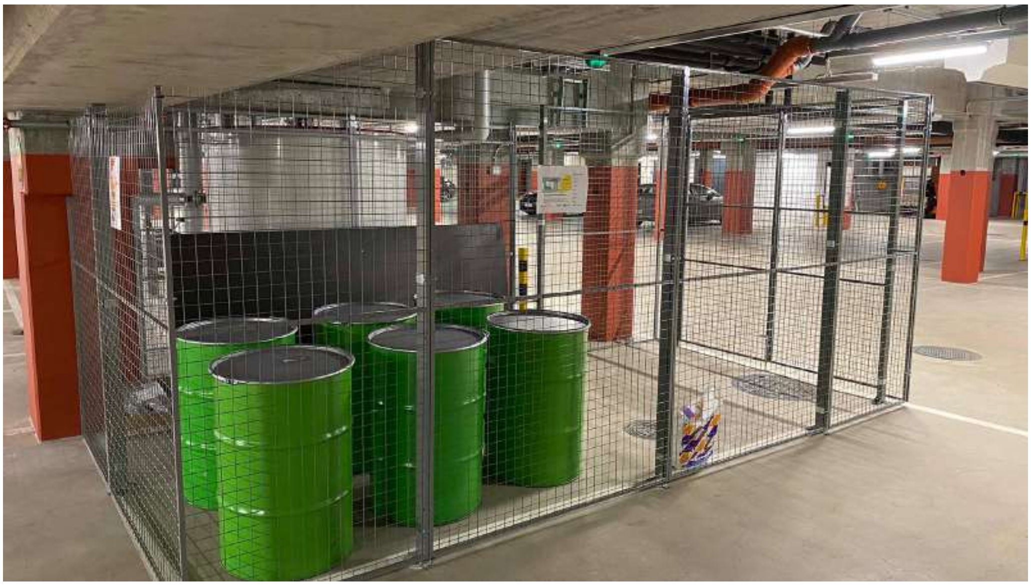

Intern : Yap Jun Ting

Internship tutor : Rauli Lautkankare

Internship supervisor : Eliane Younes

from 7 April to 29 August
Academic Year 2025

Acknowledgements

The research summarised in this report was carried out in New Energy Research Center (NERC) Turku at Turku University of Applied Sciences in Finland. These tests are performed as a part of RESINA – Resource-wise Energy Storage – project which is partly funded by European Regional Development Fund. The industrial solid wastes tested are provided by Suomen Erityisjäte Oy and Pöytyän Koneistuspalvelu Oy.

I would like to thank NERC Turku research group leader, Samuli Ranta for giving me the opportunity to join this thermal energy storage project. I would like to thank my internship tutor, Rauli Lautkankare for guiding and helping me with prompt response throughout this internship. I would like to thank my internship supervisor, Eliane Younes for her guidance throughout this internship. I would like to thank my colleagues Tero Tuomarmäki, Harri Kähkönen and Dominique Roggo for your guidance and support on my work for the internship. I would like to thank my colleague Maarit Puurunen for helping me on performing one of the important tests (sieve test) for the project. I would like to thank Leevi Yliaho whom I collaborated with at the beginning stage of my internship to build the waste heat recovery system. I would like to thank Olavi Koskinen who helped me to build the thermal energy storage installation. I would like to thank Mikael and Leena for helping me to perform one of the essential tests (thermogravimetric analysis test) for the project.

Furthermore, I would like to thank my family for their support and motivation during my internship at Turku, Finland.

Abstract

Thermal energy storage (TES) is considered as one of the most commonly used energy storage technologies and sensible heat storage is one of the essential technologies developed for thermal energy storage. The development of a sensible heat storage solution coupled with valorisation of industrial solid waste is of highly interest as this addresses not only the environmental and health problems provoked by industrial solid waste but also allows the development of a more environmentally friendly thermal energy storage technology.

This work focuses on the use of four industrial solid waste, namely: waste metal powder, crushed concrete, slag and fly ash to develop a waste heat recovery system and a thermal energy storage installation. Both TES installations have been built during this study through collaboration with colleagues of NERC Turku. The thermal characteristics and properties of the four industrial solid waste as well as the performance for both thermal energy storage installations are examined and studied through experiments and tests. Computational fluid dynamic (CFD) simulation on the waste heat recovery system has been performed to examine the system with the use of waste metal powder for TES.

The result demonstrates that the use of waste heat recovery system as open loop system for energy discharge with higher heating temperature and lower heating time is the most ideal configuration. Concerning the TES installation built, it has been revealed that crushed concrete has a better overall performance as a TES materials followed by slag and fly ash.

Keywords: thermal energy storage, sensible heat storage, industrial solid waste, waste heat recovery, waste metal powder, crushed concrete, slag, fly ash

Résumé

Le stockage d'énergie thermique (TES) est considéré comme l'une de technologie de stockage thermique les plus couramment employées. Le stockage de chaleur sensible est l'une des technologies essentielles développé au sein de stockage thermique. Le développement d'une solution de stockage de chaleur sensible couplé avec la valorisation des déchets solides industriels présent un grand intérêt car il permet non seulement d'adresser les problèmes environnementaux et de santé publique reliés avec les déchets solides industriels mais aussi de développer une solution plus écologique pour le stockage d'énergie thermique.

Ce travail se concentrent sur l'utilisation des quatre déchets solides industriels, qui sont: les déchets de poudres métalliques, béton concassé, laitier et cendre volante pour développer un système de récupération de chaleur et un système de stockage thermique. Les deux installations sont construites au cours de cette étude grâce à l'aide des collègues au NERC Turku. Les caractéristiques thermiques et propriétés des quatre déchets solides industriels ainsi que la performance des deux installations sont examinés à travers des expérimentations. Une simulation par dynamique des fluides numériques est réalisée pour examiner le système de récupération de chaleur utilisant les déchets de poudres métalliques comme matériaux pour stockage thermique.

Le résultat démontre que l'utilisation du système de récupération de chaleur en tant qu'un système ouvert avec une température de chauffage plus élevée et un plus court temps de chauffage est la plus idéale configuration. Concernant l'étude sur le système de stockage thermique, le béton concassé a une meilleure performance en tant qu'un matériel pour le stockage thermique, suivi par le laitier et la cendre volante.

Mots-clés : stockage d'énergie thermique, stockage de chaleur sensible, déchets solides industriels, récupération de chaleur, déchets de poudres métalliques, béton concassé, laitier, cendre volante

Table of Contents

List of Symbols and Abbreviations

Symbols

Q	energy
W	work done
$\dot{m}$	mass flow rate
C_p	specific heat capacity
T	temperature
t	time
η	efficiency
r	ratio
$\dot{V}$	volume flow rate
x	position across a surface
z	position along a depth

Greek

ω	moisture content
ρ	density
λ	thermal conductivity

Abbreviations

TES	Thermal energy storage
ISW	Industrial solid waste
SHS	Sensible heat storage
EST	Energy storage technology
HTF	Heat transfer fluid
CSP	Concentrated solar power
MSWI	Municipal solid waste incineration
FA	fly ash
CC	crushed concrete

1. Introduction

1.1 Background

High energy demand is an evident trait of this modern era of industrialization and digitalization. The global energy consumption was estimated to be 146,000 terawatt hours (TWh) in 2015, which is approximately 25 times more than in 1800 [1]. Similarly, the world power consumption in 2008 was estimated at around 136,129TWh, while it was documented as 161,250TWh in 2018, showing an increase of 2.9% in the last decade. In the meanwhile, the constantly increasing energy consumption is causing serious environmental issues to the world which are mainly air pollution and global warming. Fig. 1 shows the global energy-related CO_2 emissions and their annual change from 1900 to 2023 according to the report from International Energy Agency (IEA) on the CO_2 emissions in 2023 [2].

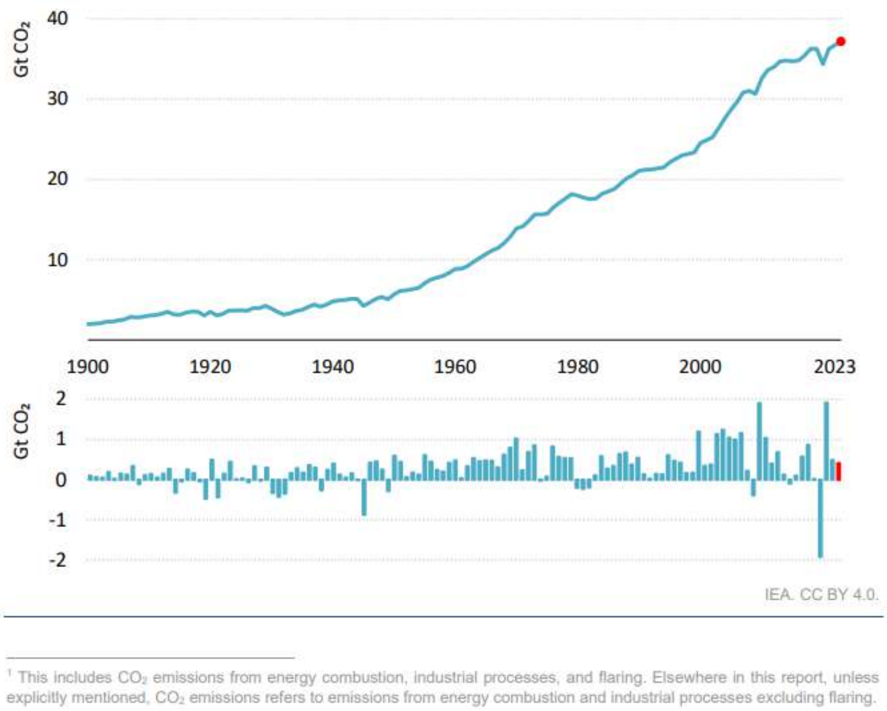

Figure 1. Global energy-related CO_2 emissions and their annual change in 1900 – 2023 [2]

37.4Gt of global CO_2 emissions are reached in 2023 and between 2019 and 2023, total energy-related emissions increased around 900Mt. According to the report, without the growing deployment of five key clean energy technologies since 2019 - solar PV, wind, nuclear, heat pumps, and electric cars - the emissions growth would have been three times larger. This illustrates the importance of clean and renewable energy as a technology capable of reducing global energy-related emissions.

Renewable energy such as solar and wind energy is a promising alternative for unsustainable fuel such as oil, natural gas and coal in terms of abundance and eco-friendliness. However, one of the main issues for renewable energy is the intermittency for energy production. The solution revolves around energy storage technology which can not only cover the mismatch between supply and demand of energy but improves the power quality stability and reliability. This makes energy storage technology one of the major components of renewable energy integration and decarbonization of world energy systems [3].

Energy storage technology can be classified into various categories, namely: electromechanical, mechanical, electromagnetic, thermodynamics, chemical and hybrid methods. Research and development have been done continuously during these years to develop energy storage technologies, which are low-cost, high efficiency and environmentally friendly.

Thermal (thermodynamics) energy storage remains as one of the principal energy storage technologies. It can be divided into three modes, namely sensible heat storage (SHS), latent heat storage (LHS) and thermochemical storage (TCS). Sensible heat storage (SHS) involves principles of increasing temperature of a medium and storing heats in liquids such as molten salts and in solids such as concrete blocks, rocks or sand-like particles. Latent heat storage (LHS) works on storing heat in a phase-change material that possesses large latent heat of phase change during melting of a solid to a liquid. Thermochemical storage (TCS) converts heat into chemical bonds, which is reversible and beneficial for long-term storage applications [8].

In recent years, with the focus on thermal energy storage (TES), the use of industrial solid waste (ISW) to develop thermal energy storage technology has attracted considerable attention because this innovative approach can not only address environmental risks and health hazards caused by industrial solid waste but also advances the energy storage technologies which is essential for the development of renewable energy. [4]

ISW-based TES materials offer a range of advantages over conventional TES materials. Firstly, the use of ISW can reduce the demand for raw materials required to build TES system, which helps to conserve natural resources while avoiding environmental degradation related to mining activities. Furthermore, the processing of ISWs into TES materials typically requires lower energy consumption than the extraction and refinement of conventional TES materials. Additionally, the use of ISWs, which are often solid waste of industrial processes, as TES materials avoids the necessity for costly disposal methods such as landfilling. The valorization of ISW also aligns with circular economy principles by transforming waste into valuable resources. Apart from that, ISW-based TES materials can significantly reduce the carbon footprint of energy storage technologies, as their production and processing generate fewer greenhouse gas emissions compared to conventional TES materials.

These advantages of ISW-based TES materials reaffirm the interest of New Energy Research Center (NERC) Turku in carrying out research activities on transforming ISW into TES materials which is the core of this study. Regarding the research activities on ISW-based TES materials, NERC Turku collaborated with two companies, namely: Suomen Erityisjäte Oy in Forssa, Finland and Pöytyän Koneistuspalvelu Oy in Riihikoski, Finland to work on two different projects of ISW-based TES (ULLEVI, RESINA).

Suomen Erityisjäte Oy, a company specializing in the treatment and recycling of municipal solid waste incineration (MSWI) bottom ash, contaminated materials and hazardous waste provides NERC Turku three different industrial wastes to be tested, which are crushed concrete, slag and fly ash. Meanwhile, Pöytyän Koneistuspalvelu Oy, a metal manufacturer specializing in the machining of medium and heavy parts provides NERC Turku one industrial waste to be tested which is waste metal powder.

1.2 Aim and scope

This work aims to carry out research to study the suitability of these four different industrial wastes to be used as materials for thermal energy storage. The crushed concrete, slag, fly ash and waste metal powder will be tested respectively as materials for sensible heat storage (SHS) installation and the general idea is to determine whether these materials can allow the SHS installation to store and release thermal energy with high efficiency. The metal powder will be tested as material for another SHS installation which serves as an installation for waste heat recovery and the general idea is to find out whether the metal powder can allow the SHS installation to recover and reuse waste heat with high efficiency. In order to evaluate the viability of the four ISWs in question to be used as materials for STES, this work highlights the following research questions:

- What is the efficiency of the SHS installations in question to charge and discharge thermal energy by employing respectively the four ISW in question?
- How will the four ISW in question behave during cycles of heating and cooling?
- How do the physical and thermal-physical properties of the four ISW in question affect their performance to store and release thermal energy? What are the main parameters for the four ISW in question that affect their performance on SHS installation?
- What are the recommendations for improving the efficiency of the SHS installation in question to charge and discharge thermal energy using respectively the four ISW in question?

This work is structured as follows. Chapter 2 introduces the background of the laboratory and the research group working on this research subject of ISW-based TES materials. Chapter 3 presents the current technologies of TES while focusing on the technology of TES using ISW through literature review. Chapter 4 describes the materials and experimental setup of this work. Chapter 5 presents the main results with detailed analysis while chapter 6 concludes and highlights the scientific relevance of this work as well as recommends ideas to further advance this research work.

2. Background of laboratory and research group

2.1 New Energy Research Center (NERC), Turku

The research mentioned in this report is being carried out in the New Energy Research Center (NERC) of Turku University of Applied Sciences in Turku, Finland. Turku University of Applied Sciences has a total of 39 research groups engaged in 5 different themes of research. Fig. 2 shows the list of all the research groups for the university. The study of ISW-based TES materials is being carried out in the New Energy Research group under the engineering field.

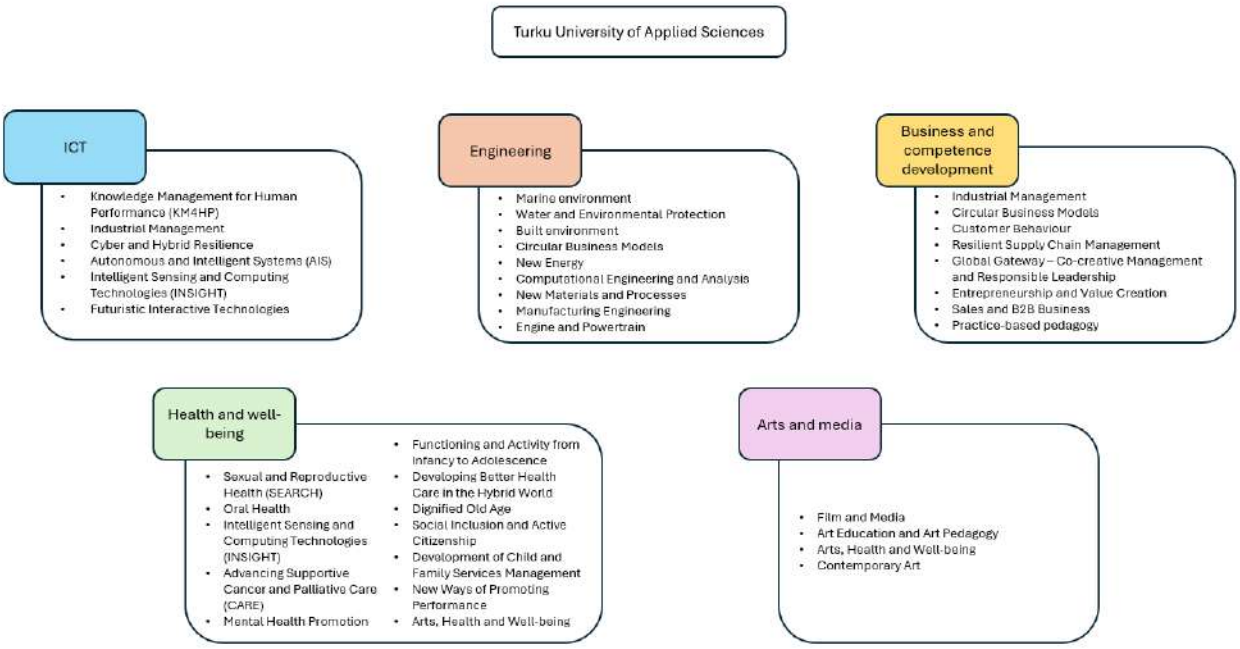

Figure 2. Research groups in different fields for Turku University of Applied Sciences

The NERC laboratory focuses its research on four core themes, namely: energy in its new ways of production, distributed energy systems, energy storages and sustainable mobility. The sustainable energy sources involved in the research include solar photovoltaic energy, wind energy hydro power and biomass. The laboratory focuses on the electrical form of energy distribution as well as on heat transfers. In the sustainable mobility research area, the team focuses on developing electric charging solutions and battery performance testing from e-bikes to e-buses. They promote activity mobility modes and public transport with simulation-based studies, hardware-in-the-loop based testing as well as impact and process evaluation of mobility measures. Concerning energy storage, the team works with storages in electrochemical, chemical and thermal form. This research focuses on energy storage in thermal form by using ISW provided by two partners of NERC laboratory in the energy storage research project.

3. Literature review

This chapter presents the state of the art in energy storage technologies (EST) with descriptions on the most commonly used energy storage technologies. The focus is then centered on thermal energy storage which is the core of this study. The second part of this chapter is dedicated to research and development related to thermal energy storage (TES) technologies coupled with valorization of industrial solid waste (ISW) as materials for heat storage.

3.1 State of the art in energy storage technology (EST)

Energy storage technology can be classified according to storage duration, response time, performance objective, type of energy stored and technology involved. Fig. 1A (in annexes) shows the classification of EST into 6 groups, namely: electrochemical, mechanical, electromagnetic, thermodynamics, chemical and hybrid [3].

Since each EST has unique characteristics in terms of efficiency, specific energy, cycle duration, self-discharge, etc., this allows the selection of suitable technology on a wide spectrum of EST based on desired application. Among the wide range of EST, the most commonly used ESTs are divided into mechanical, chemical, electrical and thermal energy storage according to the form of energy stored in the reservoir shown in the Fig. 2A (in annexes) [5-7].

Concerning thermal energy storage (TES) technology, although it has energy efficiency of around 14% to 18% which is a low value compared to other EST, one of its advantages is a rather high rated power of around 50MW to 250MW according to Fig. 3 [6].

Technology	Rated power (MW)	Specific energy (Wh/kg)	Energy efficiency (%)	Discharge at rated capacity (h)	Response time	Lifetime (cycles)	Self-discharge/day (%)
PHS	100–5000 [24], 1000–3000 [89]	0.5–1.5 [24]	65–75 [90], 75–80 [91]	1–24+ [24]	minutes [92]	>15,000 [65]	No [93], very small [65]
CAES	5–300 [24], 100–3000 [89], 50–350 [94]	30–60 [24]	41–75 [65]	1–24+ [24]	Seconds-minutes [92]	>10,000 [65]	No [93], small [65]
FES	0–0.25 [24], 0–1.65 [92], 0–10 [89]	10–30 [24], 5–80 [95]	85 [38], 80–90 [65]	0.000–0.01 [21]	<1 cycle [92]	104–107 [65]	100 [35,65]
Pb-A	0–20 [24], 0.05–10 [96], 0–40 [97]	35–50 [98], 30–50 [24]	70–80 [99], 75–80 [90]	1–5 [21]	<1/4 cycle [92]	250–1500 [65], 500–1000 [24]	<0.1 [35], 0.1 [100,101], 0.2 [102]
Li-ion	0–0.1 [24], 0.015–50 [103]	75–200 [24], 120–200 [104]	65–75 [65], 78 [105], 88 [106]	0.017–2+ [24]	<1/4 cycle [48]	600–1200 [65], <1000 [24]	1 [100], 5 [35]
Na-S	0.05–8 [24], 0.05–34 [107]	100 [108], 175 [109], 150–240 [24]	70–85 [65], 84–87 [35]	4–8 [21]	<1/4 cycle [48]	2500–4500 [65], 2500 [24]	No [110]
Ni-Cd	0–40 [24]	50–75 [24], 45–80 [98]	75 [21], 60–80 [65]	6–8 [111]	<1/4 cycle [48]	1500–3000 [65], 2000–2500 [24]	0.2 [101], 0.3 [35]
VRFB	0.03–3 [24], 12 [112]	25–35 [112], 10–30 [24]	60–75 [65], 75–85 [113]	2–12 [21]	<1/4 cycle [48]	>10,000 [65], >12,000 [24]	Small [65]
Zn-Br	0.05–2 [24]	70–90 [114], 75–85 [113]	65–75 [115], 75–85 [113]	2–5 [21]	<1/4 cycle [92]	1000–3650 [65], >2000 [24]	Very small [65]
Hydrogen	0–50 [24], 0.1–15 [38]	400–1000 [114]	35–40 [116], 42 [117]	12+ [21]	<1/4 cycle [92]	103–104 [65], >1000 [24]	0 [65]
Thermal	50–250 [83]	80–200 [24]	14–18 [118]	1–24+ [24]	–	5–15* [24]	0.05–1 [24]

* The unit is years.

Figure 3. Technical specifications of different energy storage technologies [6] (Refer to [6] for publications consulted to obtain the values given)

TES can be divided into three different categories, which are: sensible heat storage (SHS), latent heat storage (LHS) and thermochemical storage (TCS). This study focuses on SHS which has an advantage of having a large energy capacity while using inexpensive materials for thermal storage as shown in Fig. 4 [8].

	Sensible Heat Storage [5, 8-12]	**Latent Heat Storage** [5, 9, 10, 12, 13]	**Thermochemical Storage** [9, 11, 13]
Storage mechanism	Energy stored as temperature difference in solid (e.g., concrete, rock, sand) or liquid media (molten salt)	Energy stored using phase change materials (e.g., salts, metals, organics)	Energy stored in chemical bonds
Energy Density	• ~200 – 500 kJ/kg (for ~200 – 400 °C temperature differential)	• ~100 – 200 kJ/kg for nitrate salts; ~200 – 500 kJ/kg for metals; ~1000 kJ/kg for fluoride salts	• ~300 – 6,000 kJ/kg

Advantages	• Demonstrated large energy capacity (~GWh) • Inexpensive media • Solid media does not freeze and can achieve >1000°C	• Good for isothermal or low ΔT applications • Can provide large energy density with combined sensible and latent heat storage	• Large energy densities • Small heat losses • Potential for long-term storage • Compact storage system • Oxide TCES Stable at high temperatures (> 1000°C)
Challenges	• Requires insulation to mitigate heat losses • Lower energy density requires larger volumes • Molten salts freeze at ~200 °C.	• Potential for corrosion • For larger ΔT, may need cascaded systems (adds costs and complexity) • Low maturity	• Higher complexity • Low maturity • Higher capital costs • May require storage of gaseous products
Maturity	High	Low	Low
Cost	• ~$1/kg for molten salts and ceramic particles • ~$0.1/kg for rock and sands • ~$1/MJ – $10/MJ (system capital cost)	• ~$4/kg – $300/kg • ~$10/MJ – $100/MJ (system capital cost)	• ~$10/MJ – $100/MJ (system capital cost)

Figure 4. Summary of thermal storage technologies [8]

3.2 Thermal energy storage (TES) coupled with valorization of industrial solid waste (ISW)

There is a wide range of research and study on different types of ISW for thermal energy storage. Common types of ISW used for thermal storage include metallurgical slag such as blast furnace slag (BFS) and steel slag, coal fly ash (CFA), tailings and waste ceramics [4]. One example of ISW-based TES study investigates numerically the use of Electric Arc Furnace Black Slag (BS), Tundish (TN) from steel industry, as well as Demolition Waste (DW) from urban generation project as packed-bed TES materials at high temperature range [9]. A laboratory-scaled packed bed TES system which is suitable for concentrated solar power (CSP) plants is numerically analyzed with the purpose of storing heat between 290 and 565°C and molten solar salt is used as heat transfer fluid (HTF). Fig. 5 shows the design as well as the operational properties of the system.

The results revealed that all three materials have similar specific heat capacity, ranging from 0.99 to 1.14kJ/kg.K at 500°C. Tundish has the highest volumetric heat capacity at 3709.6kJ/m^3.K with 3342.2 kJ/m^3.K for black slag and 3104.5kJ/m^3.K for demolition waste. Tundish also stands out with its thermal conductivity (1.6 times higher than the others), energy storage capacity

(44.7kWh) and energy storage density (296kWh/m^3). Overall, all three materials are srong candidates for TES with molten salt as HTF, showing high efficiency in a range of 79.7-82.1%.

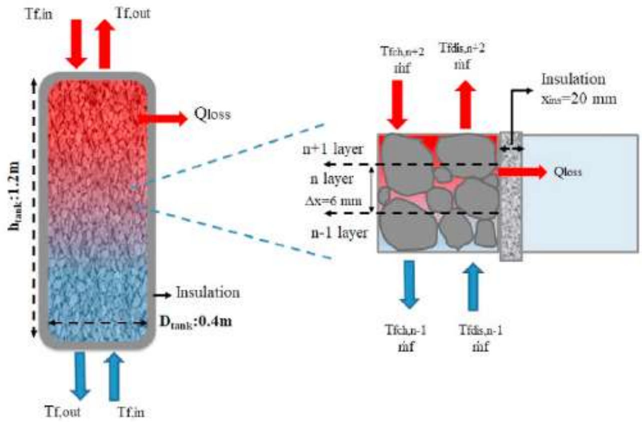

Properties	Value
Charging Temperature, T_{ch}, [°C]	290
Discharging Temperature, T_{dis} [°C]	565
Mass flow rate, $\dot{m}$, [kg/h]	100
Bed void fraction, ε, [%]	22
Diameter of storage tank, D_{tank} [m]	0.40
Height of storage tank, h_{tank} [m]	1.2
Tank Volume, V_{tank} [m^3]	0.15
Thickness of storage tank, x_{tank} [mm]	3
Thickness of insulation, x_{ins} [mm]	20
Thermal conductivity of insulation, k_{ins} [W/m°C]	0.06
Average packing material diameter, Ds [mm]	6
Mass of the storage tank, m_{comp} [kg]	40
Specific heat of the tank components, Cp_{comp} [kJ/kg°C]	0.460

Figure 5. Design and operational parameters for the TES system [9]

Another study works on the processing of demolition waste powder to become SHS material [10]. Fig. 6 shows the transformation of demolition waste (DW) sample to crushed DW powder with particle size below 1mm and finally the SHS material developed from DW powder consisting of 90% DW powder and 10% CEM I 52.5 White Portland Cement.

The study reveals that the SHS material developed from DW powder has a density of 2855kg/m^3 with a specific heat capacity of 1457J/kg.K. The SHS material developed is thermally stable up to 700°C with good physical and chemical properties and the cost of the SHS material is only at 0.001€/kg. According to the study, fine grain with an average particle size of 0.15μm is ideal to obtain low porous, high thermal conductivity and high density SHS materials by compressing and molding methods.

(a) (b) (c)

Figure 6. Images of (a) DW sample, (b) DW powder and (c) SHS material developed from DW powder [10]

A research carried out in France focuses on the use of recycled industrial ceramics made by vitrification of asbestos containing wastes (ACW) as TES materials for CSP plants [11]. The result demonstrates that ceramics obtained from vitrification of ACW are good candidates as high temperature thermal storage materials. They possess energy storage capacities

(2.5-3.2MJ/m^3.K) similar to synthetic high temperature ceramics, acceptable thermal conductivity (1.4W/m.K), low and consistent thermal expansion coefficient, very high thermal stability until 1200°C and very low raw commercial price (8€/tonne).

Another study working on a by-product from the steel industry performs a thermophysical characterization of two electric arc furnace (EAF) slag samples to investigate their suitability to be used as TES materials in medium and high temperature thermal energy storage systems [12]. Fig. 7 displays both raw EAF slag samples used in the study.

The study suggests EAF slag as a successful SHS material with a thermal conductivity of 1.41W/m.K, a specific heat capacity of 0.912 kJ/kg.K at 500 °C, a storage density of 256 kWh/m^3 and a price of 80€/tonne. Furthermore, the EAF slag remains thermally stable at a temperature up to 1100 °C which allows it to be used for different TES applications on a wide range of temperatures. This makes its implementation on the next generation CSP plants very attractive.

Figure 7. Pictures of both raw EAF slag samples, slag 1 on the left and slag 2 on the right [12]

Another study uses industrial solid waste steel slag as a supporting material to impregnate polyethylene glycol (PEG), sodium nitrate ($NaNO_3$) and sodium sulfate (Na_2SO_4) in order to create low, medium and high-temperature composite phase change materials (PCM) respectively for energy storage [13]. The research shows that the three PCMs are able to disperse uniformly in the pores of steel slag and they show a good chemical compatibility. Compared with their pure PCMs, the three PCMs impregnated within the steel slag shows an increase in thermal conductivity of 172%, 54.9% and 82.4% respectively with good phase change thermal storage properties. They also have good thermal reliability even after 100 thermal cycles, displaying their considerable application potential in different temperature areas such as building latent heat storage, solar energy storage systems and industrial waste heat recovery system. Fig. 8 presents the preparation process for the three steel slag-based composite PCMs (C-PCMs).

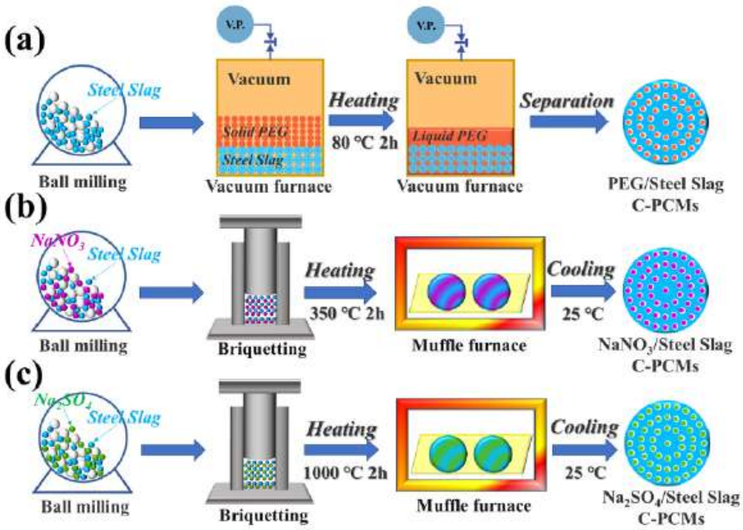

Figure 8. (a) PEG/steel slag C-PCMs, (b) $NaNO_3$/steel slag C-PCMs and (c) Na_2SO_4/steel slag C-PCMs [13]

This next research subject is not directly related to thermal energy storage. Nevertheless, this research reveals the potential of industrial solid waste in improving the geothermal heat pump system which is still closely related to the energy industry. In this study, three types of industrial waste, namely: waste steel slag, ground granulated blast furnace slag (GGBS) and waste glass powder are used to replace traditional backfill materials for ground source heat pump at varying mass fraction of 10%, 20%, 30% and 40% [14]. Fig. 9 shows the operational principle of a ground source heat pump with the use of backfill materials to connect the ground source heat pump to the soil, allowing heat extraction from the soil or heat releasing towards the soil. The three industrial wastes used to replace a portion of conventional backfill materials is shown also in Fig. 9.

Figure 9. Operational principle of ground source heat pump system and the three industrial wastes used [14]

The results show that this innovative approach is able to reduce the backfill costs by up to 5.61%-11.25% of the total borehole cost and it is expected to lower carbon emissions by up to 852.8 kg per ton of backfill material, promoting economic efficiency and environmental sustainability.

Another study about ISW-based TES uses steel slag and fly ash solid wastes to fabricate ceramics-based phase change composites (PCC) for application in thermal energy storage [15]. In this study, four samples of PCCs are prepared by encapsulating eutectic salts ($NaNO_3$-KNO_3) within pure fly ash; pure steel slag; a mixture of steel slag and fly ash; a mixture of steel slag, fly ash and kaolin. The results indicate that the steel slag-fly ash-kaolin based PCC presents excellent mechanical properties and good thermal cyclic stability with a thermal conductivity of 1.203 W/m.K. This shows the potential of steel slag and fly ash to be used as materials to fabricate low-cost PCC for application in TES system.

Once again, fly ash is being used in a research to develop electrothermal energy system for building heating by using self-heating ultra-high performance concrete (SES-UHPC) [16]. In this research, fly ash is being used as raw materials to fabricate SES-UHPC along with Portland cement, silica fume, quartz sand, water, water reducer admixture, paraffin, Al_2O_3 tubes and stainless steel wires (SSW). Due to its pozzolanic activity and large specific surface, fly ash can improve the heat storage capacity of the SES-UHPC while minimizing the thermal expansion-induced cracking. Fig. 10 shows the fabricating procedures of the SES-UHPC.

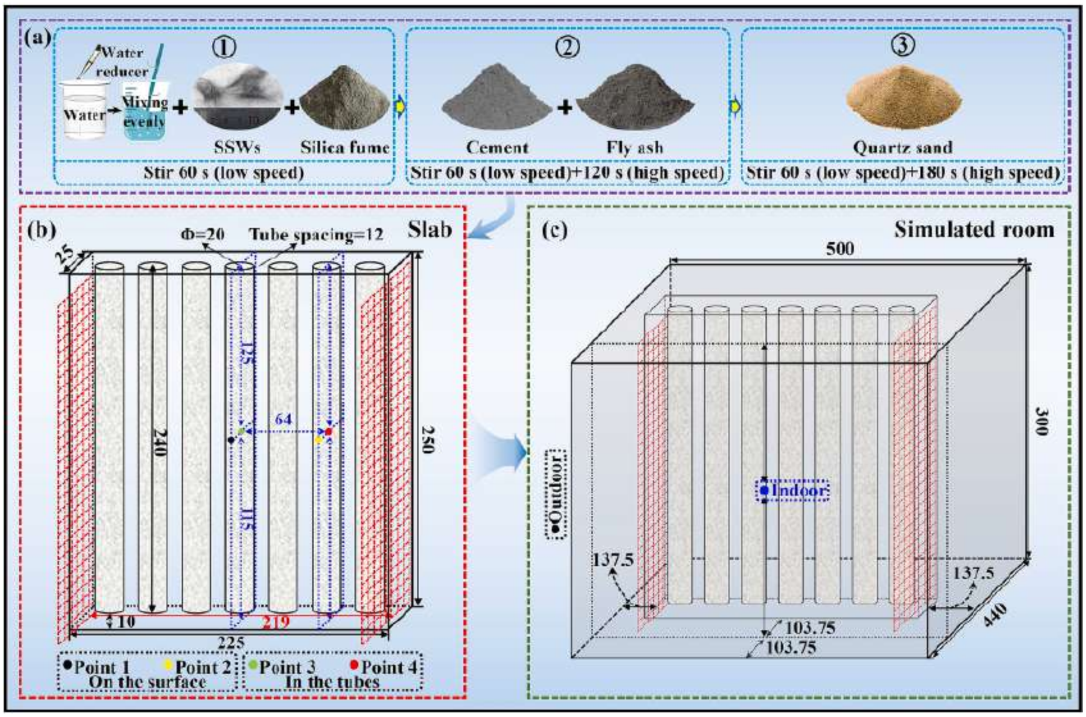

Figure 10. Fabricating procedures for SES-UHPC: (a) Mixing steps of the matrix, (b) Diagram of the SES-UHPC and (c) Diagram of the SES-UHPC in a simulated room for test (Unit: mm) [16]

The SES-UHPC fabricated demonstrates good electric thermal storage and building heating performances in the simulated environment. The SES-UHPC with 1.5 vol% of SSW and water/paraffin possess a heat supply time of 14.4/10.3h, with the outdoor temperature from -5 to -3°C and the wind speed up to 5.7m/s. According to the China's National Design standard for energy efficiency of residential buildings in severe cold and cold zones and the peak-valley time-of-use tariff policy, the use of SES-UHPC is expected to theoretically save 88.3 % of electricity tariff in an annual heat supply cycle. This illustrates the potential of SES-UHPC to be used as smart heating floors/walls in cold regions.

3.3 Current findings and shortcomings of research for sensible heat storage (SHS) using materials similar to this study

3.3.1 Fly ash

A study focusing on the use of industrial solid waste (ISW) in thermal energy storage has comprehensively examines the potential of ISW, including coal fly ash, red mud, sewage sludge, gypsum, metallurgical slag and waste concrete as TES materials [4]. This study reviews the latest research being done on TES using ISWs. Concerning the coal fly ash (CFA), the study mentions that Glosser et al. [17] has studied the sensible heat storage characteristics of different types of CFA through experiments with experimental principle shown in Fig. 11. The result concludes that if CFA is expected to be used for SHS, the total iron content of the sample should be greater than 5 % to ensure the efficiency of heat collection, which is an important selection criterion found for the use of CFA as TES materials. In another research by Agalit et al. [18] concerning physical properties of SHS of CFA, they found that the density of CFA (1.72g/m^3) is significantly lower than that of conventional high temperature SHS materials. Furthermore, they discovered that the mass decay of CFA occurs when it is heated to different temperature stages, which may be caused by incomplete oxidation of some carbon-containing components in the CFA. Therefore, it is recommended to calcine to at least 800 °C for CFA before using it as high temperature TES materials.

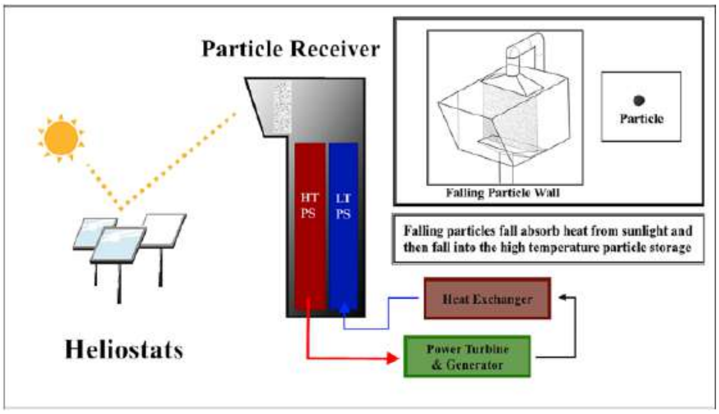

Figure 11. Working principle of CSP falling particle technology [17]

According to the research of Yin et al. [19], CFA tends to have an issue of low heat storage density (257.6kJ/kg) and specific heat capacity (0.92 kJ/kg.K). This is the main problem of CFA that may restrain the use of CFA for large-scale SHS.

3.3.2 Slag

Metallurgical slag such as steel slag and electric arc furnaces (EAF) slag has good thermal stability up to 1100°C. Therefore, they have great potential for commercial application in thermal energy storage [4]. A research work by Naimi et al. [20] has analyzed the chemical and thermal properties of 4 types of slag, namely: electric arc furnace (EAF) slag, ladle furnace (LF) slag, aluminium pot skimming (APS) and aluminium white doss (AWD) shown in Fig. 12. The four sample slags are inexpensive and widely available. The results show that there is no hazardous contents within the four slags. Among the four samples, EAF slag, LF slag and AWD remains thermally stable up to 1100°C with slight mass changes at the first thermal cycle. On the other hand, APS containing mainly carbon is degrading at high temperatures and thus it is not suitable for high-temperature TES applications. The study also concludes that most of the metallurgical industry waste produced globally can be used as high-temperature TES applications because they contain principally stable metal oxides except the ones rich in carbon dust such as APS.

Figure 12. Raw samples of slag received [20]

Agalit et al. [21] conducted a thermophysical and chemical characterization of induction furnace slags for high-temperature TES in solar tower plants. There are various type of slags depending on the employed furnace technology but they consist mainly silica (SiO_2), lime (CaO), alumina (Al_2O_3), iron oxides (Fe_2O_3) and magnesia (MgO). The induction furnace slag presented in this study is a by-product or waste generated by induction furnace while melting ferrous metal scrap and fluxes to produce steel or cast iron. Fig 13. shows the origin of induction furnace slag through the metal-making process. They are mainly composed of a non-metallic part and a small metallic part. The result reveals that they have a good specific heat capacity (700J/kg.K) and a good bilk density (2583kg/m^3). They are thermally stable up to 1000°C as well which makes them good materials for high TES application.

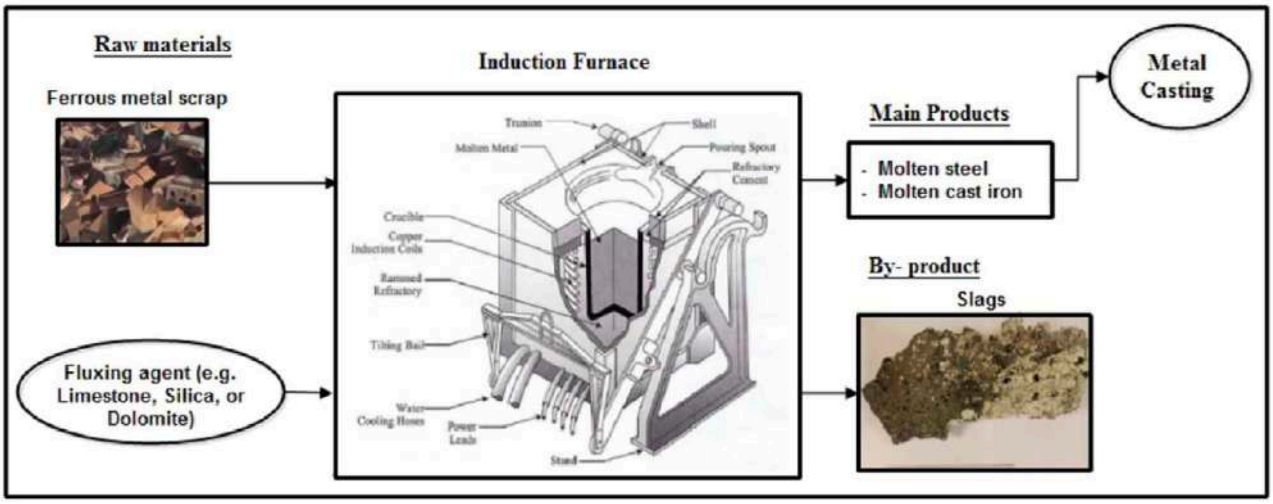

Figure 13. Metal production prcoess along with by-product, induction furnace slag [21]

Another research by Wang et al. [22] worked on two EAF slag samples from China and Spain respectively. The research indicates that the EAF slag from China has a specific heat capacity of 0.717-0.975kJ/kg.K from room temperature to 500°C while the EAF slag from Spain has a specific heat capacity of 0.713-0.858kJ/kg.K from room temperature to 500°C. Both slags shows a quasi-constant thermal conductivity of 1,7W/m.K in the test temperature and they exhibit excellent wear resistance, indicating their suitability as TES materials.

3.3.3 Waste concrete

The production of waste concrete comes mainly from the waste aggregate of construction solid waste. The waste concrete can still store heat after being crushed. Martin-kauppi et al. [23] worked on various waste aggregate and it was found that the specific heat of most samples was between 700-850J/kg.K. which was a good sign of their suitability as TES materials. Wongsa et al. [24] discovered that the thermal conductivity of clay brick recycled concrete was only 30% of that of ordinary concrete. According to the study of Lu et al. [25], the increase of water-cement ratio will lead to a decrease of thermal conductivity of recycled concrete. While having the same replacement rate of waste aggregate, the thermal conductivity of recycled concrete with water-cement ratio of 0.35 is 1.652W/m.K while that of recycled concrete with water-cement ratio of 0.55 is 1.478W/m.K with a decrease of 10.5% in thermal conductivity. Another research working on the thermal conductivity of concrete by Xiao et al. [26] revealed that the dry/wet state of sample had the greatest influence on the thermal conductivity of concrete. This reaffirms the influence of water content of concrete on its thermal conductivity. The other factors such as replacement rate of waste coarse aggregate, temperature, aggregate volume fraction, aggregate type, steel bar volume fraction, water-cement ratio and type of admixture had successively decreased impact on thermal conductivity. A study of Ding et al. [27] analyzed and simulated the relationship between porosity and thermal conductivity of foamed concrete through MATLAB and COMSOL software. It is discovered that the porosity and thermal conductivity were negatively corelated and the porosity would change the internal heat transfer path of concrete.

3.3.4 Shortcomings of research

Most of the current research on CFA focuses on the selection of the optimal CFA or the analysis of influence of proportions of each element on its properties. Few studies work on the analysis and prediction of properties of CFA by computer simulation. Although this study does not work on the analysis and prediction of properties of fly ash by computer simulation, this subject is being investigated based on the experiments carried out which helps to advance the understanding of properties of fly ash related to TES.

Concerning slag, most of the studies focuses on EAF slag and steel slag with few attentions on other type of slag. Research carried out on other slags can possibly widens the options of slag available for TES application which helps to valorize a wider range of slag. This is exactly the interest of this study as other type of slags are studied and analyzed to investigate their suitability as TES materials. Concerning waste metal powder, no research on TES using the exact same type of metal powder has been found at the moment but the waste metal powder remains similar to slags such as EAF slag and steel slag as they are all metal wastes.

On the other hand, current studies on concrete focuses mainly on the factors effecting the thermal conductivity of waste concrete through experiment and numerical simulations. However, long-term stability and thermal cycling performance of waste concrete as TES materials remain underexplored. This is exactly the interest of this study to fill the notable research gap related to the thermal stability and thermal cycling performance of waste concrete through experiment.

4. Materials and experimental setup

This chapter presents firstly the four different industrial wastes tested, namely: crushed concrete, slag, fly ash and metal powder which are obtained through the collaboration between NERC Turku and Suomen Erityisjäte Oy as well as Pöytyän Koneistuspalvelu Oy. The second part of this chapter discusses the experimental setup for different tests to study and analysis the characteristics of the materials.

4.1 Material descriptions

Suomen Erityisjäte Oy receives and processes wastes from Kiimassuo Waste Center owned by Loimi-Hämeen Jätehuolto Oy (LHJ). The crushed concrete, slag and flag ash tested are wastes collected at Kiimassuo Waste Center and they have been used as samples in this study. Fig. 14 shows the crushed concrete, slag and fly ash collected and packed by the company.

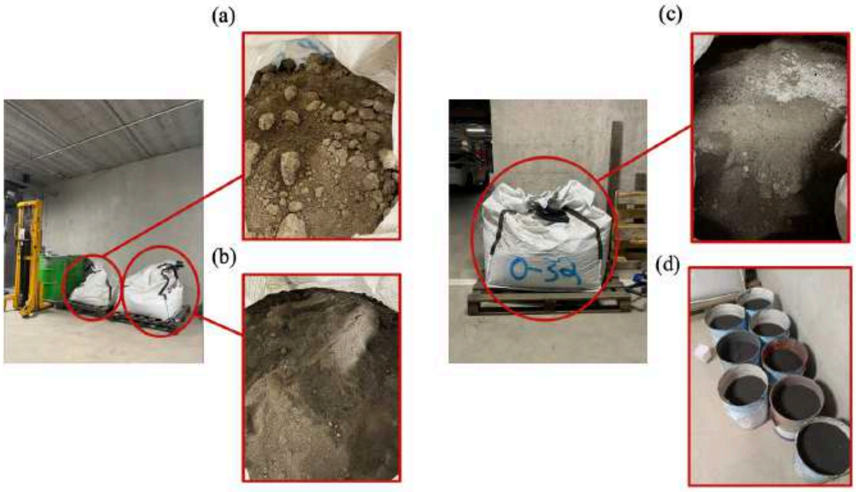

Figure 14. Industrial solid waste: (a) crushed concrete, (b) fly ash, (c) slag and (d) waste metal powder

The sample of crushed concrete is mainly comprised of crushed concrete and stone which can be construction or demolition waste. The sample of slag is waste produced by peats and wood combustion and it has been treated to remove its mineral contents in order to use the recovered valuable minerals for other purpose. The source of peats and wood combusted is unclear, but they are probably a part of biomass resources used to produce heat and electricity in Finland. The sample of fly ash is municipal solid waste incineration (MSWI) fly ash, which is the waste left after incineration of common household, commercial and institutional solid waste.

On the other hand, Pöytyän Koneistuspalvelu Oy providing a wide range of services such as core drilling, milling, turning, etc. generates metal waste during those services. The waste metal powder provided for this study is waste produced from lathe, a machine used for shaping metals. Fig. 14 shows the buckets of waste metal powder provided for this study.

4.2 Experimental setup

A total of six experiments or tests has been done to examine and analyze the thermophysical characteristics of the four industrial solid waste (ISW) provided. Two thermal energy storage (TES) installations have been built during this study before the tests are conducted. This chapter presents the experimental and installation setup as well as the methodology for each test.

4.2.1 Sieve test

The sieve test is carried out for two purposes: (i) examine the moisture content and (ii) investigate the particle size distribution of the ISWs. The sieve test for crushed concrete, slag and fly ash is done by following the SFS-EN 933-1 Finnish standard. The sieve test for waste metal powder follows the same procedure as well but with a simplified version. Fig. 15 illustrates the samples collected for the ISWs to be tested. The samples are collected randomly within the large volume of raw materials to avoid inaccuracy in the test.

(a) (b) (c)

Figure 15. (a) Crushed concrete, (b)slag and (c) fly ash collected for sieve test (without photo for waste metal powder)

4 samples are prepared for each material to ensure the repeatability and accuracy of the experiment carried out (except only 1 sample tested for waste metal powder). Fig. 16 shows the procedure for the sieve test. The prepared samples are firstly heated up in an oven at 105°C for over 16 hours to dry them. The mass of each sample is weighed before and after heating. The mass difference for the samples before and after heating designates the mass of water content for each sample. The moisture content is then calculated by equation 1:

$$\omega = \frac{m_{water}}{m_{sample\_dried}} \quad (1)$$

This method for the determination of moisture content does not take into consideration the amount of chemically bound water within the samples as the heating temperature of 105°C is not enough to break the chemical bond within the samples which contains water.

After the heating process, the samples are poured into a multilayer sieve which has different sizes of square aperture ranging from 32mm to 0.063mm. Fig. 17 shows the 10 layers of sieve used for the test. 10 layers starting from 32mm to 0.063mm have been used for crushed concrete and slag, 9 layers starting from 16mm to 0.063mm have been used for fly ash while 6 layers starting from 2mm to 0.063mm have been used for waste metal powder. The sieve is put into a shaker which shakes continuously the samples for 10 mins of sieving process. The sample retained by each layer of sieve is weighed and recorded, allowing the determination of particle size distribution for waste metal powder.

In summary, the sieve test for crushed concrete, slag and fly ash consists of: weighing the sample before heating, heating at 105°C for over 16 hours to dry the sample, weighing the sample after heating, sieving by a shaker and weighing the sample retain by each layer of sieve. The sieve test for waste metal powder follows the same procedure but without the first 2 steps (weighing before heating and heating process) because the metal powder received for this study is dry without much moisture which is justified in the Chapter 5 (*Section 5.2*).

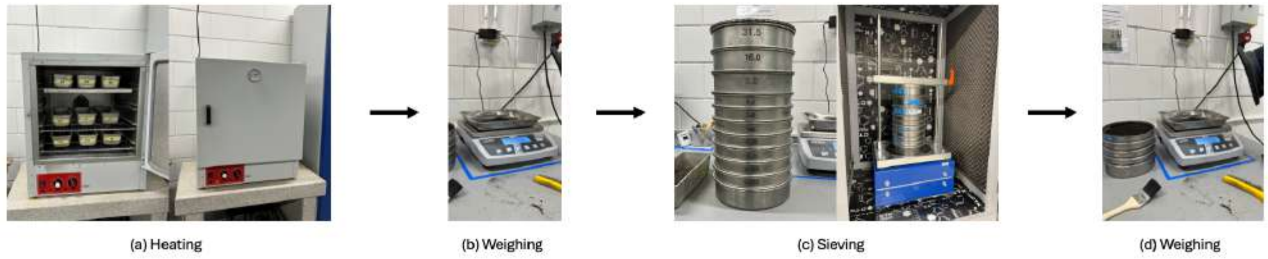

Figure 16. Procedures for sieve test according to the SFS-EN 993-1 standard

Figure 17. 10 layers of sieve with different aperture size

4.2.2 Thermogravimetric analysis (TGA)

The thermogravimetric test (TGA) is being done to examine the thermal stability of the samples from 50°C up to 950°C and to determine the thermal decomposition temperature of the samples in case where the samples decompose during the heating process. PerkinElmer TGA4000 is being used in a nitrogen environment (20 mL/min for nitrogen) to perform the TGA analysis. Fig. 18 shows the device used for TGA connected with the nitrogen tank and cooler.

After inserting the sample in the device, it is first being heated up until 50°C which the temperature will be held for 1 min. The heating then continues from 50°C until 950°C with a heating rate of 40°C/min.

Raw samples and thermally treated samples are tested respectively for each ISW to examine the samples with and without moisture. The thermal treatment refers to heating of samples in an oven at 105°C for over 16 hours to dry them. Fig 3A (in annexes) shows the samples prepared for TGA.

Figure 18. PerkinElmer TGA4000 with nitrogen tank and cooler

4.2.3 Thermal energy storage (TES) installation for metal powder: Waste heat recovery system

The waste metal powder is being used as a TES material within a waste heat recovery system connected to a sauna heater. A typical traditional Finnish sauna operates between 65°C and 90°C and the hot air of sauna room is often emitted to exterior without measures to store the high thermal energy of the air. Hence the idea is to create a heat recovery system that can collect thermal energy of hot air heated by sauna heater before releasing it to the exterior by using the waste metal powder. The type of TES involved for the waste heat recovery system is low-temperature sensible heat storage (SHS) as no phase change materials (PCM) are used and the temperature for heating is under 90°C which does not cause the melting of metal powder.

A barrel provided by Pöytyän Koneistuspalvelu Oy is used as the container for raw waste metal powder to store thermal energy released by the sauna heater. Fig 19 shows the schematic diagram of the waste heat recovery system. The sauna heater used in this study is Harvia KIP60 with a heating power of 6kW and it is filled with stones during the test as supposed to how it is used in real life. The barrel has 3 sections (top, middle and bottom section) with metal plates separating each section and only the middle section can be filled by waste metal powder as shown in Fig. 4A (in annexes). Hence only the middle part of the barrel is being filled by waste metal powder and approximately 230 kg of waste metal powder is used to fill the section. 3 temperature sensors (PT1000), which are aligned vertically, are placed in the middle section of the barrel as shown in Fig. 19 to measure the temperature of the metal powder during the tests. The homogeneity of temperature within the waste metal powder is examined also during the tests. The closed and sealed barrel is then connected to the sauna heater through a network of ventilation duct with a fan, a flow meter and a temperature regulator within the system to create an airtight and closed-loop airflow within the heat recovery system. The whole system is being insulated by ISOVER mineral wool insulation layer to minimize heat loss.

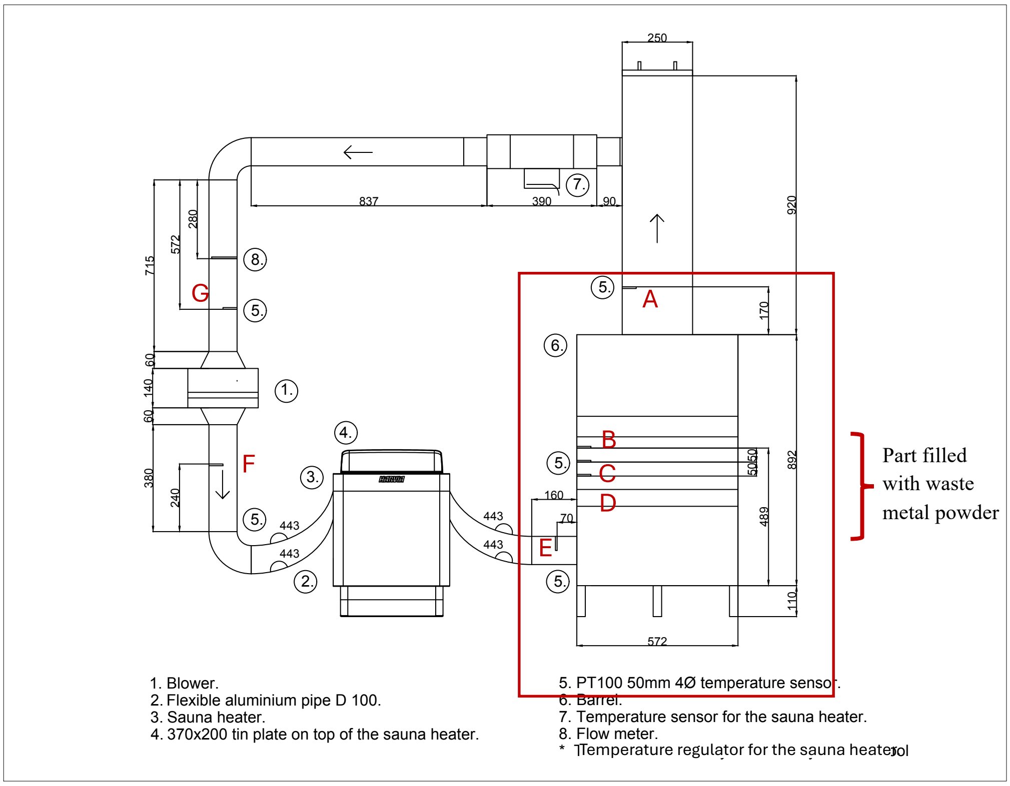

Figure 19. Schematic diagram of the waste heat recovery system (unit in mm)

A total of 7 PT1000 is placed inside the system at different position (refer to Fig. 19) to monitor the temperature at different positions. A flowmeter is also installed after the fan to measure the airflow of the system. Fig 20. illustrates the complete installation setup for the heat recovery system. In order to monitor the temperature measured by the PT1000 installed, the temperature sensors are connected to an automation unit with CentraLine NX data logger software of Honeywell Control Systems Ltd. (software shown in Fig. 5A in annexes). Cable connections have been made as shown in Fig. 6A in annexes to connect the temperature sensors with the automation unit to be able to use the data logger software.

Heating and cooling tests are then being performed to monitor the temperature evolution at different positions of the system, especially those within the waste metal powder throughout the tests. The total energy stored and released by the metal powder during the tests is determined by equation 2 and 3:

$$Heating:\ Q_{stored} = -\int_{t=0s}^{t_{final}} \dot{m}_{air} C_{p,air}\left(T_{air,exit} - T_{air,entrance}\right)dt \quad (2)$$

$$Cooling:\ Q_{released} = \int_{t=0s}^{t_{final}} \dot{m}_{air} C_{p,air}\left(T_{air,exit} - T_{air,entrance}\right)dt \quad (3)$$

It is assumed that there is no heat loss from the system towards the exterior since the system is totally insulated.

The efficiency of waste metal powder to store and release heat, also known as charge and discharge efficiency, the ratio between energy stored and expected energy stored as well as the cycle efficiency are calculated with equation 4 - 7:

$$\eta_{charge} = \frac{Q_{stored}}{W_{heater}} \quad (4)$$

$$\eta_{discharge} = \frac{Q_{released}}{W_{heater}} \quad (5)$$

$$r_{real/ideal} = \frac{Q_{stored}}{Q_{stored\_ideal}} \quad (6)$$

$$\eta_{cycle} = \frac{Q_{released}}{Q_{stored}}\ with\ t_{heating} = t_{cooling} \quad (7)$$

(a) (b)

Figure 20. Complete waste heat recovery system with (a) automation unit and (b) sauna heater with filled barrel (red arrows indicating the direction of airflow)

The thermal stability of the heat recovery system is examined during the test to study the thermal stability of the waste metal powder during heating and cooling process while ensuring that the system works well without encountering overheating issues for the sauna heater and fan.

4.2.4 Thermal energy storage (TES) installation for crushed concrete, slag and fly ash

The thermal energy storage installation built is a low-temperature sensible heat storage (SHS) installation without the use of phase change materials (PCM). Raw crushed concrete, slag and fly ash are stored respectively in a hollow barrel to build a TES installation for each ISW. Fig. 21 shows the schematic diagram of the thermal energy system. 10 temperature sensors PT1000 are placed inside the barrel to measure temperature at different positions, and the temperature sensors are connected to the automation unit shown in Fig. 20 for temperature acquisition. The PT1000 in the barrel are held by parts that are designed and 3D-printed. The 3D-printed parts then are supported by a wooden stick placed in the middle of the barrel to fix its positions as well as the positions of the temperature sensors. AutoCAD Fusion360 is used to design the 3D-printed parts as shown in Fig. 7A (in annexes). A water pipe is added inside the barrel with support by the middle wooden stick, allowing the barrel to have liquid circulation going in and out of the barrel which acts as a heat transfer fluid (HTF). Temperature sensors have been added for the liquid circulation just before entering and just after exiting the barrel to observe the temperature difference during tests.

The barrel completely filled with ISW, and with temperature sensors and water piped added is insulated by ISOVER mineral wool insulation layer to minimize heat loss during the tests. It is assumed that there is no heat loss from the system towards the exterior with the insulation layer installed. The barrel is connected to a circuit with 30 wt% ethanol and 70 wt% water as heat transfer fluid (HTF). A Sunamp Thermino 150 xPlus heater with a power of 2.8 kW is connected to the circuit for heating purpose and an Oilon heat pump (model Cube Inverter+ 3-12 03) with a power of 2.45kW is connected as well to the circuit for cooling purpose. Fig 22. shows the complete installation setup for one of the thermal energy storage systems built.

Heating tests (charge) and cooling tests (discharge) are performed for each barrel filled by crushed concrete, slag and fly ash respectively to investigate the temperature evolution of the ISW throughout the tests. The total energy stored and released by the ISW during the tests is calculated by equation 8 and 9:

$$Heating: \; Q_{stored} = -\int_{t=0s}^{t_{final}} \dot{m}_{HTF} C_{p,HTF} \left(T_{HTF,exit} - T_{HTF,entrance}\right) dt \quad (8)$$

$$Cooling: \; Q_{released} = \int_{t=0s}^{t_{final}} \dot{m}_{HTF} C_{p,HTF} \left(T_{HTF,exit} - T_{HTF,entrance}\right) dt \quad (9)$$

The charge and discharge efficiency, ratio between energy stored and expected energy stored as well as the cycle efficiency are calculated as well by equation 4, 6, 7 and 10:

$$\eta_{discharge} = \frac{Q_{released}}{W_{heat\,pump}} \quad (10)$$

The thermal stability of the ISW and the homogeneity of temperature within the barrel during the heating and cooling tests are examined and analysed to study the thermal characteristics of the ISWs tested.

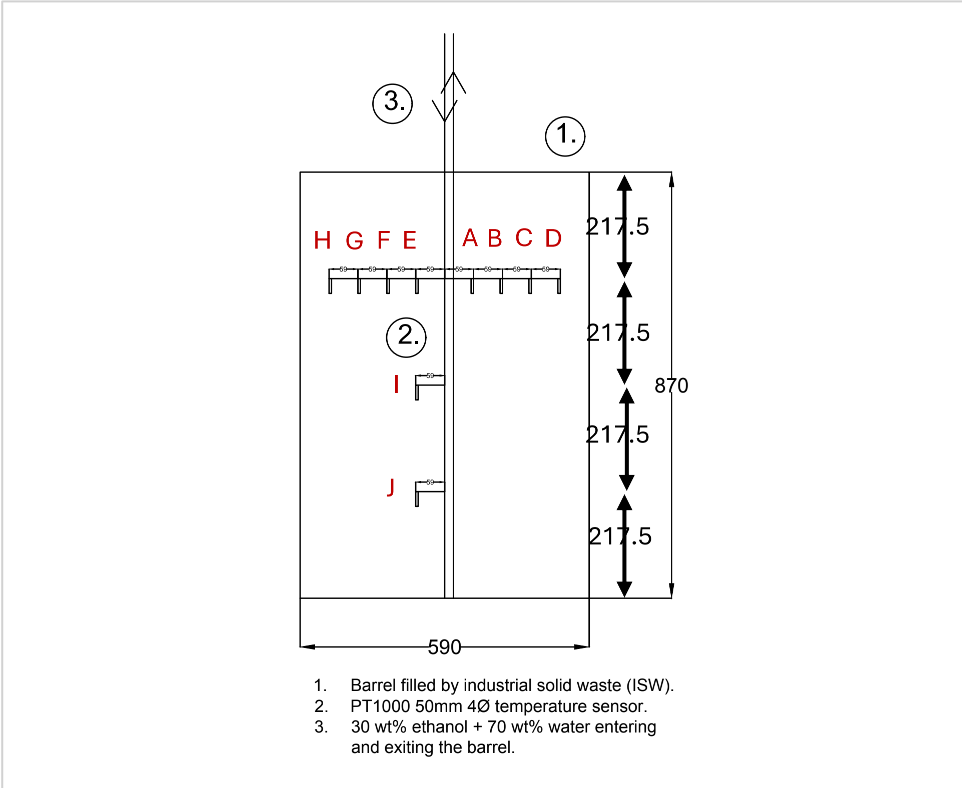

Figure 21. Schematic diagram of the thermal energy storage (TES) system (unit in mm) (distace between the 4 PT1000 adjacent to the middle stick = 59mm and distance between each PT1000 = 59mm)

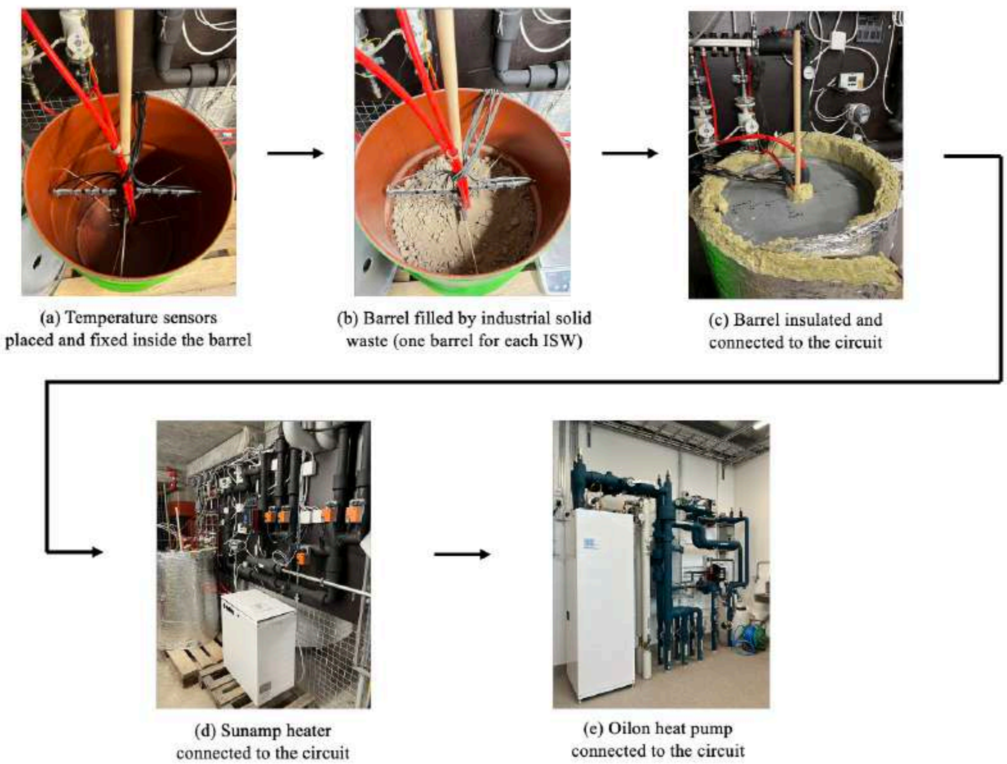

Figure 22. Complete installation setup for the thermal energy storage (TES) system

4.2.5 Computational fluid dynamic (CFD) simulation for the waste heat recovery system

Ansys simulation software is used to simulate the heating and cooling tests for the waste heat recovery system equipped with waste metal powder. Ansys Discovery is first used to draw the geometry of the system. Only the barrel filled with waste metal powder as well as the entrance and exit of the ventilation duct for the barrel is drawn using the software with the main objective to study the temperature evolution of the heat recovery system specifically at the entrance and exit of the barrel as well as within the barrel. Once the geometry is drawn, the fluid volume of the system, which is the volume taken into consideration for simulation, is extracted from the geometry. Air passes through the section of the barrel filled by waste metal powder because it is considered as porous zone which allows the air circulation a supposed to what is in real situation. The intersection of the air and the waste metal powder is then connected for the fluid volume extracted, allowing the software to know that the air and waste metal powder is adjacent at the intersection selected. Fig 23. shows the preparation of the geometry at Ansys Discovery.

The prepared geometry is imported into Ansys fluent for simulation. Fig 24 shows the geometry imported into Ansys fluent. Several assumptions have been made for the simulations which are:

- The heat recovery system is considered as adiabatic with no heat loss towards exterior.
- The metal powder inside the barrel is considered as steel powder with $\rho = 8030 kg/m^3$, $C_p = 502.48 J/kg.K$ and $\lambda = 16.27 W/m.K$ for the simulation.
- The airflow used in the simulation is the optimal airflow of the fan ($\dot{V} = 38 L/s$).
- The air entering the barrel during the heating process is supposed to be at 333 K assuming the sauna heater is heating up the air until 333 K and keeping the temperature constant throughout the test. The air entering the barrel during the cooling process is supposed to be at 300 K to cool down the barrel.

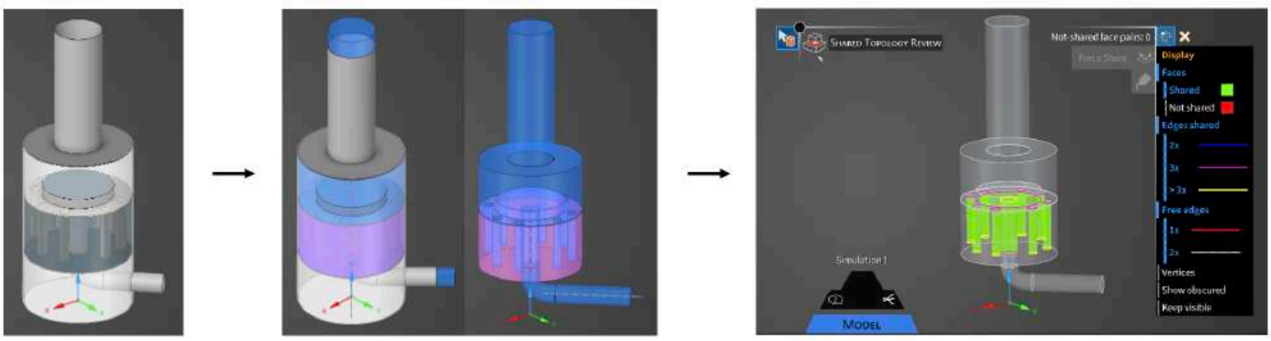

(a) Geometry drawn for the system

(b) Fluid volume extracted within the geometry

(c) Intersection of the air and waste metal powder connected

Figure 23. Preparation of geometry on Ansys Discovery for simulation

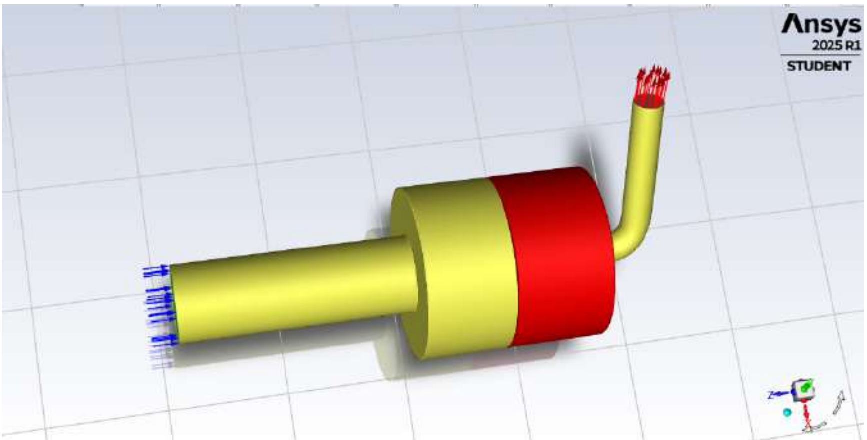

Figure 24. Geometry imported to Ansys fluent for simulation

5. Results and analysis

This chapter presents the obtained results of each test performed as well as its analysis to examine and study the thermal characteristics and performance of the four industrial solid wastes (ISW) tested.

5.1 Sieve test

5.1.1 Water content of the ISW samples

The first part of the sieve test performed (weighing and heating) allows the determination of water content for crushed concrete, slag and fly ash. Table 1 shows the water content for each sample of crushed concrete, slag and fly ash. There is no water content measurement for waste metal powder since the material is dry. It can be observed that the water content of fly ash is the highest, followed by slag and crushed concrete.

Water content (%)	Crushed concrete	Slag	Fly ash
Sample 1	7.19	13.67	39.94
Sample 2	5.11	14.21	40.39
Sample 3	7.12	14.61	40.35
Sample 4	7.26	14.23	48.82
Average	6.67	14.18	42.38

Table 1. Water content measurements for crushed concrete, slag and fly ash

The water content of fly ash corresponds well to the value found in the literature which is between 11 - 53% [28]. The MSWI fly ash mainly consists of lightweight and very fine particles, allowing it to have a large surface area. The large surface area allows fly ash to absorb water easily which can be the cause for its high water content. Apart from that, since MSWI fly ash is the waste produced from the incineration of municipal solid waste which may contain food scraps, plastics, chemicals and other materials, it is possible that the incineration and cooling of municipal solid waste can produce compounds such as chloride salts (calcium chloride) which is highly hygroscopic, indicating its ability to absorb moisture from the atmosphere. Sulfate salts such as calcium sulfate can be produced as well, which is another hygroscopic compound capable of binding water and absorbing moisture from the atmosphere. With the possibility of containing these substances within MSWI fly ash, it is highly possible for MSWI fly ash to have high water content.

The water content of slag is ranked second among the ISW. As the minerals content of slag is being removed, the main composition of slag is probably carbonaceous char or biochar. This type of substance is porous, allowing it to have a large surface area. The surface of this substance contains chemical groups that can attract and hold water molecules. Hence slag is basically porous and hydrophilic, allowing it to absorb moisture from atmosphere as well.

The crushed concrete is non-hygroscopic and only holds free surface moisture. Unlike MSWI fly ash and slag, crushed concrete and stones are inert, and they do not absorb moisture from the atmosphere. The water content of crushed concrete basically comes from water adhering to its surface or water trapped between the pores of the crushed concrete. Hence it is relevant for crushed concrete to have a lower water content. The water content of crushed concrete found aligns well with the literature which is between 3 and 8% [29-30].

On the other hand, although the water content of waste metal powder is not measured, it is assumed to have the lowest water content among the four ISWs. This is because the material is dense, non-porous and it probably does not absorb moisture from the atmosphere. Hence it has a lowest water content among the four ISWs as shown in the Section 5.2.

Fig. 25 illustrates the crushed concrete, slag and fly ash before and after heating. It can be noticed that the colour of all samples approaches grey colour after heating, indicating that the samples have been dried successfully. There is no major change visually for the samples apart from the colour change.

(a) Raw crushed concrete

(d) Heated crushed concrete

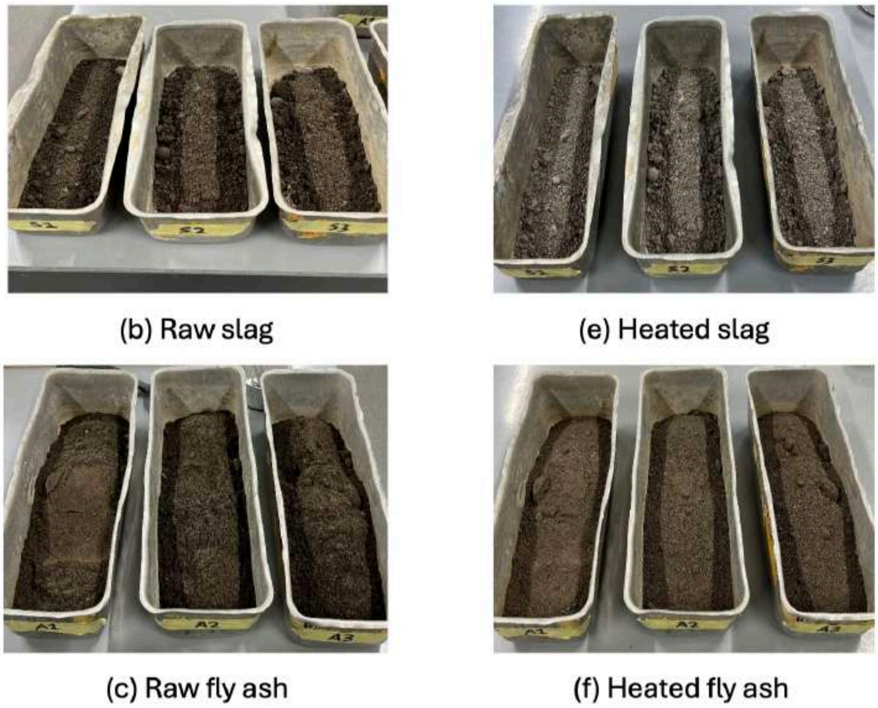

Figure 25. Samples before and after heating

5.1.2 Particle size distribution of the ISW samples

After measuring the mass of sample retained by each layer of sieves, the particle size of each ISW is determined by calculating: (i) mean, (ii) median, (iii) mode, (iv) 10th percentile and (v) 90th percentile for the particle size of the materials. Table 2 shows the value obtained from four sieve tests for each material respectively, except for waste metal powder with only one sieve test.

Crushed concrete	Mean (mm)	Median (mm)	Mode (mm)	D10 (mm)	D90 (mm)
CC1	8.69	5.32	[16, 32]	0.5	32
CC2	13.86	14.05	[16, 32]	1	32
CC3	8.14	3.61	[16, 32]	0.25	32
CC4	11.90	4.73	[8,16]	0.5	64
Average	10.64	6.93	[16, 32]	0.5	40

Slag	Mean (mm)	Median (mm)	Mode (mm)	D10 (mm)	D90 (mm)
S1	4.81	2.62	[2, 4]	0.25	16
S2	4.04	2.23	[4, 8]	0.25	16
S3	5.22	2.32	[2, 4]	0.25	16
S4	6.26	3.16	[4, 8]	0.25	32
Average	5.08	2.58	[4, 8]	0.25	20

Fly ash	Mean (mm)	Median (mm)	Mode (mm)	D10 (mm)	D90 (mm)
FA1	0.28	0.13	< 0.063	0.063	1
FA2	0.27	0.13	< 0.063	0.063	1
FA3	0.27	0.13	< 0.063	0.063	1
FA4	0.40	0.16	< 0.063	0.063	1
Average	0.31	0.14	< 0.063	0.063	1

Waste metal powder	Mean (mm)	Median (mm)	Mode (mm)	D10 (mm)	D90 (mm)
M1	0.41	0.35	[0.25, 0.50]	0.125	1

Table 2. Value obtained for each industrial solid waste (ISW) from four sieve tests

Crushed concrete has the largest average particle size of 10.64mm; 50% of the material has a particle size larger than 6.93mm; most of the crushed concrete has a particle size in the range of 16 to 32mm; 10% of the material is smaller than 0.5mm and 90% of the material is smaller than 40mm. It can be noticed that the difference between each mean and median found for crushed concrete is the most significant among the four ISWs, indicating that the material itself is not homogeneous as the value obtained for each samples differs a lot. This can be observed as well in Fig. 25 that the raw material of crushed concrete contains rocks and grains of concrete with noticeable difference in terms of particle size.

Slag has an average particle size of 5.08mm, which is 2 times smaller compared to crushed concrete; 50% of the material has a particle size larger than 2.58mm; most of the slag has a particle size in the range of 4 to 8mm; 10% of the material is smaller than 0.25mm and 90% of the material is smaller than 20mm. The difference between each sample for mean and median found of slag is smaller compared to crushed concrete. This illustrates that slag is a more homogeneous material which can be observed through Fig. 25.

Waste metal powder has an average particle size of 0.41mm, which is more than 10 times smaller than slag; 50% of the material has a particle size smaller than 0.35mm; most of the waste metal powder has a particle size in the range of 0.25 to 0.50mm; 10% of the material is smaller than 0.125mm and 90% of the material is smaller than 1mm. Hence waste metal powder consists of particles a lot finer than crushed concrete and slag. Furthermore, the waste metal powder is considered as a homogeneous material through observation.

Fly ash has the smallest average particle size of 0.31mm; 50% of the material has a particle size smaller than 0.14mm; most of the waste metal powder has a particle size smaller than 0.063mm; 10% of the material is smaller than 0.063mm and 90% of the material is smaller than 1mm. Fly ash is the material with smallest particle size among the four ISWs test. It is as well a homogenous material as the mean and median found for each sample of fly ash is similar.

Fig 26 shows the particle size distribution for each ISWs. It can be observed that more particles are passing the sieves with smaller aperture size in the ascending order: crushed concrete (CC), slag (S), waste metal powder (M), fly ash (FA), indicating that CC has the largest particle size, followed by S, M and FA. This corresponds well with the result obtained through calculation of mean and median for each ISW.

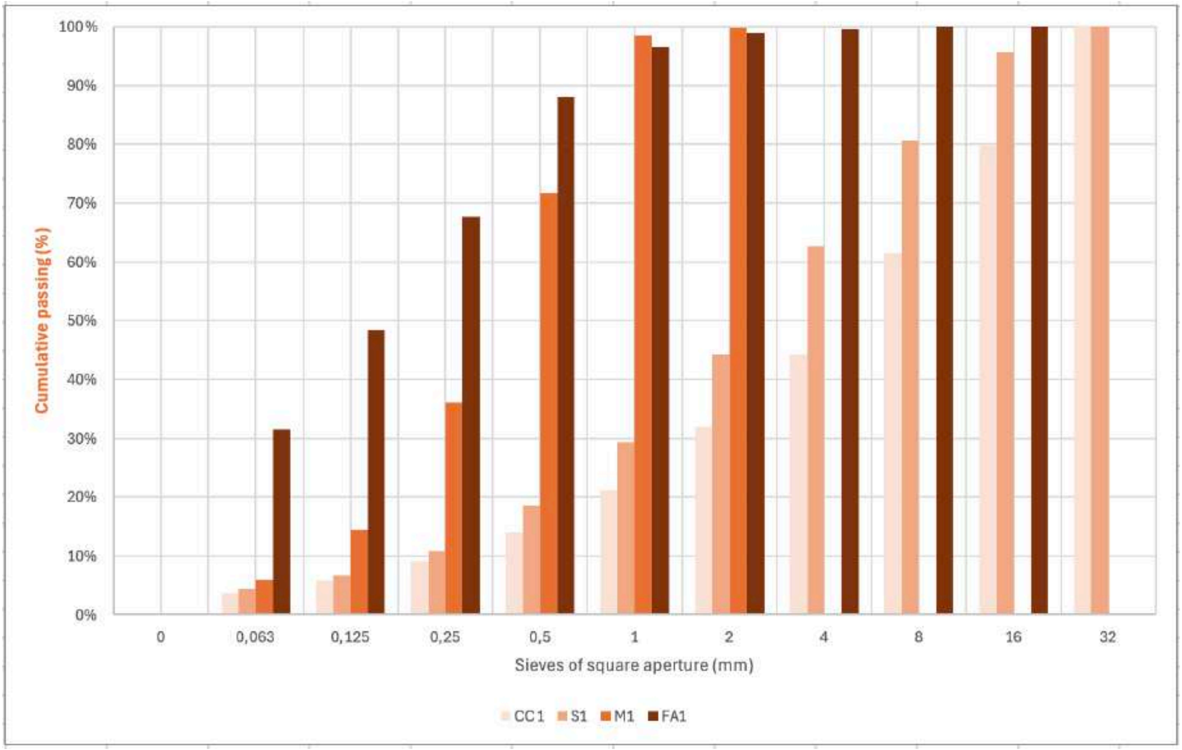

Figure 26. Particle size distribution for crushed concrete, slag, waste metal powder, fly ash

5.1.3 Partial conclusion

The sieve test provides information about the moisture content of each ISW and they can be classed according to their water content in an ascending order: waste metal powder, crushed concrete, slag, fly ash. High water content may be useful for thermal energy storage as water has a high specific heat capacity (4.186kJ/kg.K). With high water content, there is interest to transform the TES installation into latent heat storage (LHS) installation as water has an advantage of having a high latent heat of vaporization (2260kJ/kg). This study only focuses on SHS installation and further research is needed to examine the feasibility of using the four ISWs tested as materials for LHS.

Furthermore, high water content may allow the evaporation of notable quantity of water during heating process, emitting water vapour within TES installation which can cause the increase of pressure within the system. Considerations should be taken when designing the TES installation to ensure that the pressure always stays at a safe value. There is possibility to keep the water vapour within the TES installation to then recondense it during the energy discharge process. However, in the case which water vapour is removed, it is necessary to add water into the TES installation each time after the discharge to keep the same water content within the TES installation as to maintain the thermal performance of the installation.

On the other hand, the sieve test also provides information about the particle size distribution of the ISWs in which the materials are classed in the following ascending order according to their particle size: fly ash, waste metal powder, slag, crushed concrete. This is indeed an important parameter for both the waste heat recovery system using waste metal powder and the TES installation using crushed concrete, slag and fly as this affects the void fraction within the installation which then affects the performance of energy charge and discharge for TES installation.

5.2 Thermogravimetric analysis (TGA)

Thermogravimetric (TGA) has been done on samples of raw and thermally treated crushed concrete, slag, fly ash and waste metal powder.

5.2.1 Thermogravimetric analysis on waste metal powder

Fig 27 shows the result of TGA for two samples of raw waste metal powder and one sample of dried waste metal powder. Delta Y shown in the figure designates the percentage of total mass loss for the sample compared to its original mass. It can be observed that the mass loss for the raw samples is 0.433% and 0.73%. The mass loss is probably due to the thermal decomposition of remaining cutting liquid on the surface of waste metal powder. Cutting fluid is a type of coolant and lubricant used during the machining process such as turning with lathe for the purpose of cooling, reducing the friction between the machine and the metal and facilitating the cutting of the metal parts. The cutting fluid may be consisted of organic compounds which are decomposed during the process. However, since the quantity of cutting fluid remained on the waste metal powder is limited, the mass loss due to the thermal decomposition is almost negligeable. In addition, despite the fact that there is a 0.3% difference of mass loss between both raw waste metal powder, the difference remains insignificant and due to the fact that the evolution of mass loss in function of temperature for both raw waste metal powder remains similar, it is concluded that the repeatability of the test results is validated since both samples behave in the same way in terms of mass loss during TGA test.

Concerning the result for dried waste metal powder, it can be observed that the mass loss for dried waste metal powder is similar to that of raw metal powder with a difference of 0.3%. This indicates that the absence of water within the sample of waste metal powder has no effect on the result of TGA which further implies that the water content of waste metal powder is negligeable. Hence the fact that waste metal powder has the lowest water content among the four ISWs tested is justified by this TGA test.

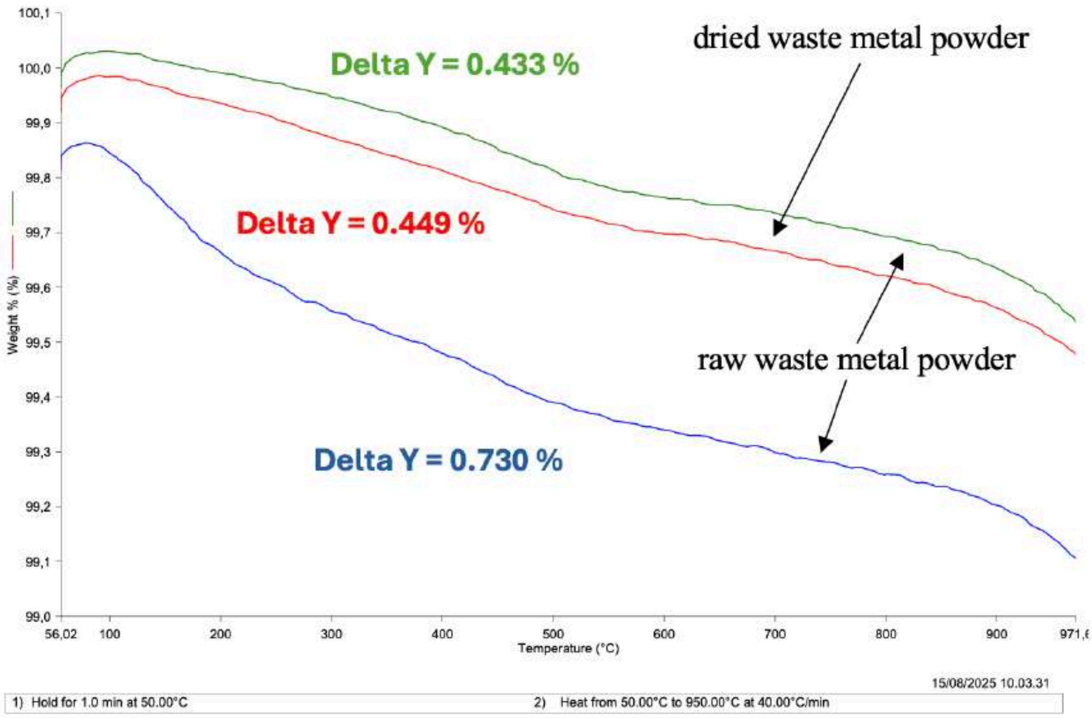

Figure 27. Results of thermogravimetric analysis for raw and dried waste metal powder

5.2.2 Thermogravimetric analysis on crushed concrete

Fig. 28 illustrates the result of TGA for two samples of raw crushed concrete and one sample of dried crushed concrete. The mass loss for both samples of raw crushed concrete is similar at around 11% (11.059% and 11.267%). This allows the validation for the repeatability of test results as both raw crushed concrete behave in the same way during TGA test. According to the TGA results, the mass loss of raw crushed concrete can be divided into two phases with each phase contributing to the mass loss through its possible corresponding mechanism:

- From 50°C until 800°C approximately, the mass loss of around 5% is mainly due to the thermal composition of ettringite, C-S-H, gypsum ($CaSO_4 \cdot 2H_2O$) and $Ca(OH)_2$ which contain chemically bound water within the compounds
- From 800°C onwards, the mass loss of around 6% is mainly caused by the thermal decomposition of carbonate compounds such as calcium carbonate.

On the other hand, it can be observed that the mass loss of dried crushed concrete (10.296%) is 1% lower compared to that of raw crushed concrete. This indicates that the effect of the absence of free surface moisture on the mass loss of crushed concrete is almost negligeable because the water adhering to the surfaces of crushed concrete is of small quantity as the water content of raw crushed concrete is only 6.67%. Hence the mass loss of dried concrete is mainly due to the same mechanisms occurred during the TGA test of raw crushed concrete with a small additional loss contributed by the evaporation of free surface moisture.

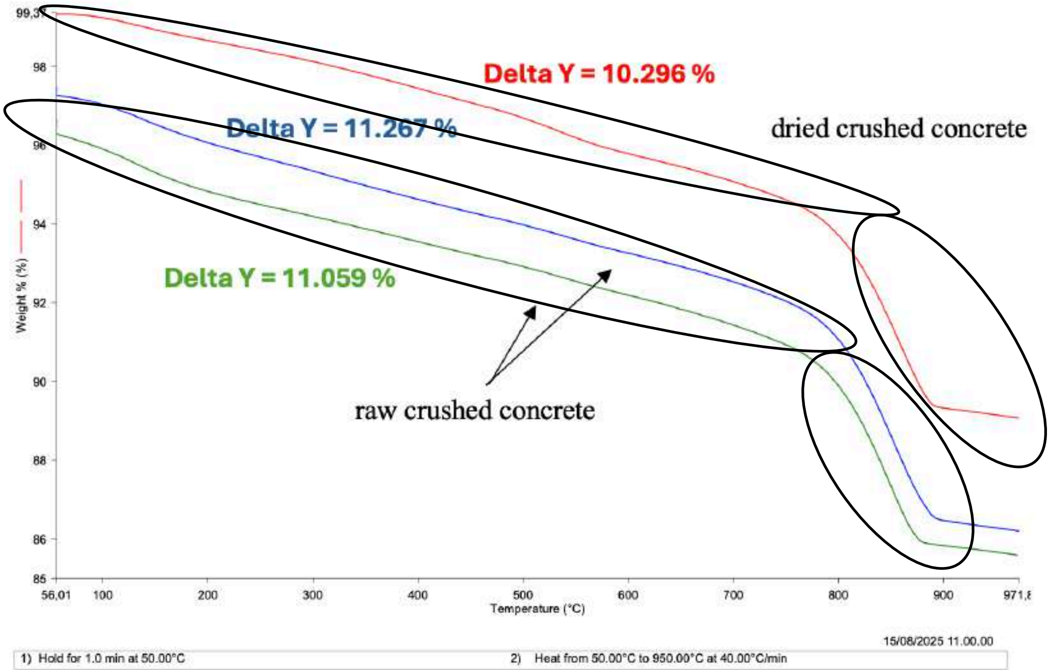

Figure 28. Results of thermogravimetric analysis for raw and dried crushed concrete

5.2.3 Thermogravimetric analysis on slag

Fig. 29 shows the TGA results for two samples of raw slag and one sample of dried slag. It can be noticed that the mass loss for the two samples of raw slag tested is similar at around 18% (17.960 and 18.260%). This validates the repeatability of the test results as both raw slags behave in the same way during the TGA test. Furthermore, the mass loss for both samples of raw slag can be divided into three phases involving possibly three different mechanisms contributing to the mass loss:

- From 50°C until 150°C approximately, the water content of slag adhering on its surface and trapped within the pores of slag is evaporated, causing a mass loss of about 10%.
- From 150°C up to 850°C approximately, the mass loss of around 6% occurs mainly due to the thermal decomposition of organic compounds remained within the slag sample.
- From 850°C onwards, the mass loss for the sample can be mainly caused by further slower thermal decomposition of stable carbon structures which accounts for about 2% of mass loss.

On the other hand, the mass loss for the sample of dried slag is 8.759%, which is around 9% lower compared to the raw slag and two different phases of mass loss is identified instead three phases for the TGA of dried slag. This illustrates the effect of free surface moisture on the mass loss of samples during the TGA test. Since raw slag has a water content of 14% which is not negligeable, evaporation of water adhering to the surface of raw slag is the principal source of mass loss during the TGA test from 50°C to 150°C which does not occur during the TGA test of dried slag because free surface water has been removed from dried slag during the drying process. Hence the mass loss for the TGA test of dried slag is mainly caused by the thermal decomposition of organic compounds remained within the sample and the thermal decomposition of stable carbon structures.

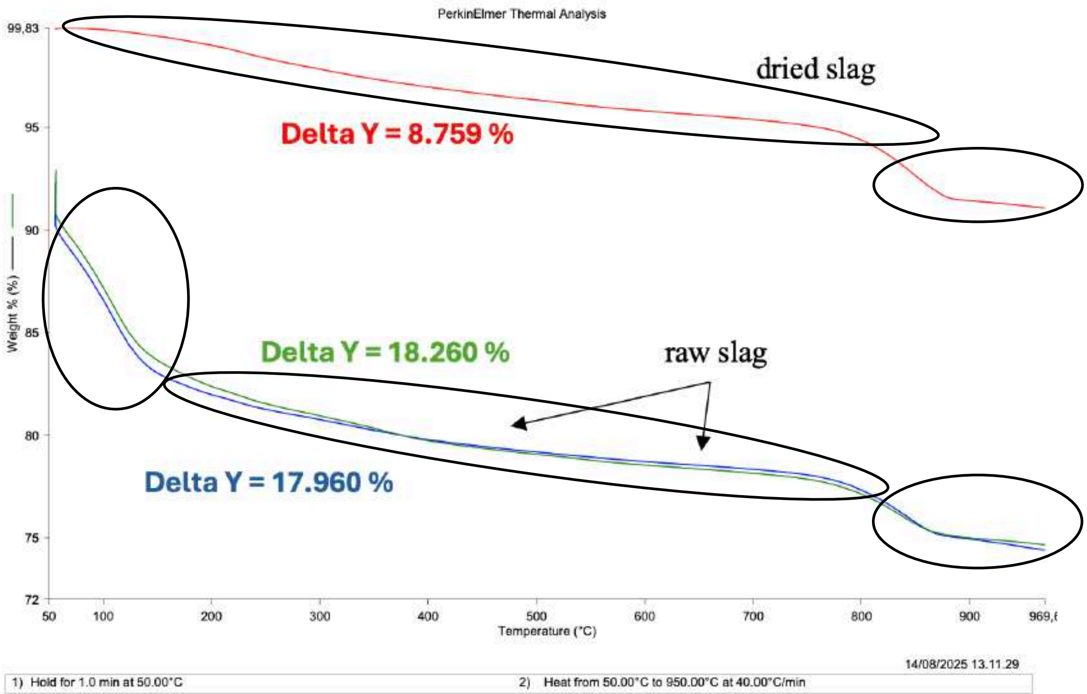

Figure 29. Results of thermogravimetric analysis for raw and dried slag

5.2.4 Thermogravimetric analysis on fly ash

Fig. 30 illustrates the TGA results for two samples of raw fly ash and one sample of dried fly ash. The mass loss for both samples of raw fly ash is similar at around 27% (26.750% and 27.341%). The repeatability of the test results is validated for fly ash since both raw fly ash behave in the same way during the TGA test. The mass loss for both raw fly ash can be divided into three phases which is similar to the TGA result for raw slag, except that there is a greater mass loss for the raw fly ash during the TGA test from 50°C to 150 °C. The three phases for the TGA results can be explained by possibly three different mechanisms, which are:

- From 50°C until 150°C approximately, the water absorbed by the raw fly ash is evaporated and removed, causing the samples to have a mass loss of around 16%.

- From 150°C until 800°C approximately, the mass loss of around 6% occurs mainly due to the thermal decomposition of the unstable carbonates and organic compound within the raw fly ash as well as dehydration of hydroxide compounds related to the loss of chemically bound water from compounds such as calcium hydroxide in fly ash.
- From 800°C onwards, the mass loss of around 5% can be mainly caused by further thermal decomposition of carbonate compounds, contributing to additional mass loss for the samples.

On the other hand, the mass loss for the sample of dried fly ash is 15.708%, which is 11-12% lower compared to raw fly ash. The difference of mass loss for raw and dried fly ash is hence more significant compared to the difference of mass loss for raw and dried slag. However, two phases have been identified for the mass loss of dried fly ash just like the result for dried slag, instead of having three phases for the mass loss. With a water content of 42% for the raw fly ash, it is relevant to conclude that the mass loss occurring for the raw fly ash during TGA test from 50°C until 150°C corresponds to the evaporation of water adhering to the surfaces of raw fly ash, which is not occurring during the TGA test for dried fly ash because the free surface moisture is removed from dried fly ash. The mass loss of dried fly ash is hence mainly due to the thermal decomposition of unstable carbonate and organic compounds as well as dehydration of hydroxide compounds.

In addition, it is observed that the absence of free surface moisture for fly ash has a more significant influence on mass loss during TGA compared to that of slag, crushed concrete and waste metal powder. This is justified once again by the fact that raw fly ash has the highest water content compared to the three other ISWs.

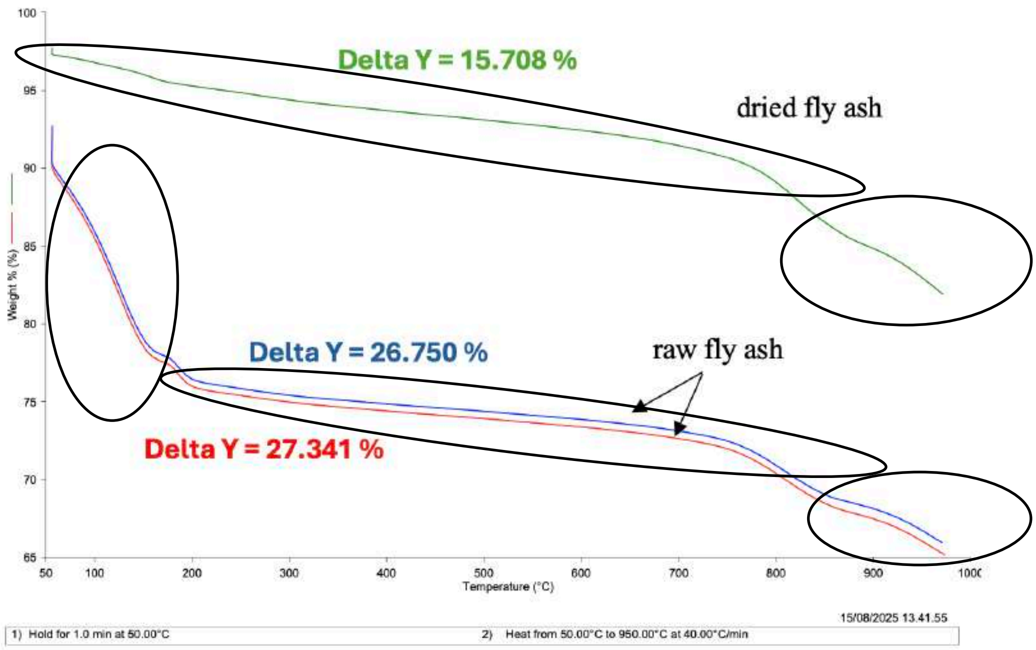

Figure 30. Results of thermogravimetric analysis for raw and dried fly ash

5.2.5 Partial conclusion

The thermal stability of the four raw industrial solid wate (ISW) tested can be classed in an ascending order: fly ash, slag, crushed concrete and waste metal powder. The principal factor degrading the thermal stability of the ISW is the water content of the samples. On the other hand, the thermal stability of the four dried industrial solid wate (ISW) tested can be classed in an ascending order: fly ash, crushed concrete, slag and waste metal powder. Table 3 presents the maximum allowed heating temperature for each raw and dried ISW with a maximum mass loss of 5%.

Industrial solid waste (ISW)	Maximum heating temperature for raw ISW (°C)	Maximum heating temperature for dried ISW (°C)
Waste metal powder	Over 950	Over 950
Crushed concrete	750	800
Slag	100	800
Fly ash	80	650

Table 3. Maximum heating temperature for raw and dried waste metal powder, crushed concrete, slag and fly ash

For waste metal powder and crushed concrete, there is less interest in using the dried materials for TES because drying the materials does not increase much their maximum heating temperature while an additional financial cost and time is necessary for the drying process. This material selection criteria is further justified by the fact that waste metal powder and crushed concrete have a lower water content or small quantity of free surface moisture and hence the drying process does not really improve their thermal properties.

However, there is strong interest in using the dried materials for slag and fly ash because drying allows a significant increment of heating temperature for slag and fly ash. This is further justified by the higher water content of slag and fly ash and hence the drying process allows the improvement of thermal properties while removing water adhering to the surfaces of materials.

5.3 Thermal energy storage (TES) installation for metal powder: waste heat recovery system

In order to investigate the suitability of waste metal powder as TES materials and the thermal performance of waste heat recovery system built, three scenarios of energy charge and discharge have been tested on the waste heat recovery system.

5.3.1 Scenario 1: Scaled-temperature heating

In this scenario, the heating process of the sauna heater starts at 60°C. After 2 hours of heating time, the heating temperature is increased to 65°C and then after 6 hours of heating time to 70°C which lasts for another 8 hours. The TES installation is then cooled down for 16 hours by switching off the sauna heater. The idea of testing scaled-temperature heating is to maximize the performance of TES installation without encountering problems caused by the limitation of the TES system. The fan of the TES installation can theoretically support a maximum temperature of 80°C. The fan will be overheated at a temperature over 80°C, causing the volume flow rate of the system to decrease until 0L/s. By heating up the fan directly at 70°C, the fan reaches a temperature over 80°C because of the thermal inertia of the TES system, causing it to be overheated. Hence, to avoid the overheating of the fan while ensuring the maximum performance of the TES installation, the heating temperature is being scaled up gradually from a lower temperature (60°C) until a possible higher temperature (70°C). This scenario can occur in real life as well when the sauna heater works at a certain temperature for a certain period then the heating temperature is increased because of the arrival of more users.

Two types of scaled-temperature heating tests are performed which is closed-loop system heating and open loop system heating. Closed-loop system heating refers to the energy charge and discharge within a closed TES system without opening to the exterior. Open loop system heating has the same setup as closed-loop system during energy charge, but the system is left open in direct contact with exterior during energy discharge by removing the connections of the ventilation duct with the sauna heater on both sides to allow airflow entering and exiting towards exterior. Fig. 31 shows the setup of open and closed-loop heating during energy discharge. The open loop heating assimilates to real life application of a heat exchanger used to heat up the airflow going into an internal space for example while the closed-loop heating assimilates to the heating of a space for industrial processes related to medical, food processing, materials processing etc. where precise temperature control is necessary. Fig. 32 shows one of the examples of real-life application for both systems.

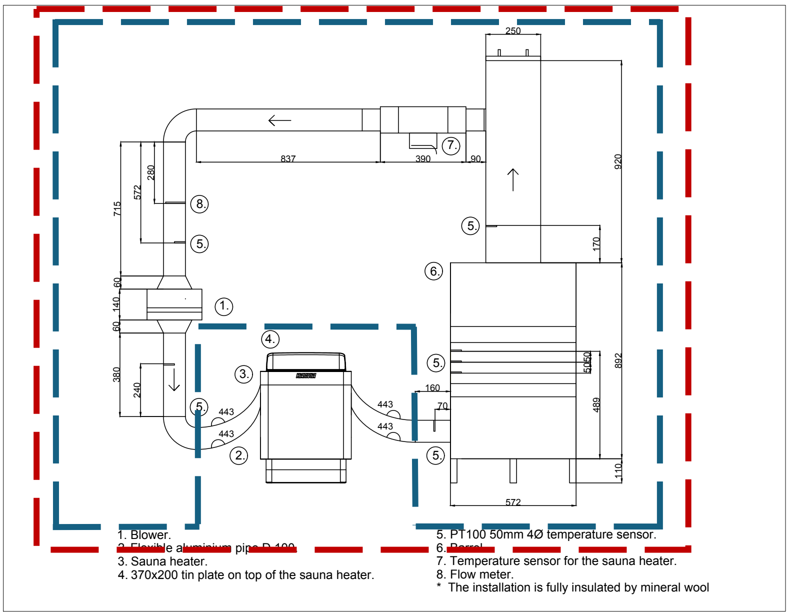

Figure 31. Open (blue) and closed-loop (red) system for waste heat recovery during energy discharge

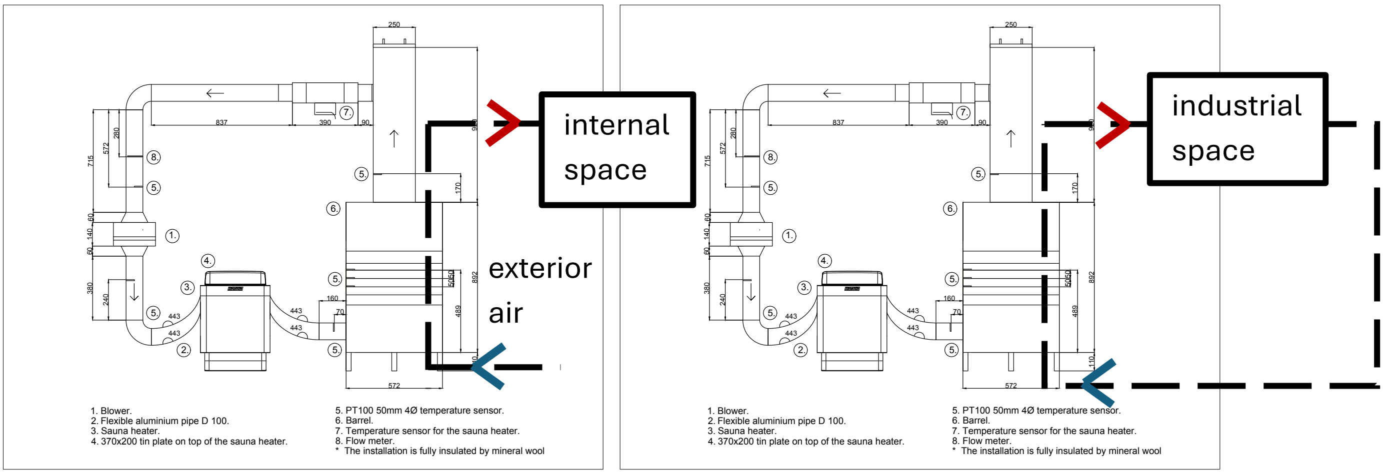

Figure 32. Illustrations for real life application of open and closed-loop system

Two tests have been performed for closed-loop system with one test for open loop system. Fig. 33 shows the temperature evolution along with time for the three tests at position B, C and D of waste heat recovery system (position of the temperature sensors shown in Fig. 19). It can be observed that the temperature evolution along with time is similar at position B, C and D, indicating that the temperature of waste metal powder is homogeneous within the heat recovery system.

Fig 34 illustrates the temperature comparison along with time for the three tests at position B, C and D respectively. Both test of closed-loop system has similar temperature evolution at position B, C and D during energy charge and discharge which validates the repeatability of the test results. The temperature evolution at position B, C and D for open loop system during energy charge has a greater gradient because the initial temperature of the test is lower. Nevertheless, the temperature evolution of open loop system during energy charge will be similar with those of closed-loop system since the setup of the test is the same for open and closed-loop system and the repeatability of test results is validated. On the other hand, the temperature evolution at position B, C and D for open loop system during energy discharge has a greater gradient because of direct contact with exterior air, implied a slightly higher heat transfer rate at the beginning of energy discharge.

Fig. 35 shows the efficiencies, total energy stored and released, average charging and discharging power, total heat loss as well as ratio between real energy stored and expected energy stored of the three tests. Concerning the charge and discharge efficiency as well as total heat loss, the open loop test has slightly better results compared to both closed-loop tests. The total energy stored and released, average charging and discharging power, cycle efficiency and ratio between real energy stored and expected energy stored have similar values for the open loop test and both closed-loop tests.

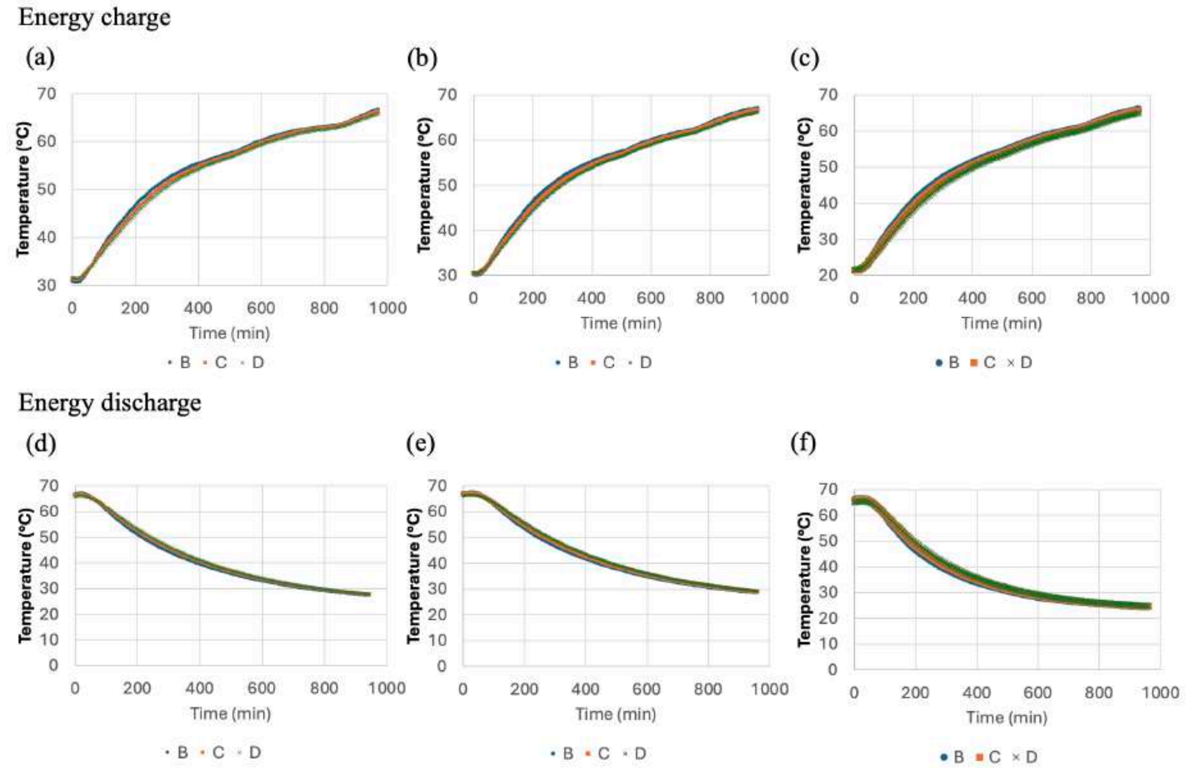

Figure 33. Evolution of temperature along with time at position B, C and D for (a) and (d): Closed-loop test 1, (b) and (e): Closed-loop test 2, (c) and (f): Open loop test 1

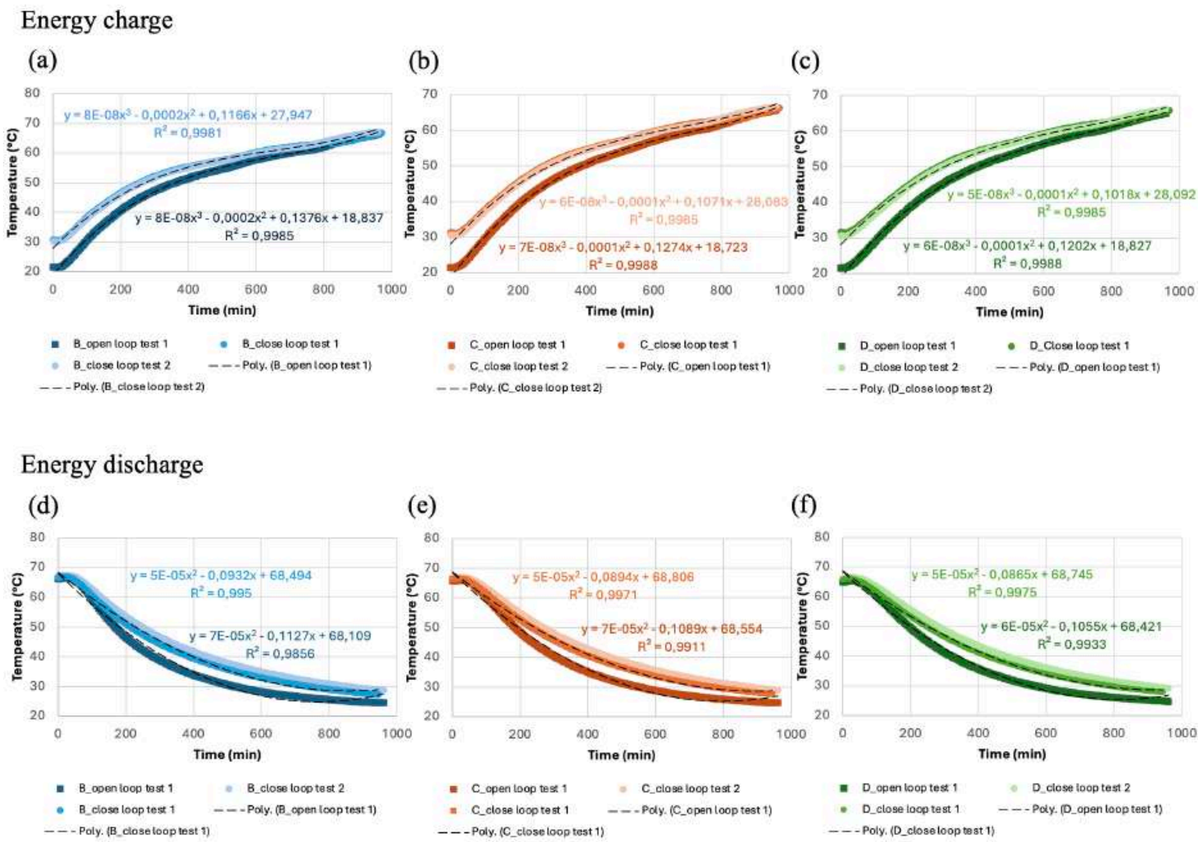

Figure 34. Temperature comparison for open and closed-loop system test at (a) and (d): Position B, (b) and (e): Position C, (c) and (f); Position D

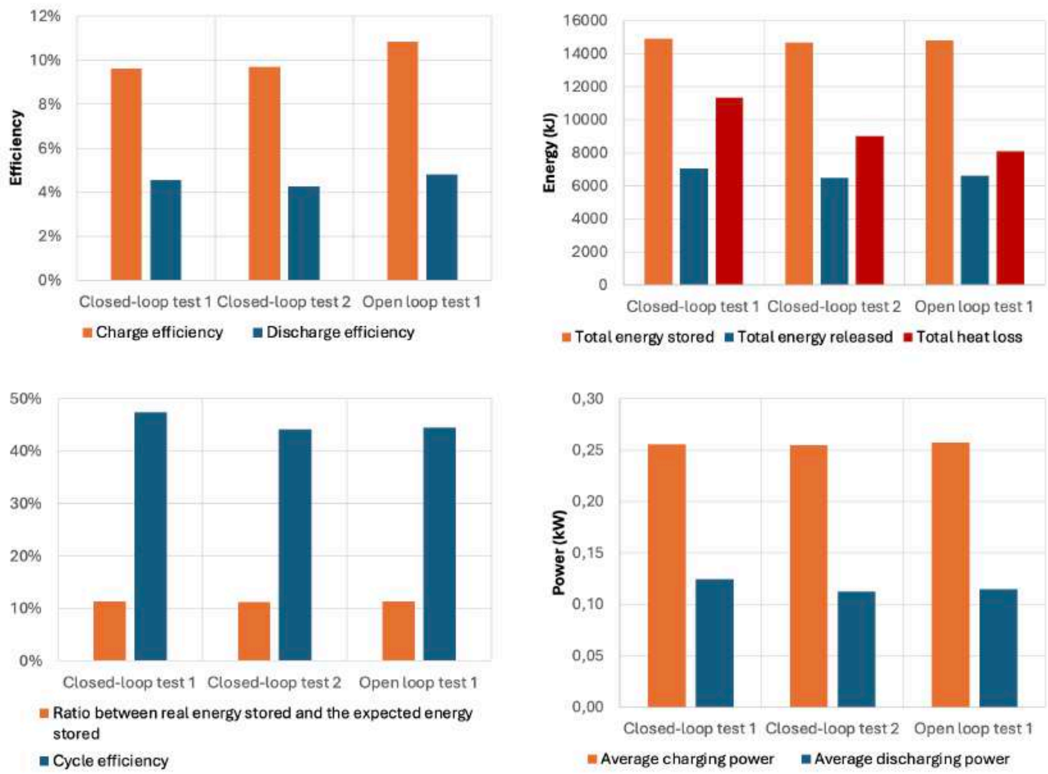

Figure 35. Efficiencies, energy stored and released, average charging and discharging power and heat loss of open and closed-loop system tests

5.3.2 Scenario 2: Constant temperature heating

Regarding to this scenario, the sauna heater works at 60°C for 4, 8 and 16 hours respectively for energy charge before the energy discharge with same amount of time (4, 8 and 16 hours respectively). This scenario can take place in real life with the sauna heater being set to work at a constant temperature for a certain amount of time before switching it off. Fig. 36 shows the temperature evolution along with time for the three tests at position B, C and D of waste heat recovery system. Concerning the energy charge, it can be noticed that all three tests have similar temperature evolution at position B, C and D during energy charge which validates the repeated behaviour of the test results. On the other hand, during the energy discharge, the gradient of temperature evolution at position B, C and D increases as the heating time increases. This is because longer heating time allows the waste metal powder to reach a higher temperature at the end of energy charge, introducing a greater temperature gradient with a better heat transfer rate at the beginning of energy discharge.

Fig. 37 shows the efficiencies, total energy stored and released, average charging and discharging power, total heat loss as well as ratio between real energy stored and expected energy stored of the three tests. As the heating time decreases, the charge and discharge efficiency, average charging and discharging power as well as ratio between real energy stored and expected energy stored increases. On the other hand, the total energy stored and released, total heat loss and cycle efficiency increases along with increasing heating time.

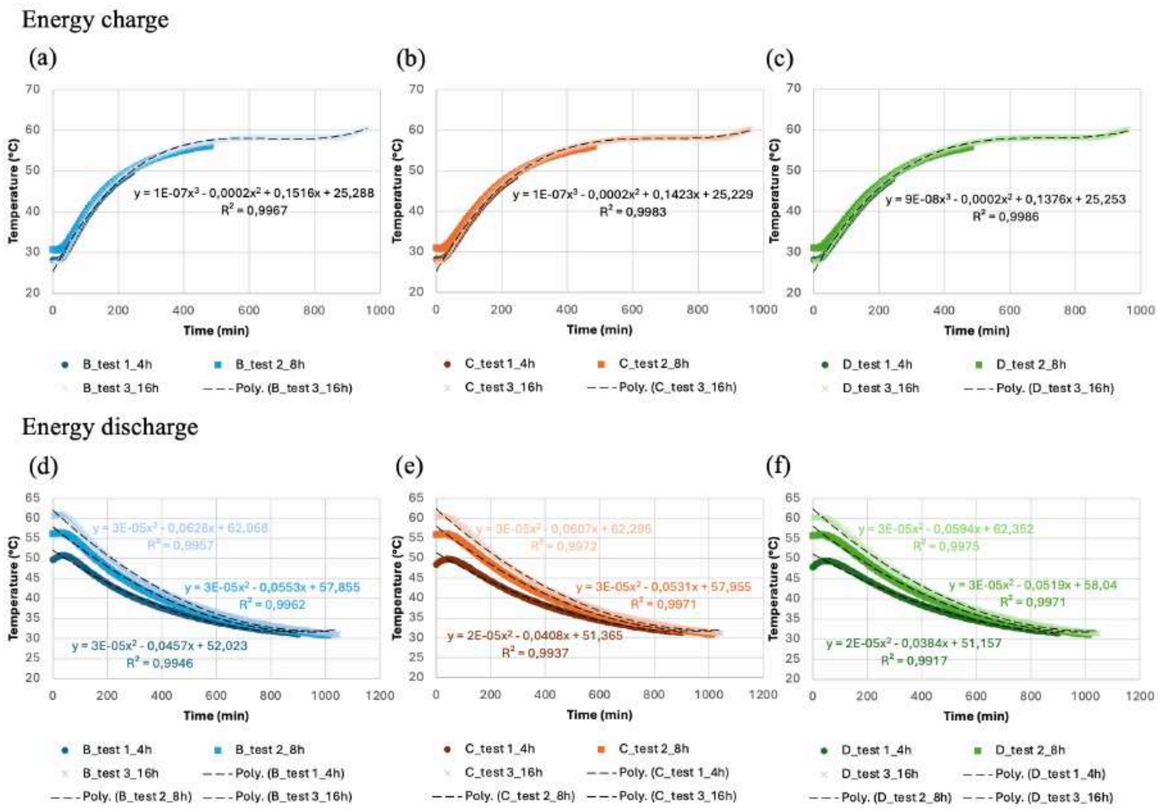

Figure 36. Temperature comparison for constant temperature heating test at (a) and (d): Position B, (b) and (e): Position C, (c) and (f); Position D

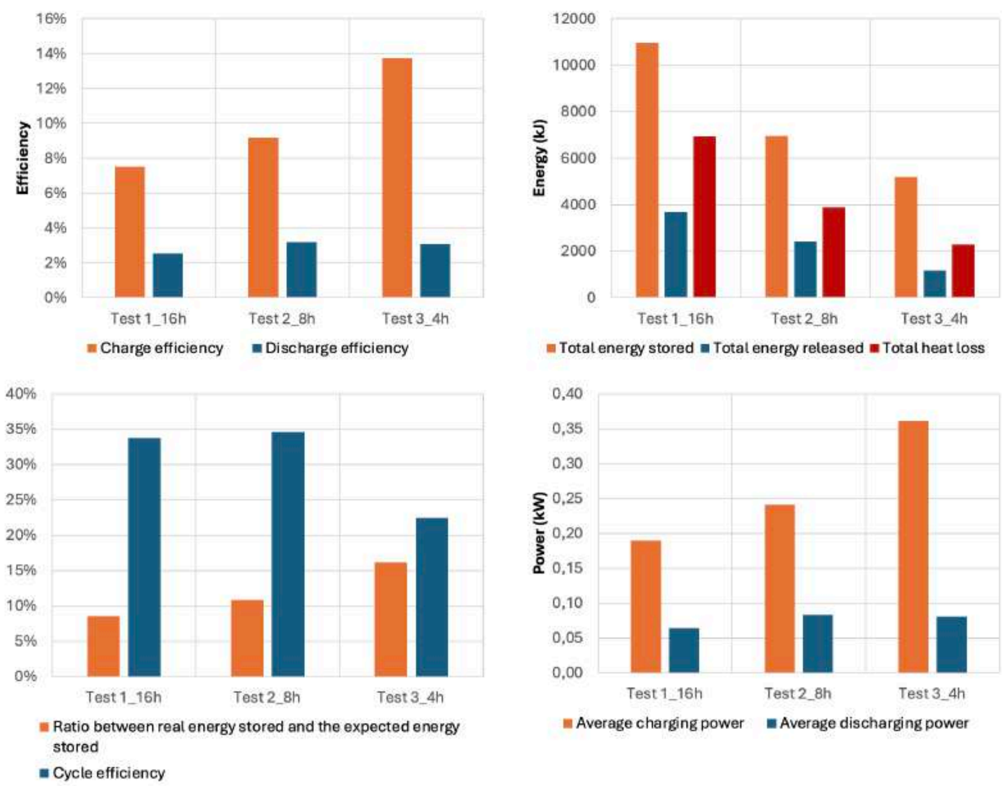

Figure 37. Efficiencies, energy stored and released, average charging and discharging power and heat loss of constant temperature heating tests

5.3.3 Scenario 3: Constant heating time

Concerning this scenario, the sauna heater works for 8 hours at 40°C, 50°C and 60°C respectively for energy charge before the 8-hours energy discharge. This scenario can occur in real life as the sauna heater works at a different temperature for a certain amount of time. Fig. 38 shows the temperature evolution along with time for the three tests at position B, C and D of waste heat recovery system. Concerning the energy charge, the gradient of temperature evolution at position B, C and D increases as the heating temperature increases, implying a better heat transfer rate during energy charge. Concerning the energy discharge, the gradient of temperature evolution at position B, C and D increases as the heating temperature increases as well, indicating a better heat transfer rate during energy discharge.

Fig. 39 shows the efficiencies, total energy stored and released, average charging and discharging power, total heat loss as well as ratio between real energy stored and expected energy stored of the three tests. As the heating temperature increases, the charge and discharge efficiency, average charging and discharging power, total energy stored and released, total heat loss and cycle efficiency increases. On the other hand, the ratio between real energy stored and expected energy stored decreases as the heating temperature increases.

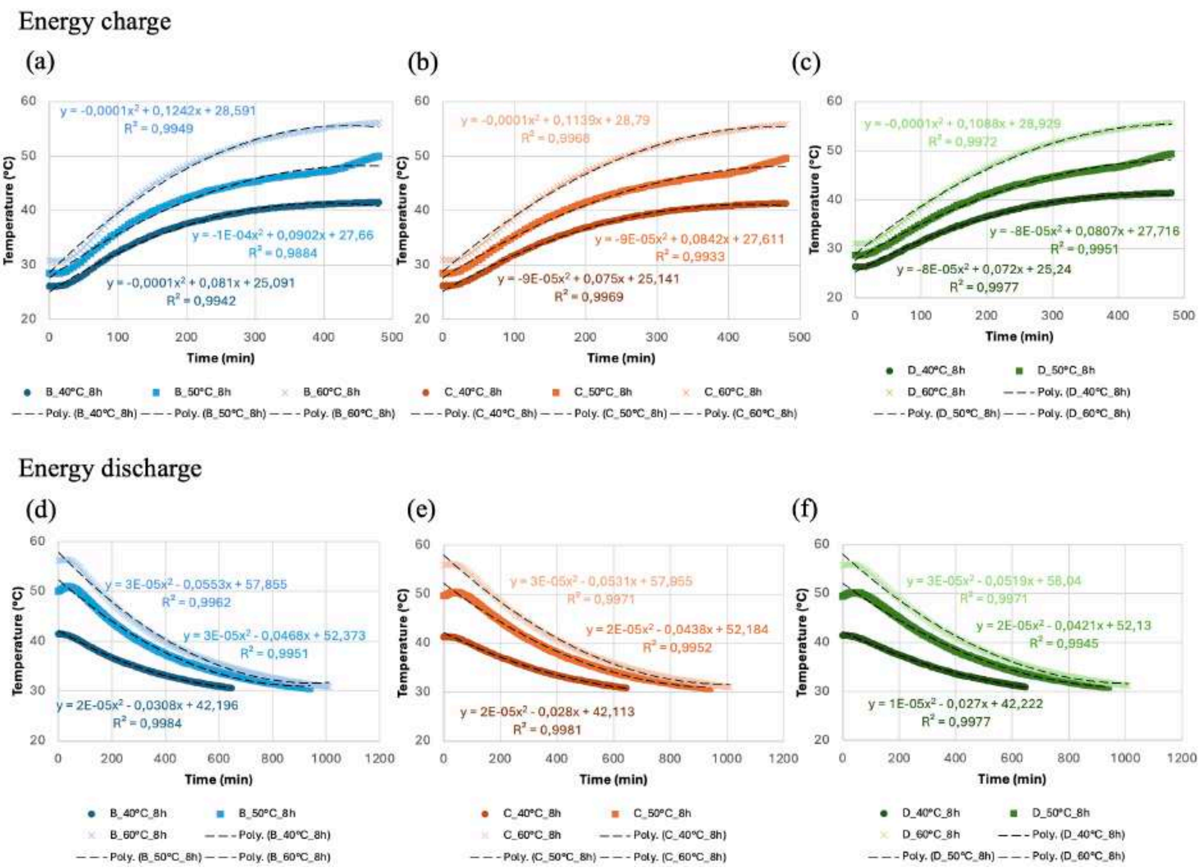

Figure 38. Temperature comparison for constant heating time test at (a) and (d): Position B, (b) and (e): Position C, (c) and (f); Position D

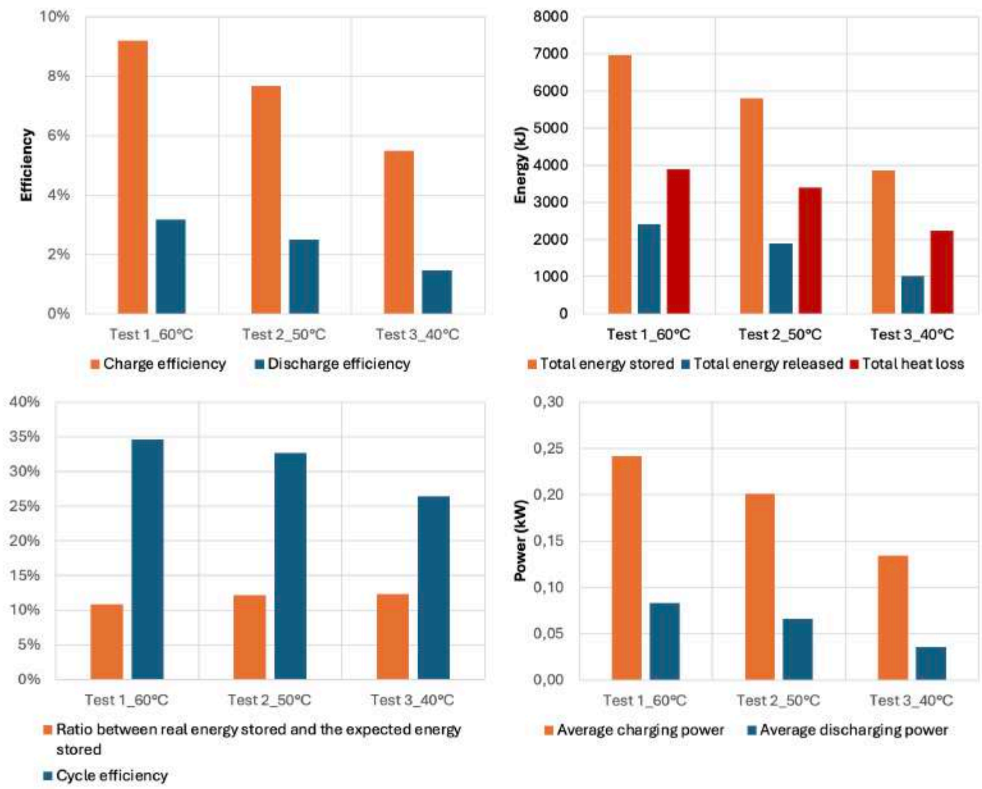

Figure 39. Efficiencies, energy stored and released, average charging and discharging power and heat loss of constant heating time tests

5.3.4 Partial conclusion

Concerning the performance of the waste heat recovery system, in comparison of open and closed-loop system test, the open loop system has a slightly better performance in terms of charge and discharge efficiency while ensuring less heat loss from the system. In comparison of constant temperature heating test with different heating time, although longer heating time does allow more energy stored and released as well as a better cycle efficiency, the performance of the test with shorter heating time is better in overall with a better average charging and discharging power, charge and discharge efficiency as well as ratio between real energy stored and expected energy stored while ensuring less heat loss. In comparison of constant heating time test with different heating temperature, it is more ideal to heat up the waste heat recovery system with a higher temperature with improvement of most parameter along with heating temperature except for cycle efficiency. Hence, the best configuration for the waste heat recovery system is the usage as an open loop system for energy discharge with higher heating temperature and shorter heating time.

In addition, the problem related to the contamination of airflow within the waste heat recovery system by the metal powder does not occur. This is further justified by a similar research done on waste heat recovery in the iron and steel industry with the use of slag as TES materials [32]. According to the research, no contamination issue occurs during energy charge and although the direction of airflow is inversed during energy discharge, there is no contamination issue as well during energy discharge. This reinforces the stability of the waste metal powder within the waste heat recovery system.

Nevertheless, the large quantity of heat loss for the TES installation is an issue to deal with. The heat loss is over 44% of energy stored for all tests performed which is significant. In the current design, the hot air has to go through the upper-side network of ventilation duct (as shown in Fig. 20) before reaching the barrel for energy storage because the temperature regulator is installed at the upper side of the barrel. The ideal configuration will be to move the regulator to the bottom side of the barrel while inversing the direction of the airflow within the heat recovery system. This allows the air heated by the sauna heater to reach directly the barrel for energy storage without the need to go through the upper-side network of ventilation duct and the energy discharge can be performed as well without going through the upper-side of ventilation duct which avoids the heat loss.

5.4 Thermal energy storage (TES) installation for crushed concrete, slag and fly ash

In order to investigate the suitability of crushed concrete, slag and fly ash as TES materials, each material is filled inside a barrel, which is then connected to the TES installation and tested respectively.

5.4.1 Thermal energy storage (TES) using crushed concrete

The TES installation with crushed concrete is heated up by Sunamp heater for 40 hours before it is being cooled down by Oilon heat pump for 24 hours. Fig. 40 shows the surface temperature evolution along with time for a total of 8 temperatures sensors from position A to H (positions of temperatures shown in Fig. 21). Position A and E have the same distance with the wooden stick in the middle of the barrel, and it goes the same for the other pairs of position (B and F; C and G; D and H). It can be observed that the homogeneity for the surface temperature of crushed concrete increases as the distance between the position and the center of the barrel increases. This is because the distance between the heat transfer fluid (HTF) and each pair of positions is not exactly identical, causing one position to receive more thermal energy than another (for example A receives more thermal energy than E). However, the effect of asymmetric reduces as the distance with the HTF increases.

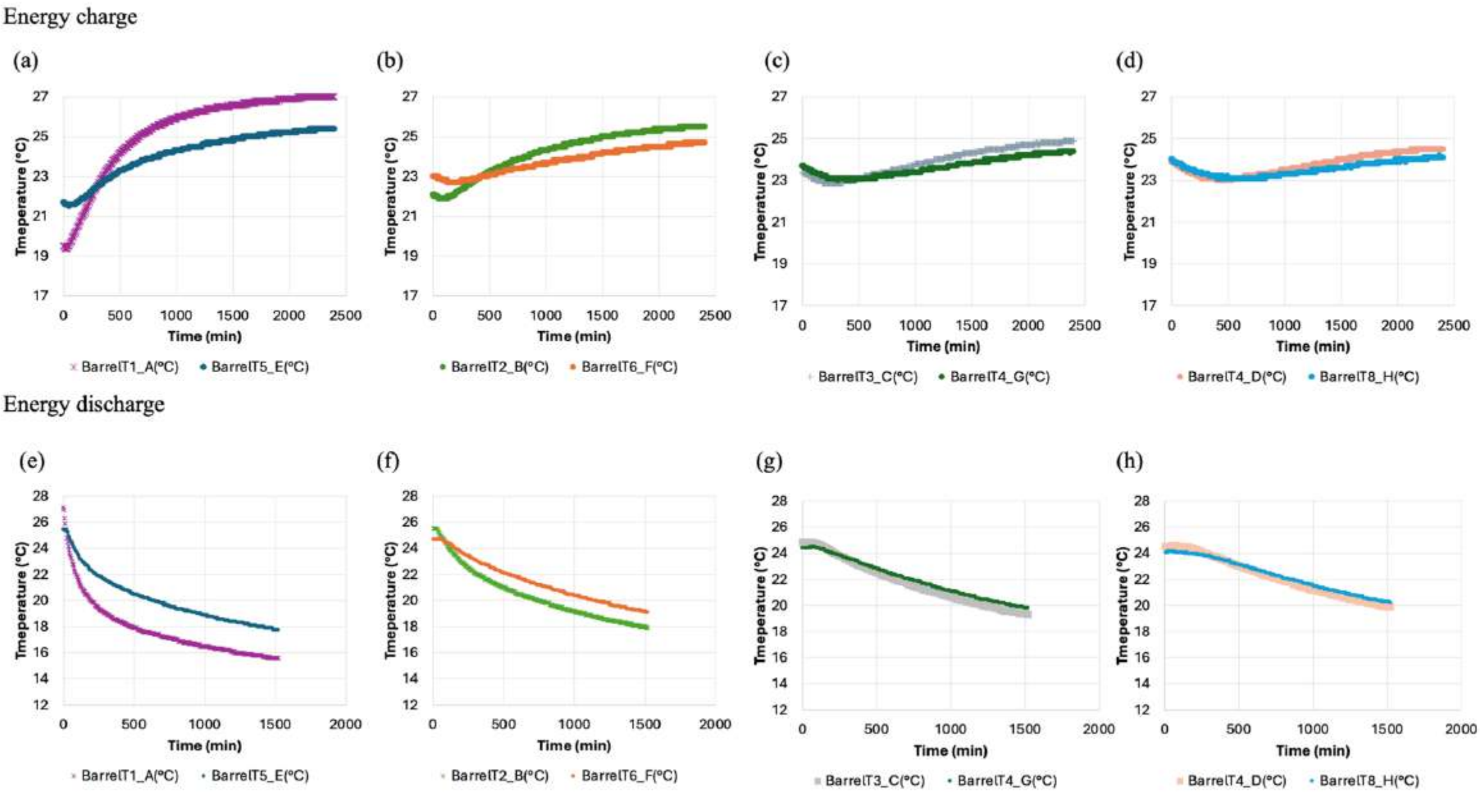

Figure 40. Surface temperature evolution along with time for 8 temperatures sensors (A, B, C, D, E, F, G, H)

Fig. 41 shows the temperature evolution across the depth along with time for 3 temperatures sensors at position E, I and J (positions of temperatures shown in Fig. 21). The temperature across the depth is not homogeneous during energy charge and discharge. During energy charge, there is heat loss from the top of the barrel towards exterior because the cover at the top of the barrel is not completely isolated. The crushed concrete at position J (lower surface) is covered and isolated by the crushed concrete above it, causing it to retain more thermal energy and thus to reach the highest temperature at the end of energy charge, followed by I (middle surface) and E (upper surface). On the other hand, during energy discharge, the HTF at 6°C has cooled down the crushed concrete along the depth. However, since the top of the barrel is not completely isolated, there is more heat gain from the exterior towards the upper surface of crushed concrete compared to those underneath it. Hence the gradient of temperature evolution at position J (lower surface) is greater compared to that at position J (middle surface) and finally at position E (upper surface), allowing position J to reach the lowest temperature at the end of energy discharge, followed by that of position I and E.

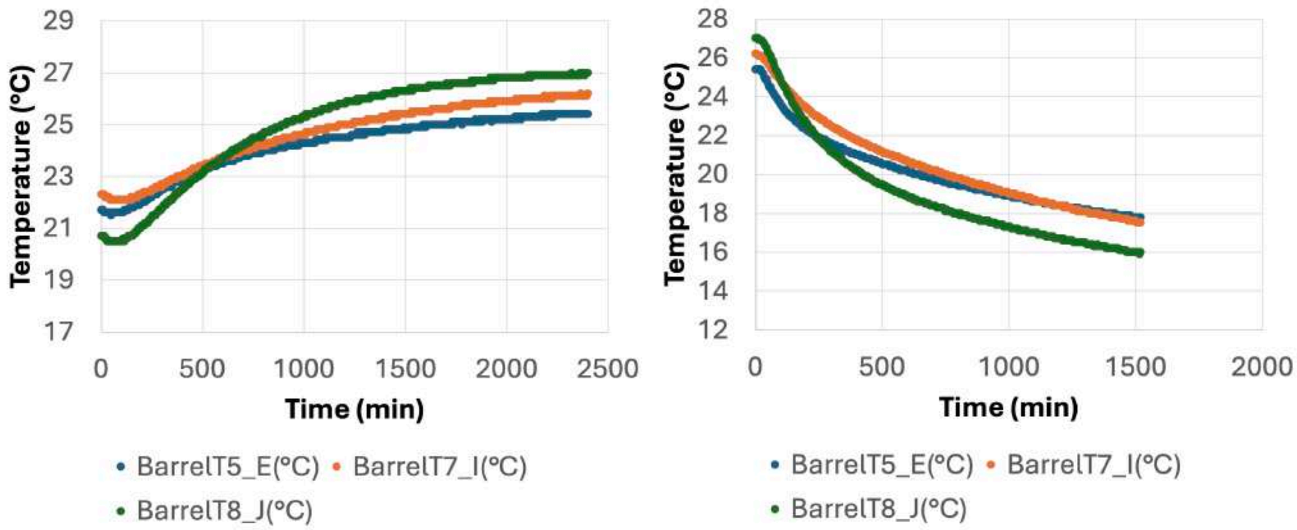

Figure 41. Temperature evolution along the depth along with time for 3 temperatures sensors at position E, I and J

5.4.2 Thermal energy storage (TES) using slag

The TES installation with slag is heated up by Sunamp heater for 41 hours before it is being cooled down by Oilon heat pump for 24 hours. Fig. 42 shows the surface temperature evolution along with time for 8 temperatures sensors from position A to H. It can be observed that the homogeneity for the surface temperature of crushed concrete increases as well as the distance between the position and the center of the barrel increases due to the similar reason with the test of crushed concrete. The effect of asymmetric reduces as the distance with the HTF increases. Furthermore, in the comparison with the test of crushed concrete, it can be noticed that slag has a better temperature homogeneity across the surface temperature compared to slag. It can be due to the fact that slag has a smaller particle size than crushed concrete, allowing a more even heat transfer across the surface which brings better temperature homogeneity across the surface temperature.

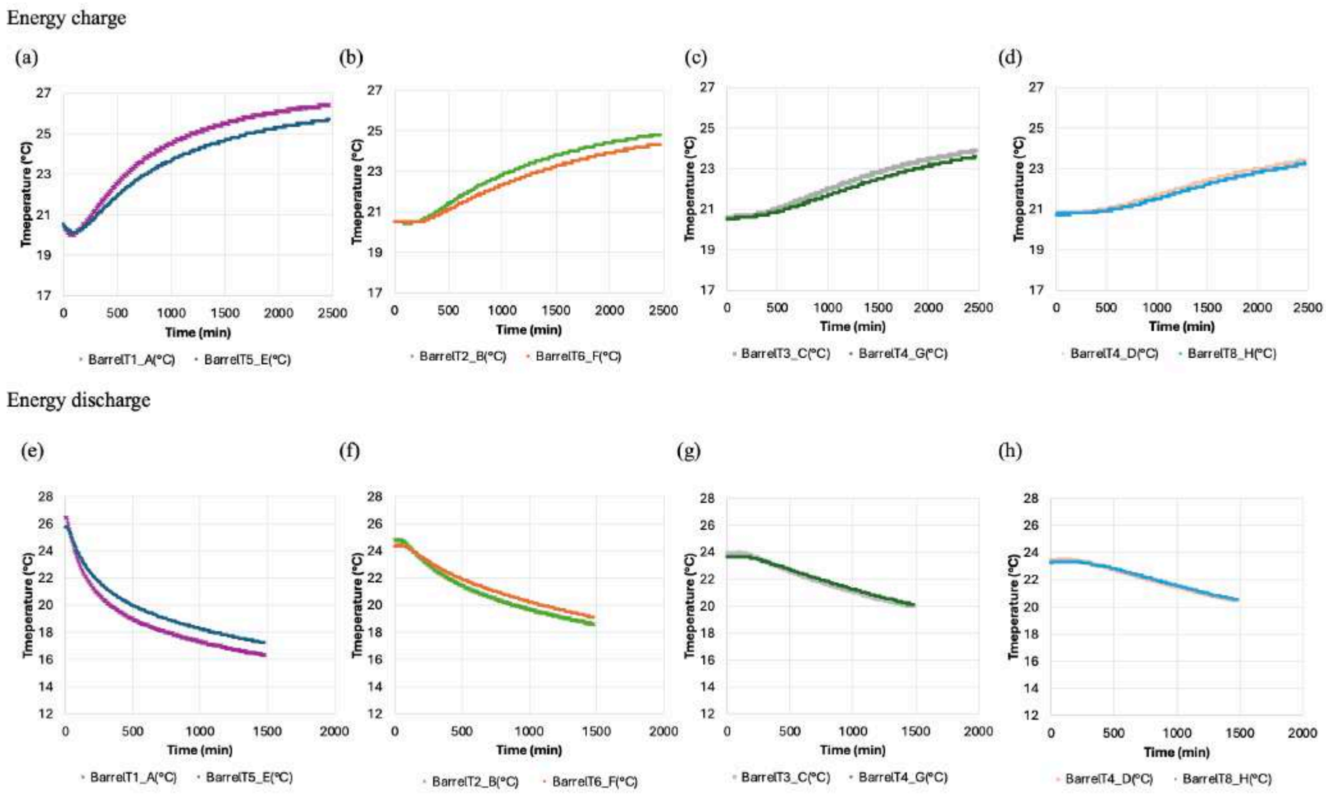

Figure 42. Surface temperature evolution along with time for 8 temperatures sensors (A, B, C, D, E, F, G, H)

Fig. 43 shows the temperature evolution across the depth along with time for 3 temperatures sensors at position E, I and J. The temperature across the depth is not homogeneous during energy charge and discharge. During energy charge, it can be observed the gradient of temperature evolution at position J (lower surface) is greater followed by that of I and E, allowing position J to reach the highest temperature at the end of energy charge, followed by position I and E due to the same reason as the test of crushed concrete. On the other hand, during energy discharge, the observation remains the same as the test of crushed concrete with the same phenomenon occurring during energy discharge.

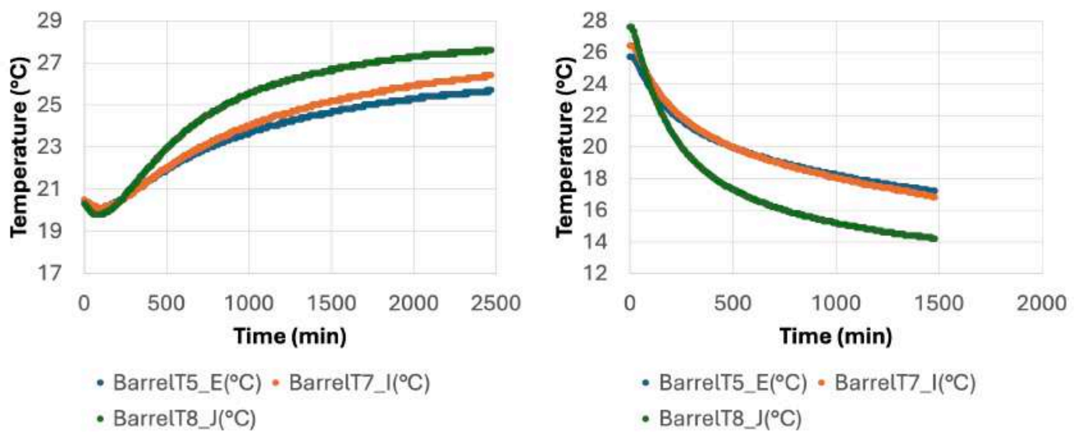

Figure 43. Temperature evolution along the depth along with time for 3 temperatures sensors at position E, I and J

5.4.3 Thermal energy storage (TES) using fly ash

The TES installation with fly ash is heated up by Sunamp heater for 40 hours before it is being cooled down by Oilon heat pump for 24 hours. Fig. 44 shows the surface temperature evolution along with time for 8 temperatures sensors from position A to H. It can be observed that the homogeneity for the surface temperature of fly ash increases as well as the distance between the position and the center of the barrel increases due to the similar reason with the test of crushed concrete. The effect of asymmetric reduces as the distance with the HTF increases. Furthermore, it can be noticed that fly ash has the best temperature homogeneity across the surface temperature compared to crushed concrete and slag. It can be due to the fact that fly ash has the smallest particle size and thus allowing an even heat transfer across the surface which brings the best temperature homogeneity across the surface temperature compared to crushed concrete and slag.

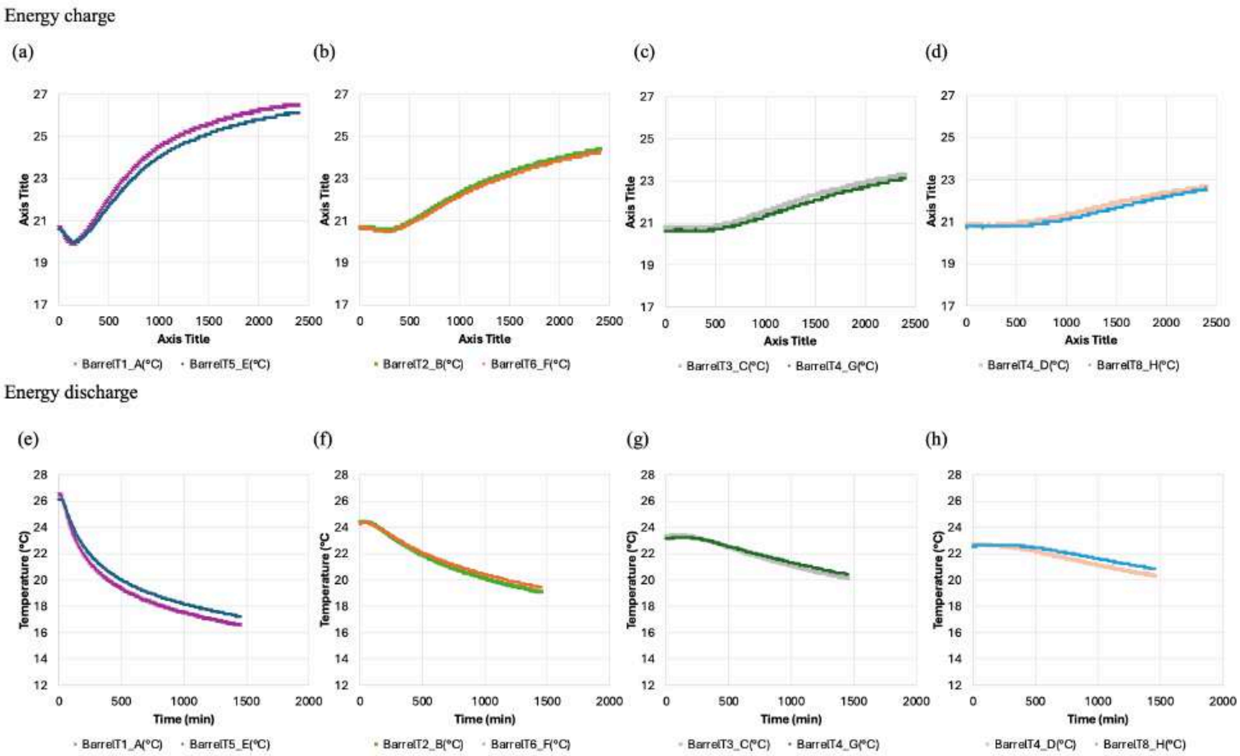

Figure 44. Surface temperature evolution along with time for 8 temperatures sensors (A, B, C, D, E, F, G, H)

Fig. 45 shows the temperature evolution across the depth along with time for 3 temperatures sensors at position E, I and J. The temperature across the depth is not homogeneous during energy charge and discharge. During energy charge, it can be observed the gradient of temperature evolution at position J (lower surface) is greater followed by that of I and E. The same phenomenon as the test with crushed concrete occurs, causing J to have the highest temperature, followed by I and E. During energy discharge, the same phenomenon occurs for fly ash as the test of crushed concrete. However, the temperature at position I remains slightly higher than that of position I which may be related to the arrangement of fly ash inside the barrel. However, the same observation as the test of crushed concrete reoccurs during the second test with fly ash, which corresponds to what is supposed to occur.

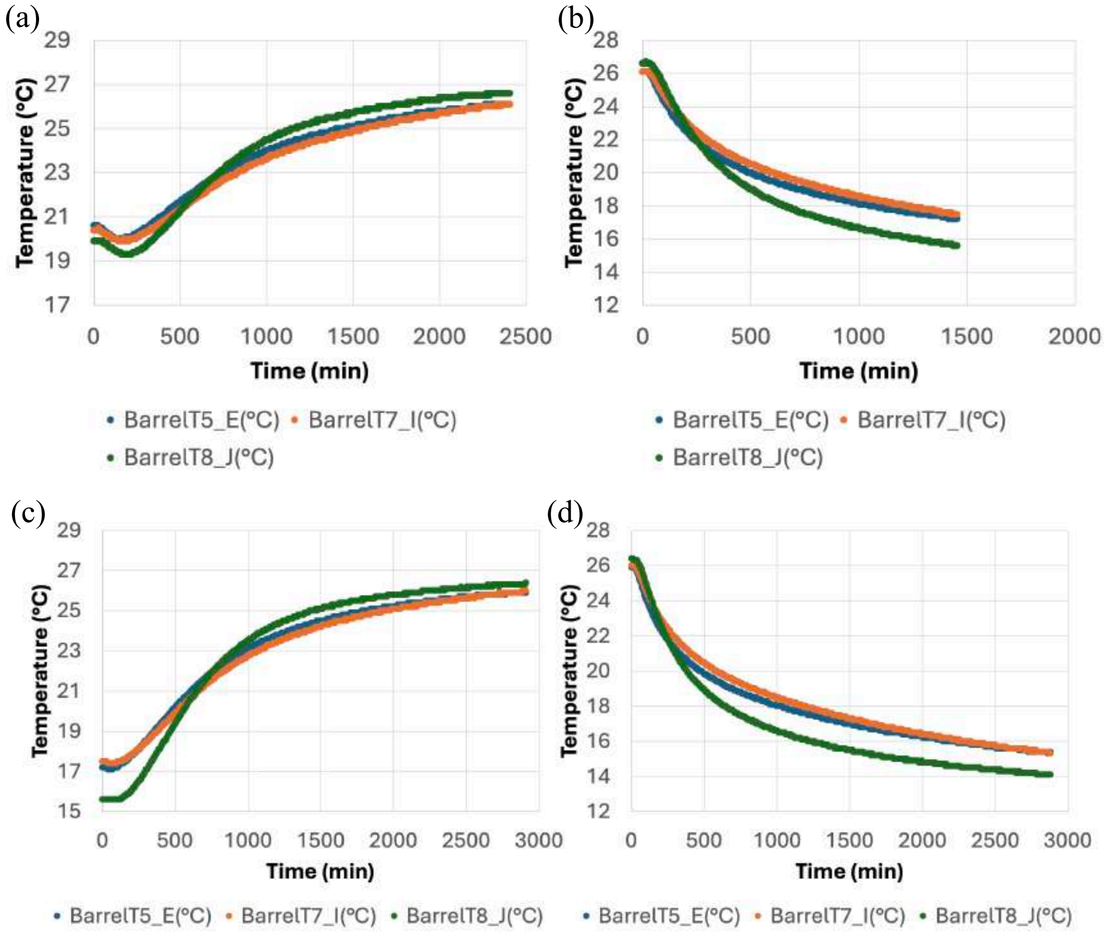

Figure 45. Temperature evolution along the depth along with time for 3 temperatures sensors at position E, I and J with (a) and (b): test 1 and (c) and (d); test 2

5.4.4 Comparison of performance of thermal energy storage (TES) installation with crushed concrete, slag and fly ash

A repetition test is performed for crushed concrete, slag and fly ash to verify the repeatability of the test results with a heating process of 46 - 48 hours and a cooling process of 48 hours. Fig. 46 shows the efficiencies, total energy stored and released as well as average charging and discharging power for both tests of each ISWs. The cycle efficiency is only determined for the repetition test as the condition of heating time is at least the same as cooling time is fulfilled. It can be observed that crushed concrete has the best overall performance as materials for TES as it has the highest charge and discharge efficiency, average charging and discharging power, total energy stored and released as well as ratio between real energy stored and expected energy stored except that its cycle efficiency is lower than slag and fly ash. Slag is a slightly better materials for TES compared to fly ash in all the parameters.

It can be observed that the cycle efficiency is higher than 100% for all three materials. This is due to the brilliance of using the heat pump to extract effectively the low-temperature thermal energy stored within the barrel. However, this does not mean that more energy is released during energy discharge than the energy stored during energy charge as the discharge efficiency is always lower than 100% and the energy consumed by the heat pump to extract the energy stored is not taken into consideration for the determination of cycle efficiency. The high cycle efficiency does indicate that there is a strong interest to use heat pump to extract successfully low-temperature thermal energy storage.

Furthermore, the repeatability of the test results for each material is validated since the values found for all the parameters are similar for the first and repetition test of each material respectively.

5.4.5 Partial conclusion

Crushed concrete has the best overall performance as TES materials, followed by slag and fly ash. This is further justified by the percentage of heat loss for the TES installation of each material with crushed concrete having the least heat loss, followed by slag and fly ash shown in Fig. 47.

The issue with the current thermal energy storage (TES) installation is related to its low charge and discharge efficiency. However, this is due to the Sunamp heater used that provides limited energy for thermal energy storage as a maximum of 28°C is reached for all the TES installations. The solution will be to find an alternative heater capable of providing more energy for energy charge. Furthermore, the top of the barrel should be insulated to minimize the heat loss towards exterior.

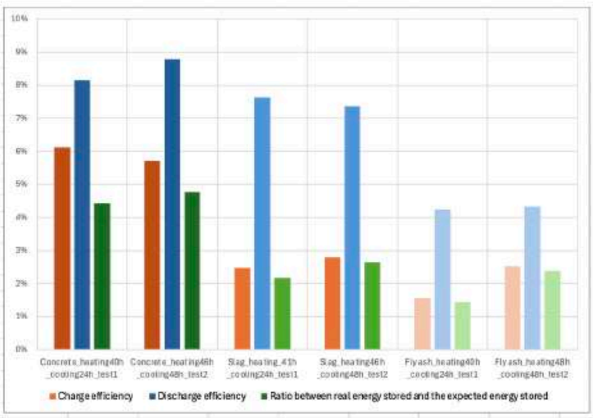

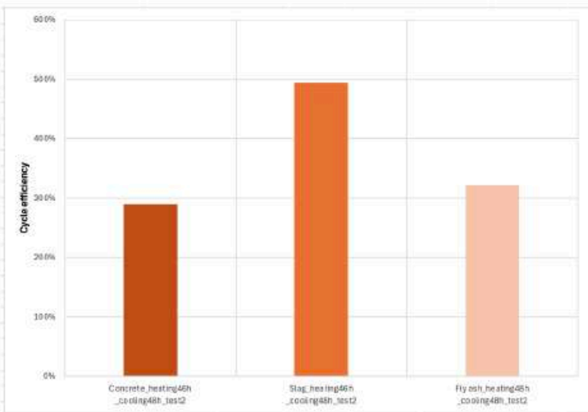

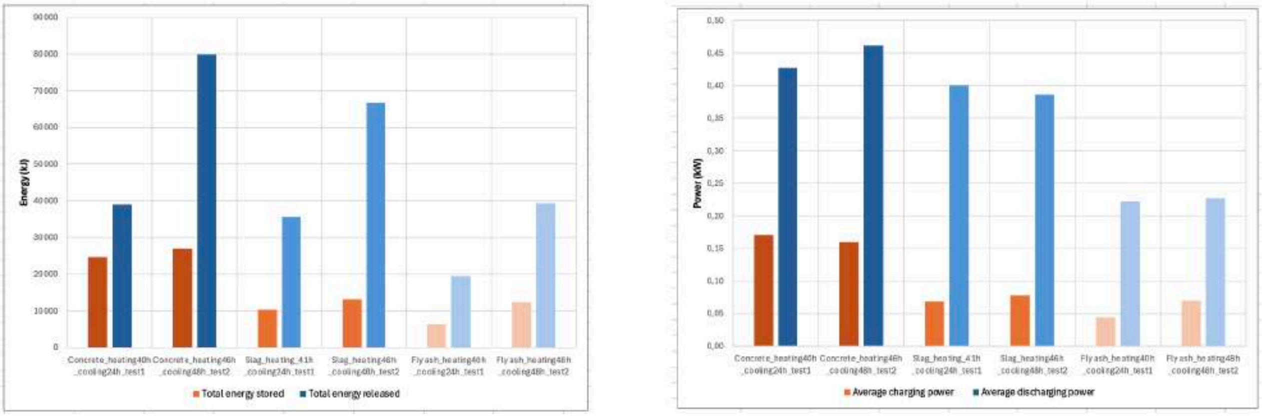

Figure 46. Efficiencies, energy stored and released, average charging and discharging power and ratio for thermal energy storage tests with crushed concrete, slag and fly ash

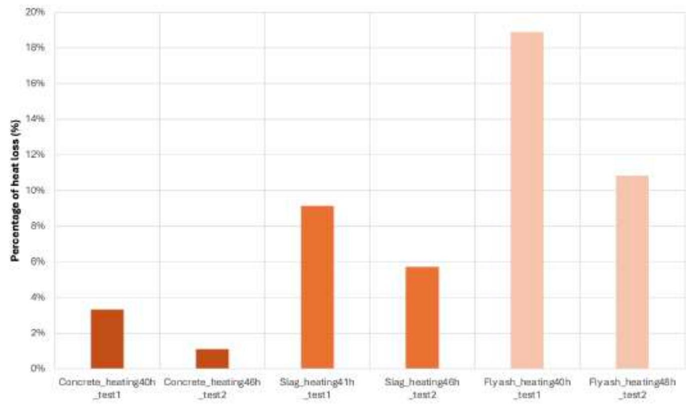

Figure 47. Percentage of heat loss for thermal energy storage tests with crushed concrete, slag and fly ash

5.5 Computational fluid dynamic (CFD) simulation for the waste heat recovery system

The initial purpose of perform CFD simulation is to build a digital model of the waste heat discovery system that is capable to predict the performance of the system with any heating temperature set for the sauna heater. however, due to the issue of unable to find the devices to measure the thermal conductivity, skeletal density and void fraction of waste metal powder, these missing information can bring inaccuracy for the simulation. Hence, the purpose of CFD is shifted to study the influence of void fraction of the metal waste powder towards the performance of TES installations. The result found through simulation may not correspond to the result in real life for the system but the comparison of the results for different scenarios is able to provide useful information about the influence of void fraction of waste metal powder towards the performance of waste heat recovery system.

5.5.1 Influence of void fraction of waste metal powder towards energy charge and discharge for waste heat recovery system

Fig. 48 shows the simulation results at t = 5 mins and 15 mins for the energy charge of heat recovery system with hot air entering at a constant temperature of 60°C and the void fraction of waste metal powder corresponds to 5, 20 and 70% respectively. It is observed that the heat recovery system heats up faster with a void fraction of 70%, indicating a better heat transfer rate for energy charge. It can possibly lead to better average charging power, better charge efficiency with more energy stored compared to waste metal powder with smaller void fraction while having the same heating time for all scenarios. Fig. 49 illustrates the simulations at t = 5 mins and 15 mins for the energy discharge of heat recovery system with the air entering at 27°C and the waste heat recovery system at 60°C. The void fraction is set at 5, 20 and 70% as well. It is noticed that the waste heat recovery system discharges heat faster with a void fraction of 70%, indicating a better heat transfer rate for energy discharge as well. It can lead also to better average discharging power, better discharge efficiency with more energy released compared to waste metal powder with smaller void fraction while having the same cooling time for all scenarios.

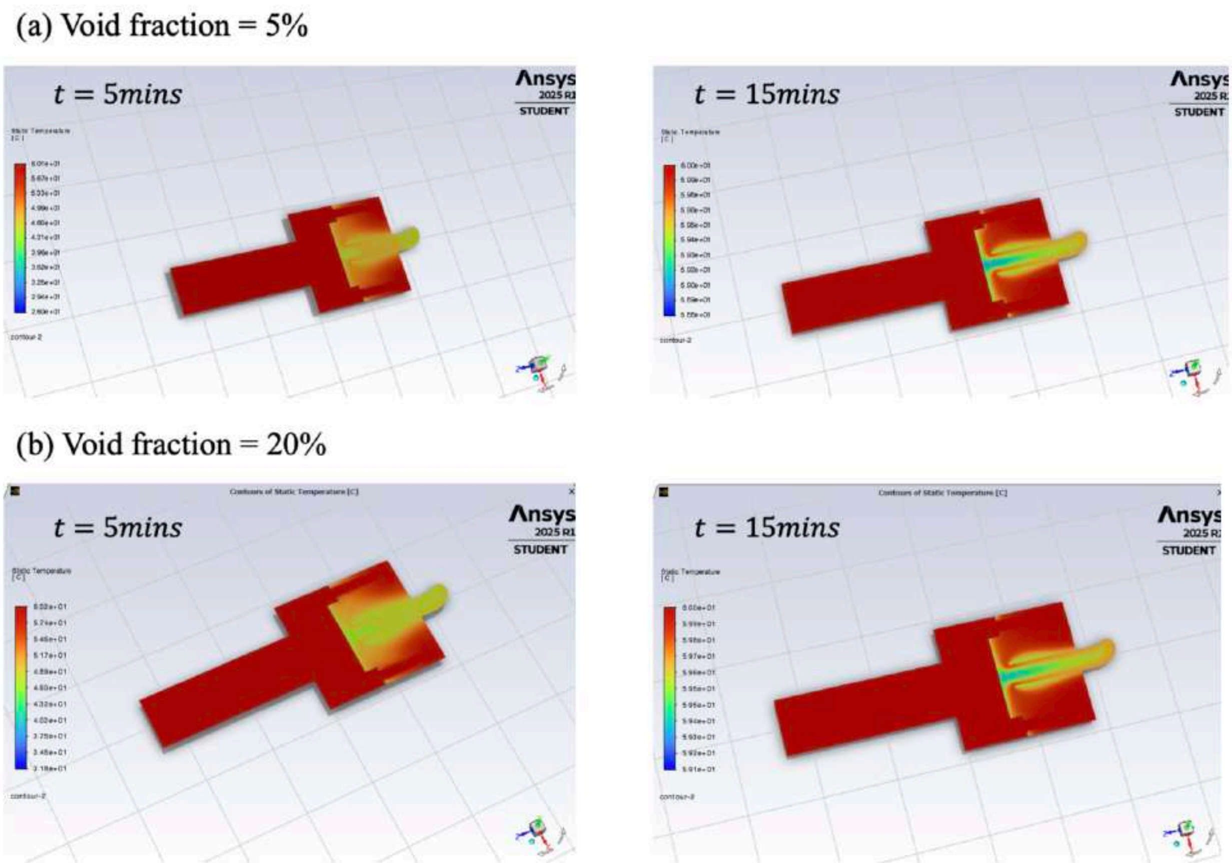

(c) Void fraction = 70%

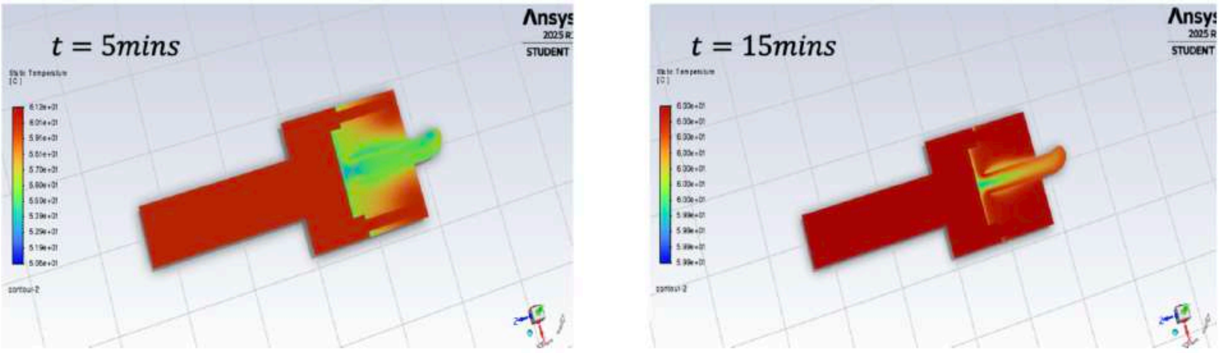

Figure 48. Simulation results for energy charge of waste heat recovery system for three scenarios at t = 5mins and t = 15 mins

(a) Void fraction = 5%

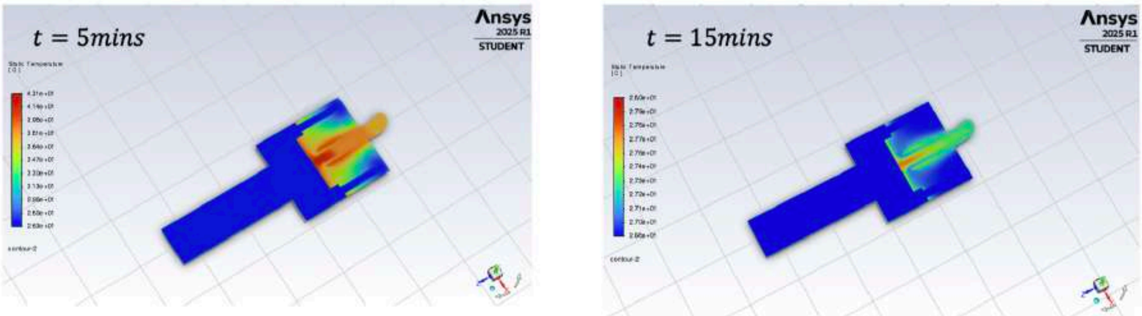

(b) Void fraction = 20%

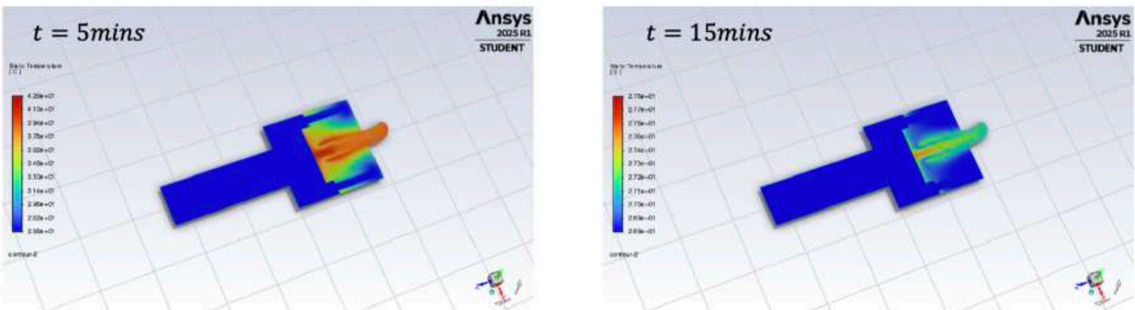

(c) Void fraction = 70%

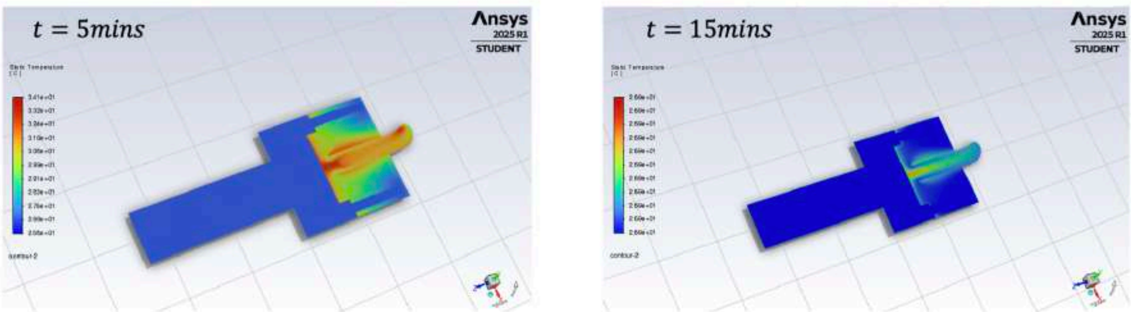

Figure 49. Simulation results for energy discharge of waste heat recovery system for three scenarios at t = 5mins and t = 15 mins

5.5.2 Partial conclusion

The use of waste metal powder with bigger void fractions is advantageous for better performance of the waste heat recovery system. The void fraction of the metal powder is a subject to work on to further the research on waste metal powder and waste heat recovery system. It will be highly interesting to carry out the measurements for thermal conductivity, specific heat capacity and skeletal density of the waste metal powder in order to perform an accurate CFD simulations capable of giving results similar to the measurements done in real life.

6. Conclusion

6.1 General conclusion

This study focuses principally on sensible heat storage (SHS) coupled with the valorisation of four industrial solid wastes (ISW), namely: waste metal powder, crushed concrete, slag and fly ash. The sensible heat storage installation built and examined in this study include waste heat recovery system and thermal energy storage (TES) installation. The main goal is to analyse the viability of valorising the industrial solid wastes as thermal energy storage materials.

The determination of the water content and particle size distribution of the four ISWs has been accomplished by performing a sieve test complying to the SFS-EN 933-1 standard. The characterisation of the particle size of ISWs is performed by calculating the mean, mode, median, 10th percentile and 90th percentile for the particle size of the materials. The homogeneity of the ISWs has been examined through the determination of particle size distribution. The results of sieve test show that fly ash is the material with highest water content, followed by slag, crushed concrete and waste metal powder. Fly ash is also the material with the smallest particle size, followed by waste metal powder, slag and crushed concrete. The thermal stability and decomposition temperature for each ISWs have been determined through the thermogravimetric analysis (TGA) test, allowing the determination of ideal maximum heating temperature for the ISWs without decomposition of the materials. The influence of free surface moisture on the result of TGA test is also studied. The results of TGA test demonstrates that waste metal powder is the most thermally stable material, followed by crushed concrete, slag and fly ash.

The built waste heat recovery system using waste metal powder as TES materials has been tested to examine the performance of the system to store and release thermal energy. Different scenarios of energy charge and discharge have been applied for the waste heat recovery system. The parameters such as charge and discharge efficiency, cycle efficiency, average charging and discharging power, total energy stored and released, ratio between real energy stored and expected energy stored as well as total heat loss have been determined through measurements and calculations, with analysis carried out on these parameters for each scenario. The temperature evolution, temperature homogeneity and repeatability of test results have been analysed and examined for the waste metal powder. The most ideal configuration for waste heat recovery system is proposed with suggestions for the improvement of the system. According to the results, the most ideal configuration is the open loop system with shorter heating time and higher heating temperature.

The built thermal energy storage installation with the use of crushed concrete, slag and fly ash as TES materials has been tested to examine the performance of the system to charge and discharge thermal energy. The same parameters measured and calculated for the waste heat recovery system have been determined and analysed for the TES installation as well. The temperature evolution, temperature homogeneity across surface and along depth of the TES installation as well as the repeatability of the test results have been studied for each ISWs used. The recommendation for the ideal material as TES material has been made with suggestions for improvement and further research on the ISWs and TES installations. According to the tests performed, crushed concrete has the best overall performance as TES materials, followed by slag and fly ash for the TES installations.

The influence of void fraction of waste metal powder towards the energy charge and discharge for waste heat recovery system is investigated through computational fluid dynamic (CFD) simulations by observing the temperature evolution of the system during energy charge and discharge. According to the simulation results obtained, it is more ideal to have larger void fraction for waste metal powder to allow energy charge and discharge in a more efficient way.

6.2 Perspectives on further research for the study

This research on the sensible heat storage coupled with valorisation of industrial solid waste is only at its early phases with works still left to be explored and performed. The possible direction for further research includes not exhaustively:

- Density test (skeletal and apparent density)
  - ⇒ Possible test device: AccuPyc 1330 Pycnometer density analyzer using gas displacement technique for determination of skeletal density
  - ⇒ Possible test device: Hall flowmeter or Carney funnel for determination of apparent density
  - ⇒ Determination of porosity and void fraction of industrial solid wastes with both density
- Thermal conductivity test
  - ⇒ Possible test device: Hot Disk TPS 2500S thermal constant analyzer
- Thermal diffusion coefficient test
  - ⇒ Possible test device: Hot Disk TPS 2500S thermal constant analyzer / NETZSCH DSC 457 MicroFlash

- Specific heat capacity test
  - ⇒ Possible test device: Hot Disk TPS 2500S thermal constant analyzer / NETZSCH DSC 404 C Pegasus / Mettler Toledo DSC 822e device / PerkinElmer DSC 6000
- Linear thermal expansion test
  - ⇒ Possible test device: NETZSCH DIL 402 C
- Computational fluid dynamics (CFD) simulation for waste heat recovery system and thermal energy storage installation with measured parameters for industrial solid wastes

References

[1] Shaqsi, A. Z. A., Sopian, K., & Al-Hinai, A. (2020). Review of energy storage services, applications, limitations, and benefits. *Energy Reports*, *6*, 288–306. https://doi.org/10.1016/j.egyr.2020.07.028

[2] IEA (2024), CO2 Emissions in 2023, IEA, Paris https://www.iea.org/reports/co2-emissions-in-2023. (Accessed 27 August 2025).

[3]Amir, M., Deshmukh, R. G., Khalid, H. M., Said, Z., Raza, A., Muyeen, S., Nizami, A., Elavarasan, R. M., Saidur, R., & Sopian, K. (2023). Energy storage technologies: An integrated survey of developments, global economical/environmental effects, optimal scheduling model, and sustainable adaption policies. *Journal of Energy Storage*, *72*, 108694. https://doi.org/10.1016/j.est.2023.108694

[4] Xiong, Y., He, M., Wu, Y., Su, Y., Li, M., Yin, M., Zhang, A., Li, X., Li, S., Yang, Y., Tian, X., & Ding, Y. (2025). A comprehensive review on the utilization of industrial solid waste in thermal energy storage field. *Solar Energy Materials and Solar Cells*, *285*, 113562. https://doi.org/10.1016/j.solmat.2025.113562

[5] Khan, M. K., Raza, M., Shahbaz, M., Farooq, U., & Akram, M. U. (2024). Recent advancement in energy storage technologies and their applications. *Journal of Energy Storage*, *92*, 112112. https://doi.org/10.1016/j.est.2024.112112

[6] Rahman, M. M., Oni, A. O., Gemechu, E., & Kumar, A. (2020). Assessment of energy storage technologies: A review. *Energy Conversion and Management*, *223*, 113295. https://doi.org/10.1016/j.enconman.2020.113295

[7] Wei, P., Abid, M., Adun, H., Awoh, D. K., Cai, D., Zaini, J. H., & Bamisile, O. (2023). Progress in energy storage technologies and methods for renewable energy systems application. *Applied Sciences*, *13*(9), 5626. https://doi.org/10.3390/app13095626

[8] Ho, C. K., & Ambrosini, A. (2018). Thermal energy storage technologies. In *U.S. DOE energy storage handbook*. U.S. Department of Energy.

[9] Koçak, B., Majó, M., Barreneche, C., Fernández, A. I., & Paksoy, H. (2024). Performance analysis of a molten salt packed-bed thermal energy storage system using three different waste materials. *Solar Energy Materials and Solar Cells*, *278*, 113199. https://doi.org/10.1016/j.solmat.2024.113199

[10] Koçak, B., Fernández, A. I., & Paksoy, H. (2021). Characterization of demolition waste powder to be processed as sensible thermal energy storage material. *Solar Energy Materials and Solar Cells*, *230*, 111283. https://doi.org/10.1016/j.solmat.2021.111283

[11] Py, X., Calvet, N., Olives, R., Meffre, A., Echegut, P., Bessada, C., Veron, E., & Ory, S. (2011). Recycled Material for Sensible Heat Based Thermal Energy Storage to be Used in Concentrated Solar Thermal Power Plants. *Journal of Solar Energy Engineering*, *133*(3). https://doi.org/10.1115/1.4004267

[12] Ortega-Fernández, I., Calvet, N., Gil, A., Rodríguez-Aseguinolaza, J., Faik, A., & D'Aguanno, B. (2015). Thermophysical characterization of a by-product from the steel industry to be used as a sustainable and low-cost thermal energy storage material. *Energy*, *89*, 601–609. https://doi.org/10.1016/j.energy.2015.05.153

[13] Liu, K., Zhao, H., Yuan, Z., Zhao, F., Chen, D., & Shi, C. (2022). Preparation and characterization of steel slag-based low, medium, and high-temperature composite phase change energy storage materials. *Journal of Energy Storage*, *57*, 106309. https://doi.org/10.1016/j.est.2022.106309

[14] Xia, X., Sun, Y., Jiang, S., Sun, W., Yang, Y., Sun, C., & Wang, Q. (2024). Strategic configuration of geothermal backfill materials using industrial solid waste for Low-Carbon building energy systems. *Journal of Building Engineering*, 111628. https://doi.org/10.1016/j.jobe.2024.111628

[15] Wu, B., Chen, G., Di, Y., Liu, J., Zhang, X., Jiao, K., Wu, L., Wei, Y., Lin, L., Jiang, Z., & Zhang, X. (2024). Using steel slag and fly ash solid wastes to fabricate ceramics-based phase change composites with excellent mechanical and thermal properties applied in thermal energy storage. *Ceramics International*. https://doi.org/10.1016/j.ceramint.2024.09.045

[16] Ding, S., Wang, X., Ashour, A., Wang, D., Sun, T., & Han, B. (2025). Developing electrothermal energy storage system for building heating by using stainless steel wires reinforced ultra-high performance concrete. *Composites Part a Applied Science and Manufacturing*, 108832. https://doi.org/10.1016/j.compositesa.2025.108832

[17] Glosser, D., Striby, P., Bellusci, M., Bottem, R., Amroun, S., & Suraneni, P. (2023). Characterization of optical and physiochemical properties of reclaimed fly ash for use as sensible thermal energy storage material in concentrating solar power systems. *Solar Energy*, *263*, 111944. https://doi.org/10.1016/j.solener.2023.111944

[18] Agalit, H., Zari, N., & Maaroufi, M. (2020). Suitability of industrial wastes for application as high temperature thermal energy storage (TES) materials in solar tower power plants – A comprehensive review. *Solar Energy*, *208*, 1151–1165. https://doi.org/10.1016/j.solener.2020.08.055

[19] S.W. Yin, J.W. Han, Y.L. Shi, L.G. Tong, L. Wang, Heat charge and discharge characteristics of non-phase change solid heat storage materials, Chem. Ind. Eng. Prog. 39 (2020) 5161–5169, https://doi.org/10.16085/j.issn.1000-6613.2020-0356.

[20] Naimi, K. M. A., Delclos, T., & Calvet, N. (2015). Industrial waste produced in the UAE, valuable high-temperature materials for thermal energy storage applications. *Energy Procedia*, *75*, 2087–2092. https://doi.org/10.1016/j.egypro.2015.07.320

[21] Agalit, H., Zari, N., & Maaroufi, M. (2017). Thermophysical and chemical characterization of induction furnace slags for high temperature thermal energy storage in solar tower plants. *Solar Energy Materials and Solar Cells*, *172*, 168–176. https://doi.org/10.1016/j.solmat.2017.07.035

[22] Wang, Y., Wang, Y., Li, H., Zhou, J., & Cen, K. (2018). Thermal properties and friction behaviors of slag as energy storage material in concentrate solar power plants. *Solar Energy Materials and Solar Cells*, *182*, 21–29. https://doi.org/10.1016/j.solmat.2018.03.020

[23] J. B. Martinkauppi, T. Syrjälä, A. Mäkiranta and E. Hiltunen, "Some Aspects of Recycling Concrete Crush for Thermal Heat Storage," *2018 7th International Conference on Renewable Energy Research and Applications (ICRERA)*, Paris, France, 2018, pp. 707-710, doi: 10.1109/ICRERA.2018.8566981.

[24] Wongsa, A., Sata, V., Nuaklong, P., & Chindaprasirt, P. (2018). Use of crushed clay brick and pumice aggregates in lightweight geopolymer concrete. *Construction and Building Materials*, *188*, 1025–1034. https://doi.org/10.1016/j.conbuildmat.2018.08.176

[25] J.F. Lu, G.Q. Yin, Z.F. Deng, Q.L. Li, S.Y. Zhou, X. Chen, Experimental study on thermal conductivity of recycled aggregate concrete, China Sci. Technol.Inform. (2012) 63, https://doi.org/10.3969/j.issn.1001-8972.2012.22.025.

[26] J.Z. Xiao, Z.W. Song, F. Zhang, An experimental study on thermal conductivity of concrete, J. Build. Mater. 13 (2010) 17–21, https://doi.org/10.3969/j.issn.1007-9629.2010.01.004.

[27] Y. Ding, M.Y. Deng, S.X. Zhou, Z.P. Wang, J.L. Dong, Y.Q. Wei, The evolution relation between Materials' Porosity and thermal conductivity based on the simulation by COMSOL software, Mater. rep. 33 (2019) 211–213.

[28] Bhatt, A., Priyadarshini, S., Mohanakrishnan, A. A., Abri, A., Sattler, M., & Techapaphawit, S. (2019). Physical, chemical, and geotechnical properties of coal fly ash: A global review.

Case Studies in Construction Materials, *11*, e00263. https://doi.org/10.1016/j.cscm.2019.e00263

[29] Zhu, P., Hao, Y., Liu, H., Wang, X., & Gu, L. (2020). Durability evaluation of recycled aggregate concrete in a complex environment. *Journal of Cleaner Production*, *273*, 122569. https://doi.org/10.1016/j.jclepro.2020.122569

[30] Bravo, M., De Brito, J., Pontes, J., & Evangelista, L. (2015). Durability performance of concrete with recycled aggregates from construction and demolition waste plants. *Construction and Building Materials*, *77*, 357–369. https://doi.org/10.1016/j.conbuildmat.2014.12.103

[31] Wang, C., Chazallon, C., Braymand, S., & Hornych, P. (2024). Thermogravimetric analysis (TGA) for characterization of self-cementation of recycled concrete aggregates in pavement. *Thermochimica Acta*, *733*, 179680. https://doi.org/10.1016/j.tca.2024.179680

[32] Schwarzmayr, P., Birkelbach, F., Walter, H., Javernik, F., Schwaiger, M., & Hofmann, R. (2023). Packed bed thermal energy storage for waste heat recovery in the iron and steel industry: A cold model study on powder hold-up and pressure drop. *Journal of Energy Storage*, *75*, 109735. https://doi.org/10.1016/j.est.2023.109735

[33] Bing, L., Biao, T., Zhen, M., Hanchi, C., & Hongbo, L. (2019). Physical and chemical properties of steel slag and utilization technology of steel slag at home and abroad. *IOP Conference Series Earth and Environmental Science*, *242*, 032012. https://doi.org/10.1088/1755-1315/242/3/032012

[34] Turunen, K. (2023). Long-term thermal energy storage with cold-crystallizing materials - Method, properties and scale-up. [Doctoral Thesis, Aalto University]. Aalto University. http://urn.fi/URN:ISBN:978-952-64-1133-0

[35] Calderón-Vásquez, I., Segovia, V., Cardemil, J. M., & Barraza, R. (2021). Assessing the use of copper slags as thermal energy storage material for packed-bed systems. *Energy*, *227*, 120370. https://doi.org/10.1016/j.energy.2021.120370

Annexes

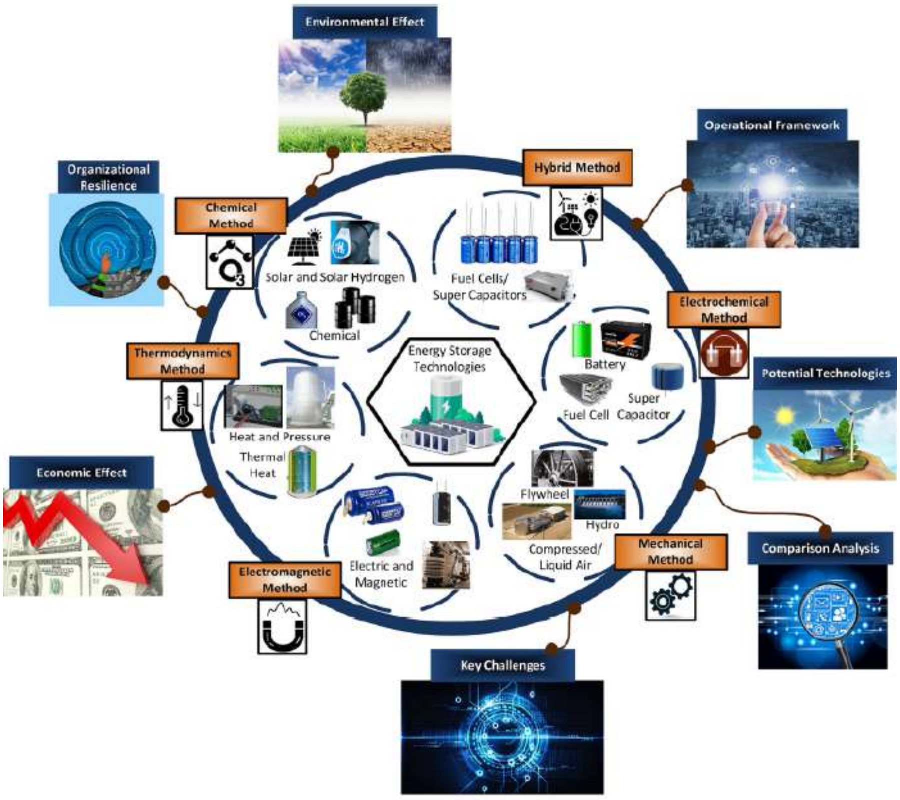

Figure 1A. Classification of energy storage technologies (EST) [3]

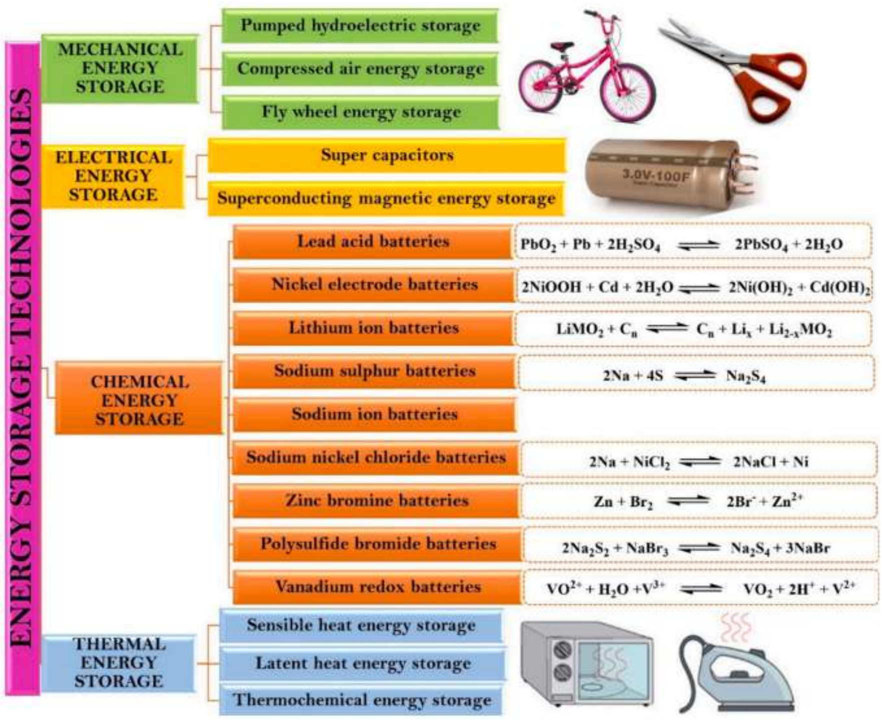

Figure 2A. Classification of energy storage technologies according to type of energy stored [5-7]

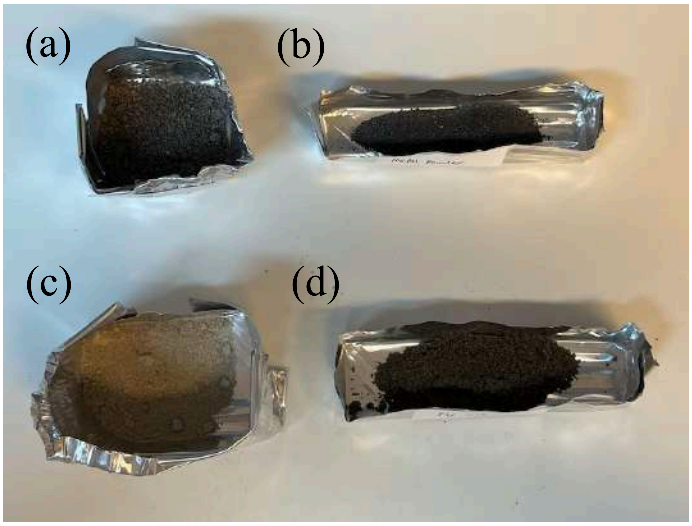

Figure 3A. (a) Slag, (b) Waste metal powder, (c) Crushed concrete and (d) Fly ash for thermogravimetric analysis (TGA)

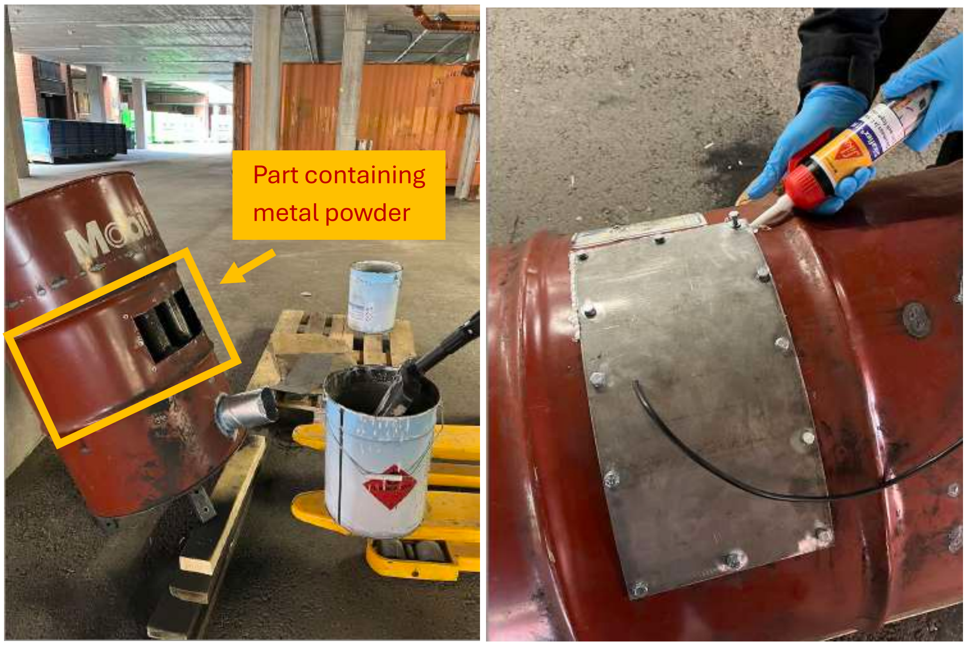

(a) (b)

Figure 4A. (a) Barrel partially filled by waste metal powder (the upper and lower side of the part filled by metal powder is being covered by metal plates which separate the barrel into 3 sections), (b) Cover for the middle section of the barrel sealed

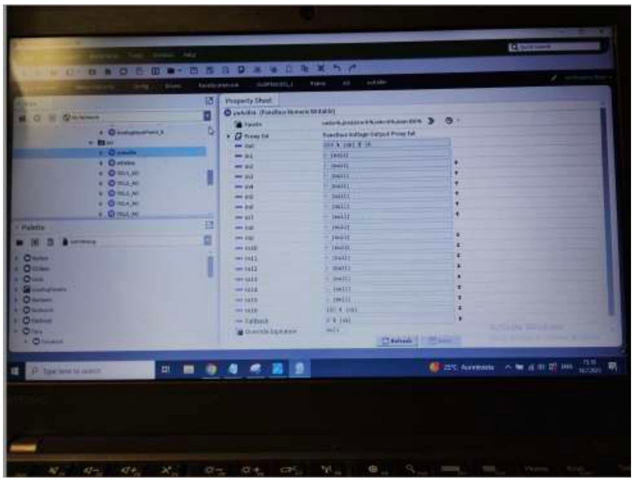

CENTRALINE
by Honeywell

Figure 5A. CentraLine NX data logger software for temperature acquisition

Figure 6A. A part of cable connection between temperature sensors and CentraLine NX software

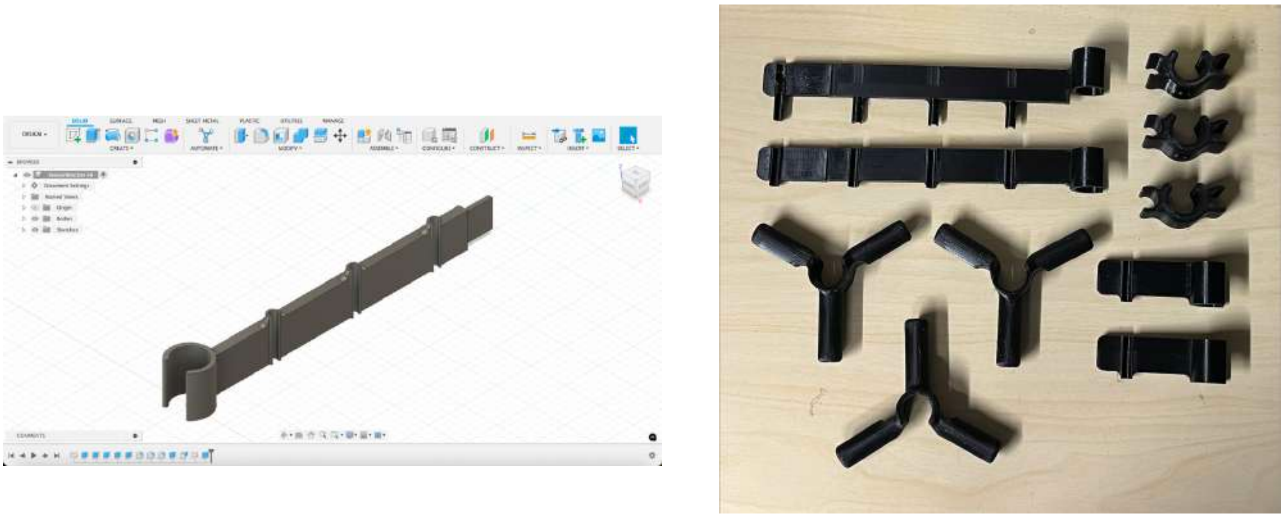

(a) (b)

Figure 7A. (a) A part of temperature sensor holder designed on AutoCAD Fusion360 and (b) A set of 3D-printed part

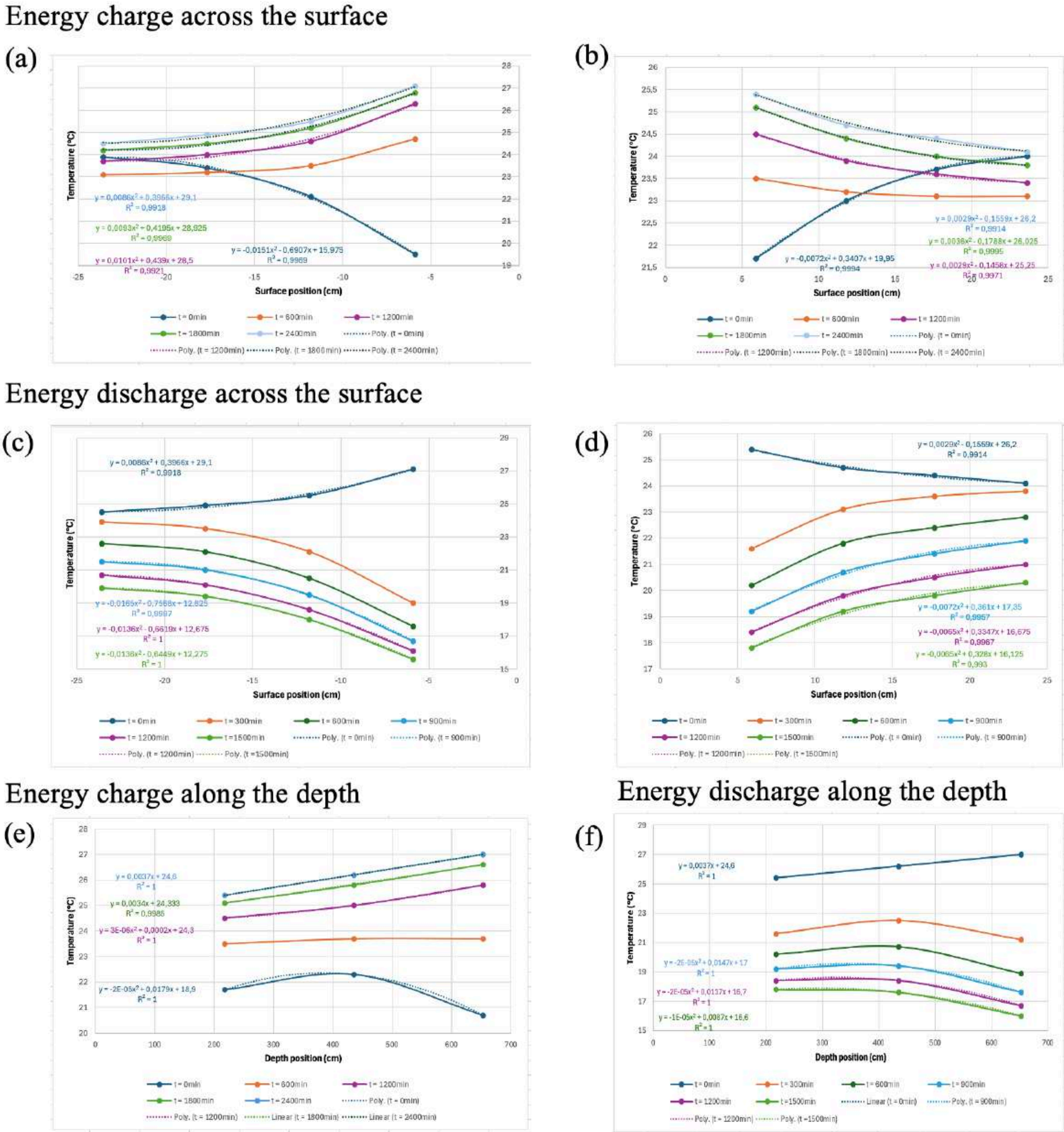

Figure 8A. Temperature evolution across the surface snd along the depth for TES installation with crushed concrete (0 represents the middle of the barrel for surface position and the top of the barrel for depth position)

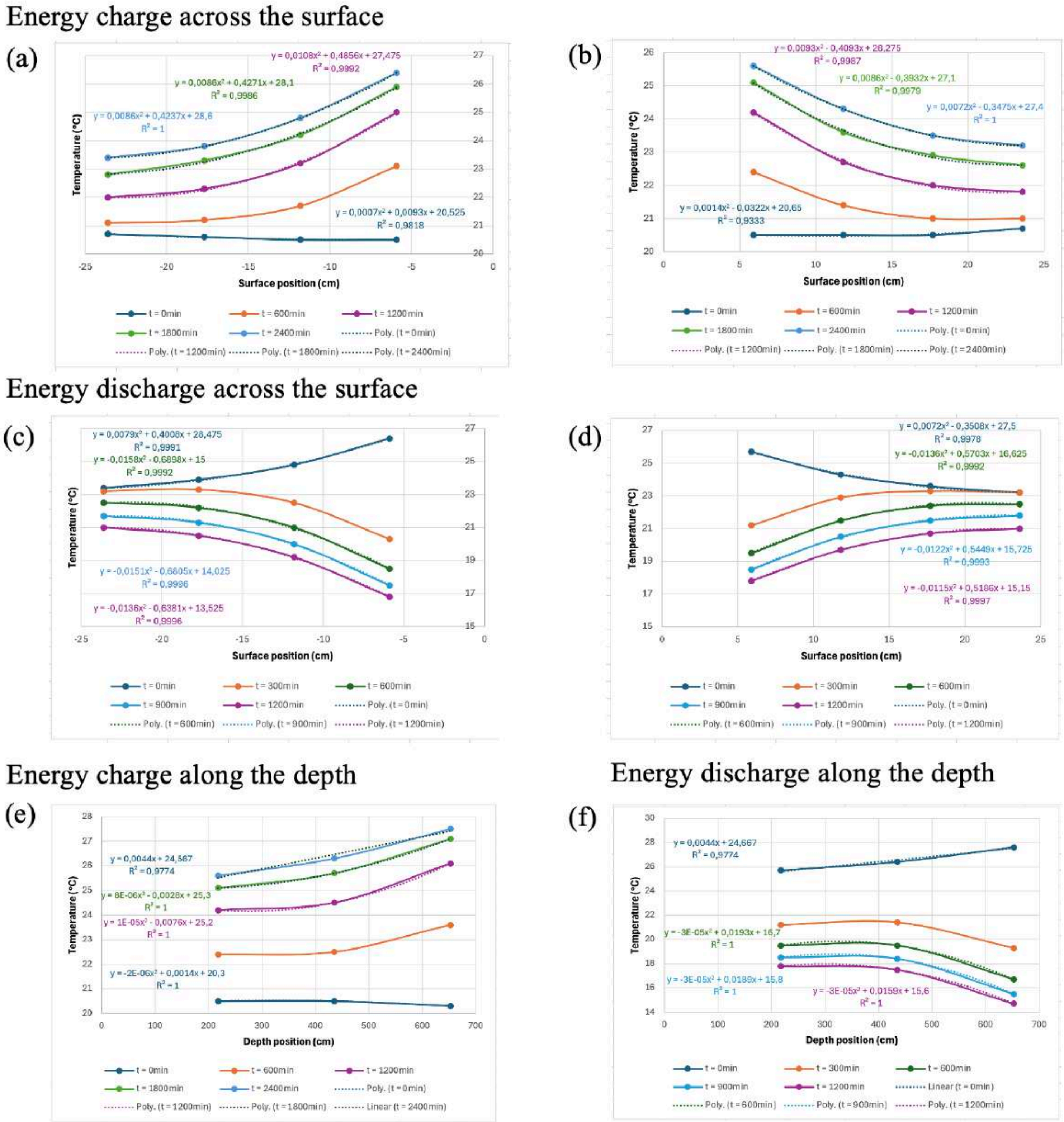

Figure 9A. Temperature evolution across the surface snd along the depth for TES installation with slag (0 represents the middle of the barrel for surface position and the top of the barrel for depth position)

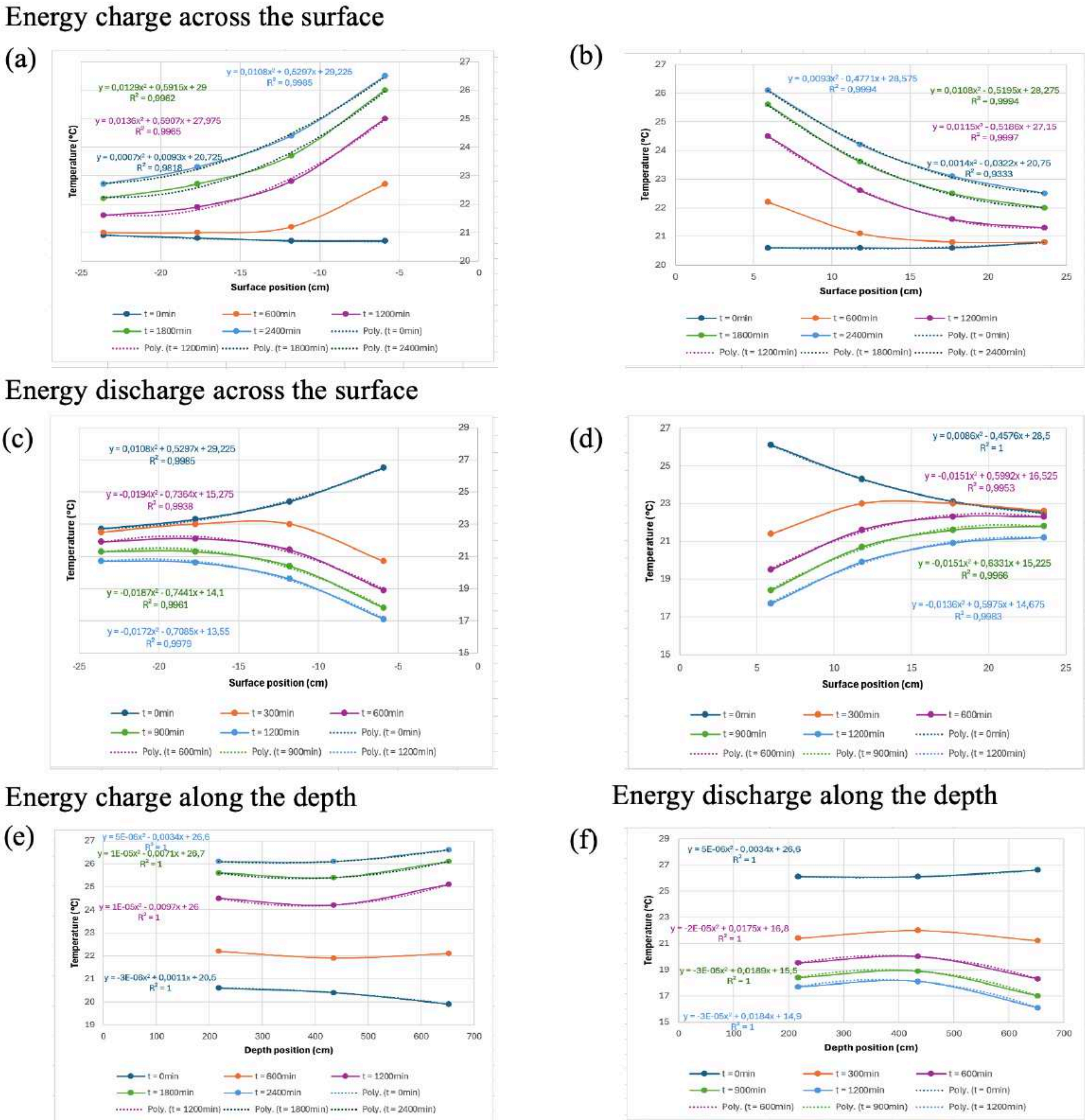

Figure 10A. Temperature evolution across the surface snd along the depth for TES installation with fly ash (0 represents the middle of the barrel for surface position and the top of the barrel for depth

Crushed concrete

Representation of the temperature evolution across the surface and along the depth (x : surface position with 0 indicating middle of the barrel, z : depth position with 0 indicating top of the barrel, y : temperature in °C):

- -23.9cm < x < -5.9cm:
  - ⇒ Energy charge: y = 0,01x^2 + 0,4x + 29
  - ⇒ Energy discharge: y = -0,01x^2 - 0,6x + 12
- 5.9cm < x < 23.9cm:
  - ⇒ Energy charge: y = 0,003x^2 - 0,2x + 26
  - ⇒ Energy discharge: y = -0,007x^2 + 0,3x + 16
- 217.5cm < z < 652.5cm:
  - ⇒ Energy charge: y = 0,004z + 25
  - ⇒ Energy discharge: y = -1E-05z^2 + 0,01x + 17

Slag

Representation of the temperature evolution across the surface and along the depth (x : surface position with 0 indicating middle of the barrel, z : depth position with 0 indicating top of the barrel, y : temperature in °C):

- -23.9cm < x < -5.9cm:
  - ⇒ Energy charge: y = 0,01x^2 + 0,4x + 29
  - ⇒ Energy discharge: y = -0,01x^2 - 0,6x + 14
- 5.9cm < x < 23.9cm:
  - ⇒ Energy charge: y = 0,01x^2 - 0,3x + 27
  - ⇒ Energy discharge: y = -0,01x^2 + 0,5x + 15
- 217.5cm < z < 652.5cm:
  - ⇒ Energy charge: y = 0,004z + 25
  - ⇒ Energy discharge: y = -3E-05z^2 + 0,02z + 16

Fly ash

Representation of the temperature evolution across the surface and along the depth (x : surface position with 0 indicating middle of the barrel, z : depth position with 0 indicating top of the barrel, y : temperature in °C):

- -23.9cm < x < -5.9cm:
  - ⇒ Energy charge: y = 0,01x^2 + 0,5x + 29
  - ⇒ Energy discharge: y = -0,02x^2 - 0,7x + 14
- 5.9cm < x < 23.9cm:
  - ⇒ Energy charge: y = 0,01x^2 - 0,5x + 29
  - ⇒ Energy discharge: y = -0,01x^2 + 0,6x + 15
- 217.5cm < z < 652.5cm:
  - ⇒ Energy charge: y = 1E-05z^2 -0,003z + 27
  - ⇒ Energy discharge: y = -3E-05z^2 + 0,02z + 15